การรับรู้แอนไอออนและกรดอะมิโนชนิดแอลฟาโดยใช้สารประกอบเชิงซ้อนไดนิวเคลียร์ของคอปเปอร์(II) และซิงก์(II) กับลิแกนด์กลุ่มไตรโพดัลแอมีนโดยวิธีการแทนที่อินดิเคเตอร์

นายสรายุทธ เวชสิทธิ์

จุฬาลงกรณ์มหาวิทยาลัย
Chulalongkorn University

บทคัดย่อและแฟ้มข้อมูลฉบับเต็มของวิทยานิพนธ์ตั้งแต่ปีการศึกษา 2554 ที่ให้บริการในคลังปัญญาจุฬาฯ (CUIR)
เป็นแฟ้มข้อมูลของนิสิตเจ้าของวิทยานิพนธ์ ที่ส่งผ่านทางบัณฑิตวิทยาลัย
The abstract and full text of theses from the academic year 2011 in Chulalongkorn University Intellectual Repository (CUIR)
are the thesis authors' files submitted through the University Graduate School.

วิทยานิพนธ์นี้เป็นส่วนหนึ่งของการศึกษาตามหลักสูตรปริญญาวิทยาศาสตรดุษฎีบัณฑิต
สาขาวิชาเคมี ภาควิชาเคมี
คณะวิทยาศาสตร์ จุฬาลงกรณ์มหาวิทยาลัย
ปีการศึกษา 2558
ลิขสิทธิ์ของจุฬาลงกรณ์มหาวิทยาลัย

# SENSING OF ANIONS AND α-AMINO ACIDS USING DINUCLEAR COMPLEXES OF Cu(II) AND Zn(II) WITH TRIPODAL AMINE LIGANDS UNDER INDICATOR DISPLACEMENT ASSAY APPROACH

Mr. Sarayut Watchasit

A Dissertation Submitted in Partial Fulfillment of the Requirements
for the Degree of Doctor of Philosophy Program in Chemistry
Department of Chemistry
Faculty of Science
Chulalongkorn University
Academic Year 2015
Copyright of Chulalongkorn University

| | |
|---|---|
| Thesis Title | SENSING OF ANIONS AND α-AMINO ACIDS USING DINUCLEAR COMPLEXES OF Cu(II) AND Zn(II) WITH TRIPODAL AMINE LIGANDS UNDER INDICATOR DISPLACEMENT ASSAY APPROACH |
| By | Mr. Sarayut Watchasit |
| Field of Study | Chemistry |
| Thesis Advisor | Professor Thawatchai Tuntulani, Ph.D. |
| Thesis Co-Advisor | Assistant Professor Chomchai Suksai, Ph.D. |

Accepted by the Faculty of Science, Chulalongkorn University in Partial Fulfillment of the Requirements for the Doctoral Degree

.....Dean of the Faculty of Science
(Associate Professor Polkit Sangvanich, Ph.D.)

THESIS COMMITTEE

.....Chairman
(Associate Professor Vudhichai Parasuk, Ph.D.)

.....Thesis Advisor
(Professor Thawatchai Tuntulani, Ph.D.)

.....Thesis Co-Advisor
(Assistant Professor Chomchai Suksai, Ph.D.)

.....Examiner
(Professor Orawon Chailapakul, Ph.D.)

.....Examiner
(Assistant Professor Soamwadee Chaianansutcharit, Ph.D.)

.....External Examiner
(Assistant Professor Jaray Jaratjaroonphong, Ph.D.)

สรายุทธ เวชสิทธิ์ : การรับรู้แอนไอออนและกรดอะมิโนชนิดแอลฟาโดยใช้สารประกอบเชิงซ้อนไดนิวเคลียร์ของ คอปเปอร์(II) และซิงก์(II) กับลิแกนด์กลุ่มไตรโพดัลแอมีนโดยวิธีการแทนที่อินดิเคเตอร์ (SENSING OF ANIONS AND α-AMINO ACIDS USING DINUCLEAR COMPLEXES OF Cu(II) AND Zn(II) WITH TRIPODAL AMINE LIGANDS UNDER INDICATOR DISPLACEMENT ASSAY APPROACH) อ.ที่ปรึกษาวิทยานิพนธ์หลัก: ศ. ดร.ธวัชชัย ตันฑุลานิ, อ.ที่ปรึกษาวิทยานิพนธ์ร่วม: ผศ. ดร. จอมใจ สุกใส, 127 หน้า.

งานวิจัยนี้ได้ทำการสังเคราะห์สารประกอบเชิงซ้อนชนิดไดนิวเคลียร์และโมโนนิวเคลียร์ของไอออนโลหะ คอปเปอร์(II) และซิงก์(II) กับลิแกนด์ที่เป็นอนุพันธ์ของไตรโพดัลแอมีน ($Cu_2L2$, $Zn_2L2$, CuL3 และ ZnL3) และทำการพิสูจน์โครงสร้างของสารประกอบที่สังเคราะห์ได้ด้วยเทคนิคมาตรฐานทางเคมีวิเคราะห์ จากนั้นได้ทำการศึกษาความสามารถในการนำไปใช้ตรวจวัดแอนไอออนและกรดอะมิโนชนิดแอลฟาด้วยวิธีการแทนที่อินดิเคเตอร์

จากการศึกษาความเป็นไปได้ในกรตรวจวัดแอนไอออนไพโรฟอสเฟต (PPi) ด้วยสารประกอบเชิงซ้อนชนิดไดนิวเคลียร์กับอินดิเคเตอร์ชนิดต่างๆ พบว่าสารประกอบเชิงซ้อนที่เตรียมจากสารประกอบ $Zn_2L2$ กับ อินดิเคเตอร์ MTB สามารถตรวจวัด PPi ได้อย่างจำเพาะเจาะจง จากการศึกษาด้วยเทคนิค $^{1}$H-NMR, $^{31}$P-NMR และ เทคนิคทางเคมีคำนวณพบว่า โครงสร้างของสารประกอบเชิงซ้อนที่เกิดขึ้นมีอัตราส่วนของ $Zn_2L2$:PPi เท่ากับ 2:2 และได้ค่าขีดจำกัดการตรวจวัด PPi เท่ากับ 0.3 μM

การตรวจวัดกรดอะมิโนฮิสทิดีน (His) ด้วยสารประกอบ CuL3 และ ZnL3 ด้วยวิธีการแทนที่อินดิเคเตอร์โดยใช้ PAR เป็นอินดิเคเตอร์ พบว่าสารประกอบ CuL3 สามารถตรวจวัด His ได้อย่างจำเพาะเจาะจง ซึ่งแตกต่างจากสารประกอบ ZnL3 ที่จะถูกรบกวนด้วยแอนไอออนที่มีหมู่ฟอสเฟตเป็นองค์ประกอบ ผลการทดลองยังแสดงให้เห็นว่าระบบดังกล่าวสามารถตรวจวัด His ในตัวอย่างปัสสาวะได้ มีค่าขีดจำกัดการตรวจวัดเท่ากับ 0.5 μM.

| | |
|---|---|
| ภาควิชา เคมี | ลายมือชื่อนิสิต ..... |
| สาขาวิชา เคมี | ลายมือชื่อ อ.ที่ปรึกษาหลัก ..... |
| ปีการศึกษา 2558 | ลายมือชื่อ อ.ที่ปรึกษาร่วม ..... |

# # 5373830223 : MAJOR CHEMISTRY
KEYWORDS: PYROPHOSPHATE / INDICATOR DISPLACEMENT ASSAY / HISTIDINE / ANIONS / DINUCLEAR COMPLEXES / MONONUCLEAR COMPLEXES / TRIPODAL AMINE / **α**-AMINO ACIDS

SARAYUT WATCHASIT: SENSING OF ANIONS AND **α**- AMINO ACIDS USING DINUCLEAR COMPLEXES OF Cu(II) AND Zn(II) WITH TRIPODAL AMINE LIGANDS UNDER INDICATOR DISPLACEMENT ASSAY APPROACH. ADVISOR: PROF. THAWATCHAI TUNTULANI, Ph.D., CO-ADVISOR: ASST. PROF. CHOMCHAI SUKSAI, Ph.D., 127 pp.

In this research, the dinuclear and mononuclear copper( II) and zinc( II) complexes with anthracene based tripodal amine ligands ($Cu_2L2$, $Zn_2L2$, CuL3 and ZnL3) were synthesized and characterized by standard analytical techniques. The sensing abilities towards anions and **α**- amino acids were investigated using the indicator displacement assay (IDA) approach.

The detection of pyrophosphate anion ( PPi) by $Zn_2L2$ with four complexometric indicators was carried out. The results indicated that the [$Zn_2L2$•MTB] ensemble could discriminate the PPi from other phosphate containing anions. $^{1}H$ and $^{31}P$ NMR spectroscopy as well as DFT calculations confirmed that PPi bound to $Zn_2L2$ in a 2 : 2 manner. The detection limit of PPi for the reported IDA system was 0.3 μM.

The mononuclear complexes with tripodal amine based IDA receptors (ML3), where M = $Cu^{2+}$ and $Zn^{2+}$, for anions were investigated for colorimetric histidine (His) sensor under displacement assay using PAR as an indicator. [CuL3·PAR] can detect histidine selectively while [ ZnL3·PAR] can be interfered by phosphate containing anions. Furthermore, [CuL3·PAR] can be used to detect His in real urine samples with limit of detection of 0.5 μM.

| | | | |
|---|---|---|---|
| Department: | Chemistry | Student's Signature | ..... |
| Field of Study: | Chemistry | Advisor's Signature | ..... |
| Academic Year: | 2015 | Co-Advisor's Signature | ..... |

## ACKNOWLEDGEMENTS

I would like to express my sincere gratitude and deep appreciation to my advisor, Prof. Dr. Thawatchai Tuntulani for his valuable guidance, advice and encouragement throughout this study. I wish to thanks Asst. Prof. Dr. Chomchai Suksai my co-advisor for her comments and suggestions. I am also grateful to Asst. Prof. Dr. Jaray Jaratjaroonphong, the principal examiner, for his advice and criticism. Prof. Orawon Chailapakul and Asst. Prof. Soamwadee Chaianansutcharit for valuable suggestions and comments as committee member and thesis examiner. I am also grateful to thank Assist. Prof. Dr. Chaveng Pakawatchai for X-ray crystallography experiments and many useful suggestions.

Financial support from the Royal Golden Jubilee Ph.D. Program and the Thailand Research Fund RTA5380003 are also gratefully acknowledged.

I would like to express my deepest gratitude to my parents and family for their love, kindness, encouragement, and financial support throughout my life. Finally, I would like to thank Chulalongkorn University and Burapha University for financial support.

Sarayut Watchasit

จุฬาลงกรณ์มหาวิทยาลัย
Chulalongkorn University

**CONTENTS**

Page

THAI ABSTRACT ..... iv

ENGLISH ABSTRACT ..... v

ACKNOWLEDGEMENTS ..... vi

CONTENTS ..... vii

LIST OF FIGURES ..... xi

LIST OF TABLES ..... 1

LIST OF SCHEMES ..... 1

CHAPTER I INTRODUCTION ..... 1

1.1 Statements and significance of the problems ..... 1

CHAPTER II THEORETICALS AND LITERATURE REVIEWS ..... 5

2.1 Concept of supramolecular chemistry ..... 5

2.2 Molecular recognitions to chemical receptors and chemical sensors ..... 6

2.3 Chemosensing ensembles ..... 7

2.3.1 Metal complexing indicator–displacement assays (M-IDA): Anion sensing strategy ..... 8

CHAPTER III EXPERIMENTS ..... 15

3.1 Instruments ..... 15

3.2 Chemical reagents ..... 15

3.3 Synthesis and characterization of ligands L2 and L3 ..... 16

3.3.1 Preparation of (E)-1-(pyridin-2-yl)-N-(pyridin-2-ylmethylene) methanamine (a) ..... 16

3.3.2 Preparation of bis-pyridin-2-ylmethylamine (b) ..... 17

3.3.3 Preparation of 2-[bis(2-pyridylmethyl)aminomethyl]nitrobenzene (c) ..... 18

จุฬาลงกรณ์มหาวิทยาลัย
CHULALONGKORN UNIVERSITY

Page

3.3.4 Preparation of 2-[bis(2-pyridylmethyl)aminomethyl]aniline (d) ..... 19

3.3.5 Preparation of 9,10-bis(chloromethyl)anthracene (e) ..... 20

3.3.6 Preparation of anthracene-9,10-dicarboxaldehyde (f) ..... 21

3.3.7 Preparation of (*N*,*N*'*E*,*N*,*N*'*E*)-*N*,*N*'-(anthracene-9,10-diylbis(methan-1-yl-1-ylidene))bis(2-((bis(pyridin-2-ylmethyl)amino)methyl)aniline) (h) ..... 22

3.3.8 Preparation of ligand L2 ..... 23

3.3.9 Preparation of (*E*)-*N*-(anthracen-9-ylmethylene)-2-((bis(pyridin-2-ylmethyl)amino)methyl)aniline (g) ..... 24

3.3.10 Preparation of ligand L3 ..... 25

3.4 Synthesis and characterization of metal complexes of Cu(II) and Zn(II) with ligand L2 and L3 ..... 26

3.4.1 Preparation of dinuclear complex $Cu_2L2$ ..... 26

3.4.2 Preparation of dinuclear complex $Zn_2L2$ ..... 27

3.4.3 Preparation of mononuclear complex CuL3 ..... 28

3.4.4 Preparation of mononuclear complex ZnL3 ..... 29

3.5 Screening tests for selective sensing of anions and **α**-amino acids sensing ..... 30

3.5.1 Screening tests of indicators for selective PPi sensing ..... 30

3.5.2 Screening tests of indicators for selective histidine sensing ..... 30

3.6 UV-vis titrations under indicator displacement assay ..... 30

3.6.1 UV-vis titrations under indicator displacement assay for PPi detection ..... 30

3.6.2 UV-vis titrations under indicator displacement assay for histidine detection ..... 31

3.7 NMR titration experiments ..... 31

3.8 Tolerances limit study by UV-Visible spectrophotometry ..... 32

จุฬาลงกรณ์มหาวิทยาลัย
Chulalongkorn University

Page

3.9 Urine samples preparation for histidine detection under indicator displacement assay ..... 32

CHAPTER IV RESULTS AND DISCUSSION ..... 33

4.1 Synthesis and characterization of ligands L2 and L3 ..... 33

4.1.1 Synthesis and characterization of L2 ..... 33

4.1.2 Synthesis and characterization of ligand L3 ..... 35

4.2 Synthesis and characterization of dinuclear complexes $Cu_2L2$ and $Zn_2L2$ and mononuclear complexes CuL3 and ZnL3 ..... 37

4.2.1 Synthesis and characterization of $Cu_2L2$ ..... 37

4.2.2 Synthesis and characterization of $Zn_2L2$ ..... 38

4.2.3 Synthesis and characterization of CuL3 ..... 40

4.2.4 Synthesis and characterization of ZnL3 ..... 41

4.3 Sensing of PPi under an indicator displacement assay ..... 43

4.3.1 Screening tests of indicators for selective PPi sensing ..... 43

4.3.2 Binding studies of $Zn_2L2$ with PPi by $^{1}H$ and $^{31}P$ NMR spectroscopy ..... 45

4.3.3 Binding studies of dinuclear complex $Zn_2L2$ with MTB and displacement studies with PPi using $^{1}H$ NMR spectroscopy ..... 49

4.3.4 Studies of $Zn_2L2$–indicator ensembles by UV-vis spectrophotometry ..... 51

4.3.5 PPi sensing studies by UV-vis spectrophotometry ..... 54

4.3.6. Studies of interferences and limit of detection ..... 56

4.4 Sensing of histidine under an indicator displacement assay ..... 57

4.4.1 Sensing abilities studies of Zn2L2 based ensemble towards α-amino acids 57

จุฬาลงกรณ์มหาวิทยาลัย
Chulalongkorn University

Page

4.4.2 Sensing abilities studies of ZnL3 based ensemble towards α-amino acids 60

4.4.3 DFT Calculations of the adduct structure between ZnL3 and His ..... 63

4.4.4 His sensing studies by [ZnL3•PAR] ensemble in biological samples ..... 64

4.4.5 Sensing abilities studies of CuL3 based ensemble towards α-amino acids 65

4.4.6 Analytical Performance for His detection..... 69

CHAPTER V CONCLUSIONS..... 73

Suggestions for future works..... 74

REFERENCES..... 75

VITA..... 127

จุฬาลงกรณ์มหาวิทยาลัย
Chulalongkorn University

# LIST OF FIGURES

**Figure 1.** Dyes employed in displacement assays for the chromogenic and fluorogenic sensing of anions and amino acids. ..... 3

**Figure 2**. The structures of the proposed complex receptors employed in this work. ..... 4

**Figure 3**. The complementary shape and size of the host and guest as they interact non-covalently ..... 6

**Figure 4.** Schematic representation of chemical sensor process. ..... 7

**Figure 5.** Sensing mechanism of indicator displacement assay (IDA) ..... 8

**Figure 6**. The structures of organic compound receptor having three guinidium groups and carboxy fluorescein indicator and citrate anion ..... 10

**Figure 7**. The structures of dicopper (II) complex **1** and coumarin indicator **2**. ..... 11

**Figure 8**. The structures of dicopper (II) complex **3** and indicators **4** and **5** ..... 12

**Figure 9**. The structures of dinuclear zinc(II) complex **6** and chromogenic indicator **7** ..... 12

**Figure 10**. The structures of dinuclear zinc(II) complexes **8** and **10** and fluorescence indicator **9** ..... 13

**Figure 11**. $^{1}$H NMR spectrum of ligand **L2** in $CDCl_3$ ..... 34

**Figure 12**. Mass spectrum of ligand **L2** ..... 34

**Figure 13**. $^{1}$H NMR spectrum of ligand **L3** in $CDCl_3$ ..... 36

**Figure 14**. Mass spectrum of ligand **L3** ..... 36

**Figure 15**. ORTEP plot of ligand **L3** ..... 37

**Figure 16**. Mass spectrum of dinuclear complex **$Cu_2$L2** ..... 38

**Figure 17**. $^{1}$H NMR spectrum of complex **$Zn_2$L2** in 20% $D_2O/CD_3CN$ ..... 39

**Figure 18**. Mass spectrum of complex **$Zn_2$L2** ..... 39

จุฬาลงกรณ์มหาวิทยาลัย
CHULALONGKORN UNIVERSITY

**Figure 19**. Mass spectrum of mononuclear complex **CuL3**..... 40

**Figure 20**. ORTEP plot of mononuclear complex **CuL3** ..... 41

**Figure 21**. Comparison of $^{1}$H NMR spectra of ligand **L3** and mononuclear complex **ZnL3** in $CDCl_3$ ..... 42

**Figure 22**. Mass spectrum of mononuclear complex **ZnL3** ..... 42

**Figure 23**. Structures of indicators employed in **PPi** sensing under the IDA studies... 43

**Figure 24**. Color changes of the **$Zn_2$L2**-based (20 μM, 2 mL) ensembles (Ens) with various indicators (Dye) (400 μM, 0.2 mL) at a 1:2 receptor to indicator ratio (a) **PV**, (b) **BPG**, (c) **MTB** and (d) **XO** in the presence of various anions (1 mM, 0.3 mL) in 80/20 (%v/v) acetonitrile/aqueous solution buffered at pH 7.4 with HEPES. ..... 44

**Figure 25**. (a) structure of dinuclear complex **$Zn_2$L2** (b) $^{1}$H NMR spectra of (I) free **$Zn_2$L2**, (II) **$Zn_2$L2** + **PPi** 0.5 equiv., (III) **$Zn_2$L2** + **PPi** 1.0 equiv., (IV) **$Zn_2$L2** + **PPi** 1.5 equiv., (V) **$Zn_2$L2** + **PPi** 2.0 equiv. And (VI) **$Zn_2$L2** + **PPi** 2.5 equiv. in 20% $D_2O/CD_3CN$. ..... 46

**Figure 26**. $^{31}$P NMR spectra of **$Zn_2$L2** (5 mM) upon addition of various concentrations of **PPi** (0.05 M) in 80/20 (%v/v) $CD_3CN/D_2O$..... 47

**Figure 27**. The most stable DFT-calculated structure of the dimeric 2:2 species, 2**$Zn_2$L2**·2**PPi** complex..... 49

**Figure 28.** $^{1}$H NMR titration spectra of (I) free **$Zn_2$L2** (5 mM), (II) **MTB**, (III) **$Zn_2$L2·MTB**, (IV) **$Zn_2$L2**·2**MTB**, (V) **$Zn_2$L2·MTB** + 2.0 equiv. of **PPi** and (VI) **$Zn_2$L2**·2**MTB** + 2.0 equiv. of **PPi** in 80/20 (%v/v) $CD_3CN$ /$D_2O$, where * is the residue of free **MTB** present in the ensemble. ..... 50

**Figure 29.** (a) UV-vis spectra obtained by the addition of **$Zn_2$L2** (400 μM) to a solution of **MTB** (20 μM), inset: Job's plot analysis of the **MTB**-based ensemble and (b) color changes upon increasing the amount of **$Zn_2$L2** (400 μM) to the **MTB** (20 μM) solution: (i) free **MTB**, (ii) 0.1 equiv., (iii)

0.2 equiv., (iv) 0.3 equiv., (v) 0.4 equiv., (vi) 0.5 equiv., (vii) 0.6 equiv., (viii) 0.7 equiv., (ix) 0.8 equiv., (x) 0.9 equiv. and (xi) 1.0 equiv. ..... 52

**Figure 30**. Concentration profiles of the species present at equilibrium in the UV-vis titration of **MTB**-base ensemble, where % is referred to the total concentration of **MTB**. ..... 53

**Figure 31**. (a) UV-vis spectra obtained for the addition of **PPi** (1 mM) to a 1:2 ensemble solution of **$Zn_2$L2** and **MTB** (20 μM) and (b) concentration profiles of the species present at equilibrium in the UV-vis titration of **PPi** displaced [**$Zn_2$L2·MTB**] ensemble. ..... 56

**Figure 32**. (a) Sensing of **PPi** in the presence of competitive anions (7.5 equivalents) in 80/20 (%v/v) acetonitrile/aqueous solution buffered at pH 7.4 with 10 mM HEPES (b) Calibration curve for detection of **PPi** using [**MTB·$Zn_2$L2]** ensemble. ..... 57

**Figure 33**. Color changes of (a) **[$Zn_2$L2·PAR]** and (b) **[$Zn_2$L2·MTB]** ensembles (20 μM) in the presence of various amino acids (1 mM) in 80/20 (%v/v) $CH_3CN/H_2O$ buffered at pH 7.4 with HEPES. ..... 58

**Figure 34**. (a) UV/vis titration spectra obtained by addition of **$Zn_2$L2** (400 μM) to a solution of **PAR** (20 μM) (b) concentration profiles of the species present at equilibrium in the UV-vis titration of **[$Zn_2$L2·PAR]** base ensemble, where % is referred to the total concentration of **PAR** (c) Job's plot analysis in HEPES buffered pH 7.4 in 80/20 (% v/v) acetonitrile/aqueous solution and (d) A plot of absorption against concentration of **$Zn_2$L2** titrated in **PAR**. The red solid line is nonlinear least-squares fittings of the titration profiles using SPECFIT32 program.... 60

**Figure 35.** (a) UV/vis spectra obtained by addition of **ZnL3** (400 μM) to a solution of **PAR** (20 μM) in HEPES buffered pH 7.4 in 80/20 (% v/v) acetonitrile/aqueous solution (b) a plot of absorption against concentration of **ZnL3** titrated in **PAR**. The red solid line is nonlinear least-squares fittings of the titration profiles using SPECFIT32 program

and (c) color changes of **[ZnL3·PAR]** ensemble (20 μM) in the present of various amino acids (12.5 equiv.). ..... 61

**Figure 36**. $^{1}$H NMR spectra of **ZnL3** (5 mM) upon addition of various concentrations of **His** (0.05 M) in 50% (v/v) $D_2O/CD_3CN$; (i) free **ZnL3**, (ii) **ZnL3** + **His** 0.2 equiv., (iii) **ZnL3** + His 0.4 equiv., (iv) **ZnL3** + **His** 0.6 equiv., (v) **ZnL3** + **His** 0.8 equiv. and (vi) **ZnL3** + **His** 1.0 equiv. ..... 63

**Figure 37.** The most stable DFT-calculated structure of complex of [**ZnL3•His**]..... 64

**Figure 38**. Color changes of [**ZnL3•PAR**] ensemble (20 μM) in the present of various anions in 10 mM HEPES buffered pH 7.4 in 80/20 (% v/v) acetonitrile/ aqueous solution. ..... 65

**Figure 39**. (a) color changes of **[CuL3·PAR]** ensemble (20 μM) in the present of various amino acids (12 equiv.) (b) color changes of [**CuL3·PAR]** ensemble (20 μM) in the presence of various anions (12 equiv.) and (c) UV–vis spectra obtained by addition of various amino acids (7.5 equiv) to [**CuL3•PAR**] (20 μM) ensemble in 10 mM HEPES buffered pH 7.4 in 80/20 (% v/v) acetonitrile/aqueous solution. ..... 67

**Figure 40**. Square wave voltammograms of $Cu^{2+}$ and **CuL3** in the presence of **His** 3 equivalents scan rate 100 mV/s. ..... 68

**Figure 41**. UV-Visible spectra obtained by addition of **His** (1 mM) to an ensemble solution of [**CuL3•PAR**] ensemble (20 μM), in HEPES buffered pH 7.4 in 80/20 (% v/v) acetonitrile/aqueous solution. ..... 69

**Figure 42**. Absorption response of [**CuL3•PAR**] ensemble 20 μM to various amino acids in HEPES buffered pH 7.4 in 80/20 (% v/v) acetonitrile/aqueous solution. The blue bars represent the absorption of [**CuL3•PAR**] in the presence of amino acids 12.5 equivalents. The red bars represent the change of the absorption that occurs upon the subsequent addition of **His** to the various amino acids to the solution of [**CuL3•PAR**]. The intensities were recorded at 512 nm. ..... 70

จุฬาลงกรณ์มหาวิทยาลัย
Chulalongkorn University

**Figure 43**. Calibration curve for detection of **His** using [**CuL3•PAR**] ensemble. ..... 71

**Figure 44**. Structures of dinuclear complexes **$Cu_2$L2** and **$Zn_2$L2** and mononuclear complexes **CuL3** and **ZnL3**. ..... 73



จุฬาลงกรณ์มหาวิทยาลัย
Chulalongkorn University

# LIST OF TABLES

**Table 1**. Stepwise ensemble formation constants (log $\beta$) between **$Zn_2L2$** and the indicators ..... 54

**Table 2**. Analytical results for **His** in human urine samples..... 72

# LIST OF SCHEMES

**Scheme 1**. The synthetic pathway for ligand **L2** ..... 33

**Scheme 2.** The synthetic pathway for ligand **L3** ..... 35

# CHAPTER I

# INTRODUCTION

## 1.1 Statements and significance of the problems

The multifaceted role of anions and α-amino acids in biology and the environment has led researchers to develop various means of detecting these species. Anions play fundamental roles in many phenomena, including biological processes such as the transport hormones, proteins biosynthesis, DNA regulation, and the activity of enzymes[1]. Amino acids are very important markers in biochemistry and molecular biology, which require high resolution techniques for determinations[2]. Therefore, the important roles of those anions and amino acids have inspired chemists to devote significant efforts toward the design of practical chemosensors for the detection of various anions and amino acids in both qualitative and quantitative manners.

Among essential amino acids, histidine (**His**) has been recognized as being extremely important for human growth as well as acting as a neurotransmitter in the central nervous system of mammals[2]. Histidine-rich proteins are found to play many important roles in humans and their abnormal level could indicate a variety of diseases[3]. The deficiency of **His** is involved in many syndromes, for instances epilepsy, Parkinson's disease[4], and nerve deafness[5]. However, high levels of His in physiological fluids could induce metabolic disorders such as histidinemia[6].

Not only amino acids can act as biomarker for diseases but also anions have attracted chemists attention due to their importance in living systems[1]. Great attention has been given to the design of chemical sensors for the pyrophosphate anion, $P_2O_7^{4-}$ or **PPi**[7-9]. Such an interest stems from the fact that **PPi** plays an important role in many biological processes. In particular, **PPi** participates in ATP hydrolysis and is involved in DNA or RNA polymerase reactions[10-12]. Moreover, the amount of **PPi** has recently been monitored in patients with calcium pyrophosphate dihydrate (CCPD) crystal deposition disease (also known as chondrocalcinosis), as the disease has been shown to cause high synovial fluid **PPi** levels in patients.

Therefore, detection of **His** and **PPi** in biological fluids has become an important goal and several conventional sophisticated techniques, like high performance liquid chromatography (HPLC)[13], capillary electrophoresis (CE)[14, 15] and voltammetry[16-19] have been employed to detect amino acids but have shown limitation in operational convenience, skilled personnel and analysis cost. However, the optical detection based on specially designed small synthetic organic molecular scaffolds-chemosensors are becoming more attractive and reliable due to their simplicity and sensitivity. Therefore, the interest in developing optical chemosensors based on specially designed small synthetic organic molecular specifically recognizing a target amino acid has grown steadily[20-27].

Thus far, most of anion and amino acid chemosensors have been synthesized by attaching a dye, usually a colorimetric and fluorescence dye, to an anion-binding site giving a convenient visual “by eye” detection provided by colorimetric assays and highly sensitive fluorescence spectroscopy[28]. However, this mechanism does not always work well. Recently, indicator displacement assays (IDA) employing fluorescence and chromogenic indicators are becoming an increasingly popular method of detecting various analytes[29, 30]. The dyes used in the development of IDA are depicted in Figure 1. Many physiologically and environmentally important targets, such as phosphate[31, 32], pyrophosphate[33-38], citrate[39, 40], carbonate[41], amino acids[42-46], and biological molecules[47-51], can now be detected and quantified through indicator displacement assays. This approach is somehow employed in displacement reactions in immunoassay protocols[52].

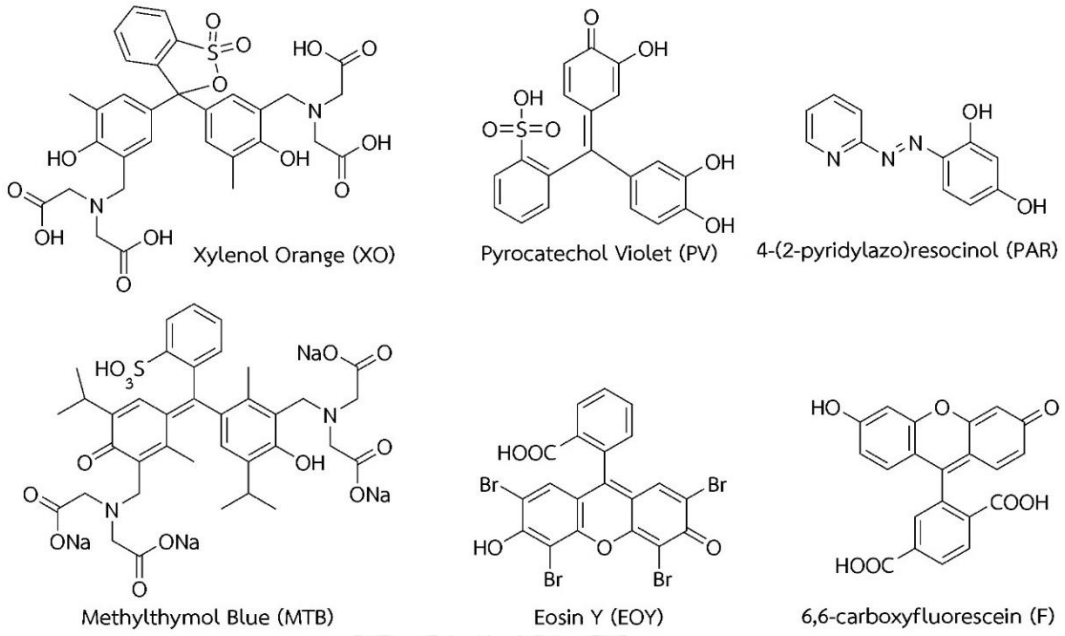


**Figure 1.** Dyes employed in displacement assays for the chromogenic and fluorogenic sensing of anions and amino acids.

Traditionally, the selected receptor (usually a metallic complex) forms an inclusion complex with a dye. Upon addition of the target anion, the receptor binds to the anion and releases the dye to the solution. Perhaps the most interesting feature of this approach is that the non-covalent anchoring of binding sites and indicator groups allows testing a large number of combinations in order to obtain tuned sensing systems. Additionally, most of the designed ensembles usually display sensing features in water or mixed organic–aqueous solutions allowing the design of realistic sensing protocols. For sensing anions and amino acids, the metal complexing IDA (M-IDA) are usually favorable since the pioneering work of Fabbrizzi[41] and Anslyn[42]. The advantages of an M-IDA are that it can operate in highly polar and solvating solvents (aqueous ethanol or pure water), and displays strong affinity toward anionic substrates[53].

In previous studies[38], I found that a dinuclear $Cu^{2+}$ complex of a calix[4]arene derivative containing tripodal amine units, **$Cu_2$L1**, could successfully be an IDA receptor

for pyrophosphate anion (**PPi**) in aqueous acetronitrile buffer at pH 7.4 using pyrocatechol violet (**PV**) as colorimetric indicator. Bearing these result in mind, I expect that dinuclear complexes could have sensing potentials toward **PPi** with respect to other phosphate containing anions using IDA strategy by changing the ligand structures, metal center type and reporting indicators[38]. In my continuing endeavor to develop assays for detecting anions and α-amino acids, I decided to investigate whether my two IDA complexes, **$Cu_2$L2** and **$Zn_2$L2**, would be suitable for achieving the required selectivity for other anions and α-amino acids. Moreover, we study the IDA approach of mononuclear complexes, **CuL3** and **ZnL3,** in order to compare results with those of **$Cu_2$L2** and **$Zn_2$L2**. The sensing abilities could be tuned by the topological difference of the complexes and indicators employed. The structures of complex receptors employed in this work are presented in Figure 2.

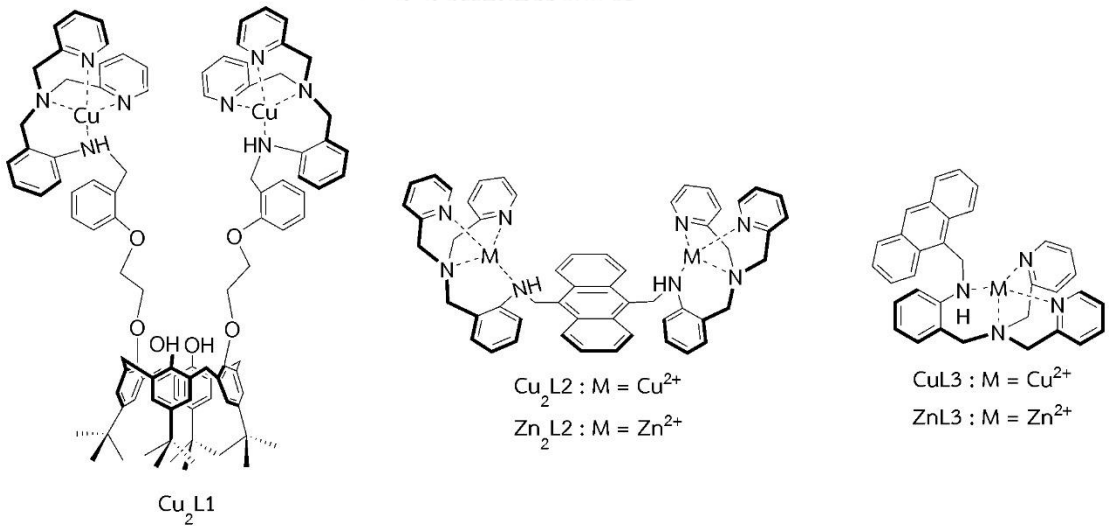


**Figure 2**. The structures of the proposed complex receptors employed in this work.

# CHAPTER II
# THEORETICALS AND LITERATURE REVIEWS

## 2.1 Concept of supramolecular chemistry

Supramolecular chemistry is a young discipline dating back to the late 1960s and early 1970s. Jean-Marie Lehn, who won the noble prize in 1987, has defined the term of *"supramolecular chemistry"* as "the chemistry of molecular assemblies and of the intermolecular bonds"[54]. However, many attempts have tried to mention supramolecular chemistry as "chemistry beyond the molecule" or "the chemistry of the noncovalent bond" as well as "nonmolecular chemistry".

Non-covalent interactions for examples electrostatic interactions, hydrogen bonding and metal-ligand coordination have a profound importance in chemistry and biochemistry. Where these interactions occur with strength and selectivity, molecular recognition may occur allowing highly complex systems consisting of discrete molecules to form and operate. Furthermore, non-covalent interactions may be used to control and accelerate the formation and breaking of covalent bonds[54].

In supramolecular chemistry, the interaction between two or more molecules in a unique structural arrangement is known as host-guest chemistry. A host molecule is one that contains a cavity or a hole within the molecule. This cavity must be complementary to its guest, with can be fit inside the cavity. Typically, the host is a larger molecule with a pocket or cavity possessing convergent binding sites for selectivity of a specific guest[54]. The guest molecule possesses divergent binding sites and can vary in size from a single atom to a complex biological assembly as shown in Figure 3. An advanced and challenging target in host-guest chemistry is the construction of a host molecule having the ability of specific recognition with a guest molecule.

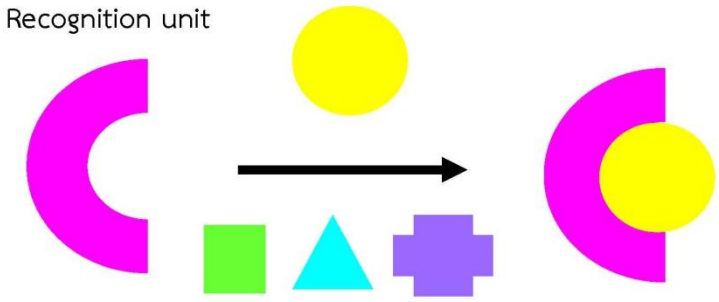


**Figure 3**. The complementary shape and size of the host and guest as they interact non-covalently

Ideally, construction of supramolecular chemistry host-guest complexes concern the stability of complex which is being formed. In addition, in the complicated system not only the interactions between host and guest are considered but also many molecular recognition events, involving the making and breaking of many interactions between host-guest and the solvent, and within the solvent itself and effect to conformational changes should not be forgotten. Consequently, the synthesis of successful artificial host-guest systems is still a challenge.

## 2.2 Molecular recognitions to chemical receptors and chemical sensors

One of the current challenges in the area of supramolecular chemistry involves the development of chemical receptors and chemical sensors with high selectivity for specifically targeted guest molecules. The system could have an important role to play in a variety of applications, including sensing[55], analysis[56], waste remediation[57], and drug development[58]. Chemical sensors are usually understood to be devices that transform chemical information into analytically useful signals[59]. The basic design principle of a chemosensor is that the sensing event has to be related to an easy-to-measure signal. Nowadays, many chemosensors display changes in color[60], fluorescence[61] and electrochemical properties[62] in the presence of a certain guest molecule. Especially, the design of optical chemosensors has continuously evolved. In the first approach explored, the sensors feature the receptor

unit as part of the chromophore/fluorophore. In these systems, which have been named *intrinsic chemosensors*, the interaction between the bound substrate and the dye (chromophore or fluorophore) leads directly to the modification of its emission properties, as shown in Figure 4.

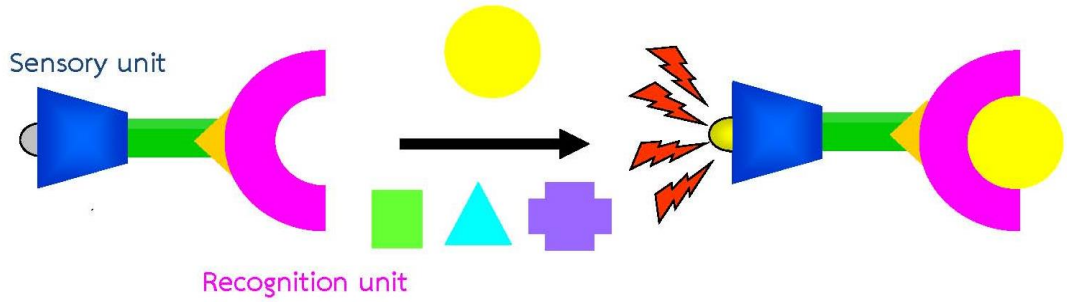


**Figure 4.** Schematic representation of chemical sensor process.

## 2.3 Chemosensing ensembles

These self-assembled chemosensors are made by mixing a dye, a substrate, and a receptor which is able to interact with both chemical species, but with different binding strength. Following the design principle, these systems have been named *chemosensing ensembles*. The chemosensing ensemble strategy is based on a competition assay in which the dye and the substrate compete for the receptor[29]. The displacement of the dye from the complex results in a change of its optical properties. The supramolecular version of this assay uses a recognition unit, designed for selective interaction with a desired analyte, along with an external indicator (a UV-visible chromophore or a fluorescence dye) that associates with the recognition unit in the absence of the analyte. This method is also referred to as *indicator displacement assay* (IDA)[30]. The IDA sensing mechanism is shown in Figure 5.

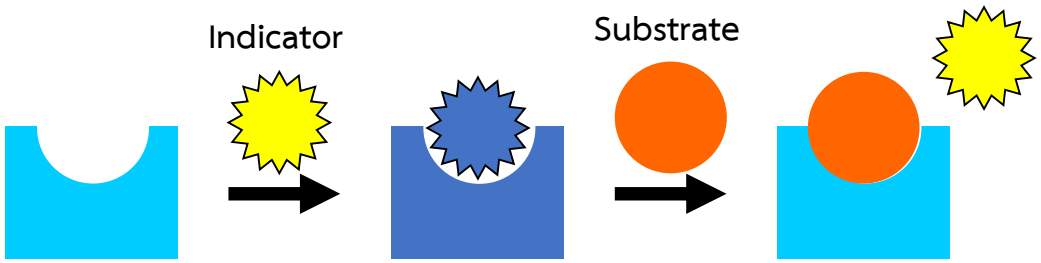


**Figure 5.** Sensing mechanism of indicator displacement assay (IDA)

The IDA offers many advantages over traditional sensing assays. First, the method does not require the indicator to be covalently attached to the receptor. Second, since there are no covalent bonds between the receptor and the indicator, one can employ several different indicators with the same receptor. Third, the assay works well in both organic and aqueous media, and lastly, the assay is easily adapted to different receptors and platforms for quick analysis. Nguyen et al.[30] have classified three types of IDAs as follow. First, the colorimetric IDA (C-IDA) which employs colorimetric indicators. The second class is the fluorescent IDA (F-IDA) which uses fluorescent indicators, and the third class is the metal complexing *IDA* (M-IDA) that utilizes a metal center with either a colorimetric or fluorescent indicator. Therefore, a M-IDA is a subset of both a C-IDA and a F-IDA.

จุฬาลงกรณ์มหาวิทยาลัย
CHULALONGKORN UNIVERSITY

### 2.3.1 Metal complexing indicator–displacement assays (M-IDA): Anion sensing strategy

Anions play fundamental roles in many phenomena, including biological processes such as the transport of hormones, proteins biosynthesis, DNA regulation, and the activity of enzymes. The important roles of anions have inspired chemists to design of practical chemosensors for the detection of anions, both qualitatively and quantitatively. It has long been known that the coordination chemistry of anion recognition has some specific characters that need to be speculated[63]. Therefore, when constructing the receptor for a certain anion, the geometry and shape of the

anion to recognize its charge, which can be varied as a function of the hydrophobicity and its pH should be taken into account[64].

Normally, it can be said that the anions receptors use similar type of interactions as biological receptors. Those can be basically classified into hydrogen bond formation, interactions with metal centers and electrostatic interactions. Electrostatic interactions with anions are found using positively charged receptors having for instance guanidinium groups[65], quaternary ammoniums[66] and isothiouranium and protonated amines[67]. Hydrogen-bonding interactions have been widely for anion recognition, for example amides[68]), ureas and thioureas[69], calix[4]pyrroles[70] and porphyrins[71].

Not only organic compounds have been exploited as anion receptors, but also metal complexes have also been used as anion binding sites[53]. Metal complexes can bind anions, forming stronger bonds than those generally observed using electrostatic or hydrogen-bonding interactions. Especially, metal complexes with open coordination sites, unsaturated complexes, have found wide use in molecular recognition. The metal ion should be coordinated in a thermodynamically and kinetically stable fashion. Coordination to metal ions occurs typically with a single coordinated bond from a guest to a metal complex host may provide sufficient binding energy to result in stable and defined aggregates at micromolar concentrations in water. However, not all coordinatively unsaturated metal complexes are suitable binding sites for molecular recognition of guest molecules. The coordinative bond between the metal complex and the bound guest should be strong but not too tight. Importantly, a reversibly bound Lewis basic guest should not displace the metal ion from the ligand. Therefore, multidentate ligands have been used as ligands for metal complex host molecules[72].

As I mentioned before, in M-IDA strategy an indicator (chromophore or fluorophore) is allowed to coordinate with both the metal center and the receptor. Addition of an analyte to the system causes the displacement of the indicator from the metal and the receptor. This results in optical changes that can be measured to derive binding affinity. The advantages of a M-IDA are that it can operate in highly polar

and solvating solvents (aqueous ethanol or pure water), and displays strong affinity toward anionic substrates.

The first pioneered in IDA is Professor Anslyn. He discovered the organic compound receptor having three guinidium groups can use as receptor for citrate anion under IDA approach by using 5-carboxy fluorescein as reporting indicator and they applied this system for determination of citrate in beverages[73], as shown in Figure 6.

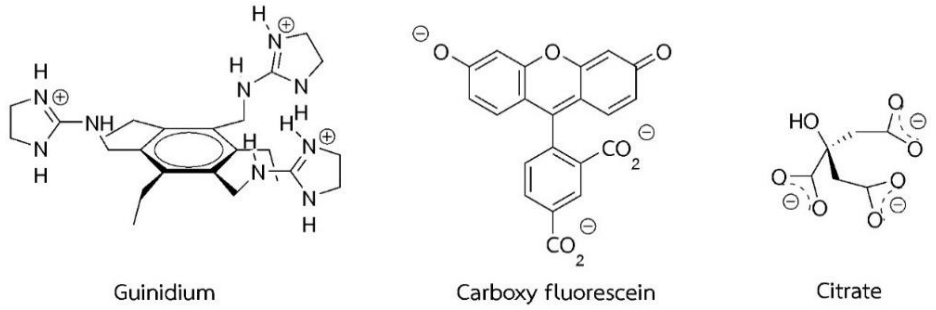


**Figure 6**. The structures of organic compound receptor having three guinidium groups and carboxy fluorescein indicator and citrate anion

Another one of the pioneers of this method is the Fabbrizzi group[74]. They have shown that the ensemble system between dicopper (II) complex **1** and fluorescence coumarin **2** indicator, as shown in Figure 7, possessed the high selectivity to carbonate anion in aqueous solution. The carboxylate group of coumarin is capable of bridging the two copper centers of **1**. This coordination quenches the fluorescence of coumarin **2**. Addition of carbonate anion to the ensemble solution regenerated the fluorescence due to the displacement of **2** from **1** by carbonate anion.

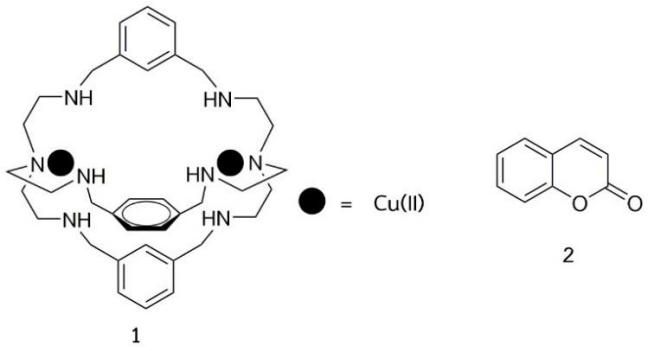


**Figure 7**. The structures of dicopper (II) complex **1** and coumarin indicator **2**.

The same strategy was used by Fabbrizzi in the detection of pyrophosphate (PPi)[33] and histidine in water[43]. Pyrophosphate anions play important roles in bioenergetic and metabolic processes[65, 66]. Receptor **3** was designed to incorporate two copper ions to gain affinity for the analytes. Eosine Y **4** was one of the indicators used in this study. Results from these studies showed that **3** could bind to pyrophosphate better than monophosphate due to the ability of pyrophosphate to coordinate the two copper centers. The same sensing ensemble [**3•4**] was also able to discriminate histidine from glycine, phenyl alanine, valine, leucine, and proline. This is because histidine possesses an imidazole residue which coordinates to dicopper centers, resulting in higher selectivity.

Moreover, Hu and Feng[75] has shown that the ensemble system between dinuclear Cu(II) complex **3** with fluorescence Eosin Y **4** and fluorescein **5** indicator possess the high selectivity to oxalate anion in aqueous solution, as shown in Figure 8. The result showed that, receptor **3** possessed higher binding affinity for **4** over **5.** Noticeably **4** based ensemble can discriminate oxalate from malonate, which is often found as a strong competitor in oxalate sensing. The detection limit of **4** based ensemble for oxalate is calculated to be 0.079 mM.

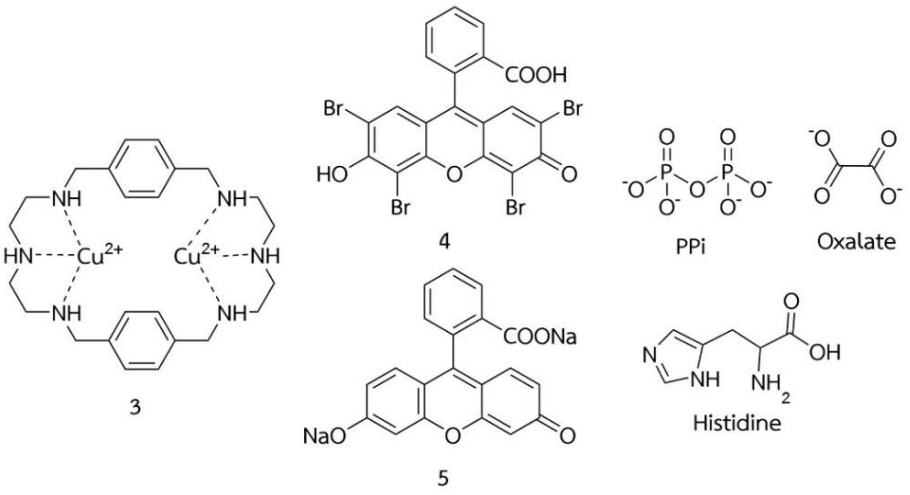


**Figure 8**. The structures of dicopper (II) complex **3** and indicators **4** and **5**

Interestingly, the dinuclear zinc phosphoesterase enzyme models have been exploited as M-IDA receptors. Kim and Han[31] have used an ensemble of $Zn^{2+}$-dipicolylamine complex **6** and pyrocatechol violet or PV **7** as anion sensor to detect both phosphate (**Pi**) and **PPi** at pH 7.4 in 10 mM HEPES buffer, as shown in Figure 9. It was found that the Zn–Zn distance in complex **6** is 3.0 Å which is less than that in phosphotriesterase (3.5 Å). This may be the reason why **6** can bind both Pi and **PPi**. Therefore, the Zn–Zn distance played a key role in analyte preference.

จุฬาลงกรณ์มหาวิทยาลัย
CHULALONGKORN UNIVERSITY

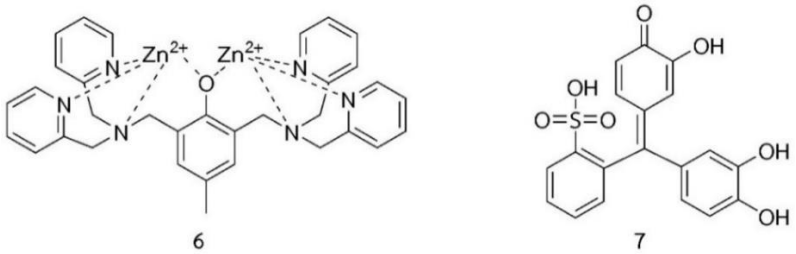


**Figure 9**. The structures of dinuclear zinc(II) complex **6** and chromogenic indicator **7**

Anion binding capabilities of a diketopiperazine-based receptor **8** bearing two $Zn^{2+}$ dipicolylamino binding sites were studied by using IDA strategy with a fluorescent coumarin derivative **9**[68]. Receptor **8** was able to quench the fluorescence emission of **9** at 37°C in water (HEPES, pH 7.4 and NaCl to mimic physiological pH and ionic strength) as shown in Figure 10. The titration profiles indicated the formation of a 1:1 complex between **8** and **9**. An equimolar solution of **[8•9]** was then titrated with aliquots of the anions $NO_3^-$, $SO_4^{2-}$, $Br^-$, $I^-$, $AcO^-$, (+)-tartrate, citrate, $HPO_4^{2-}$, **PPi**, phosphotyrosine, phosphothreonine, **AMP**, cAMP, **ADP**, **ATP** and GTP. Selective fluorescence enhancement for di- and triphosphate oxoanions over all other anions was observed in the order: **PPi** > **ATP** ≈ GTP > **ADP**. These results are not as selective as the results obtained in a previous study using receptor **10** which better matches **PPi** due to the larger distance between the two $Zn^{2+}$ metal centers. The work points towards the importance of the correct scaffold choice in the design of receptors for phosphate oxo anions.

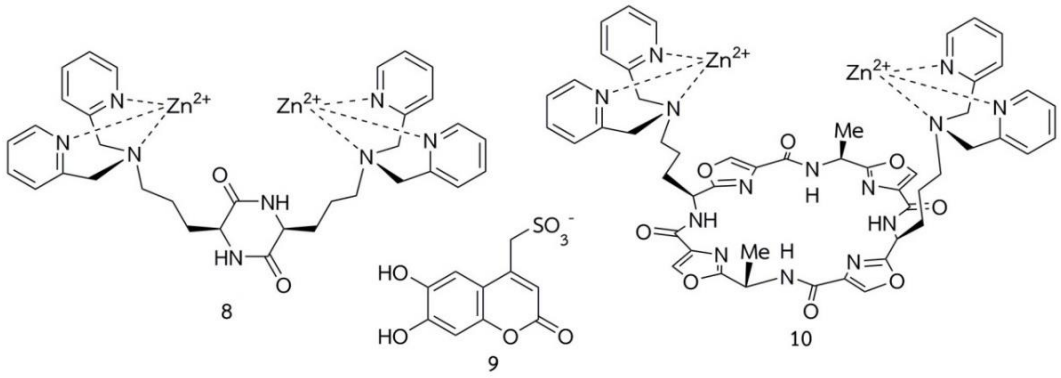


**Figure 10**. The structures of dinuclear zinc(II) complexes **8** and **10** and fluorescence indicator **9**

Watchasit and co-workers have synthesized dinuclear Cu(II) complex of *p-tert*-butylcalix[4]arene containing two tripodal amine units (**$Cu_2$L1**) and the complex has been exploited as **PPi** sensor by the IDA approach[38]. It was found that the new

ensemble between (**$Cu_2$L1**) and **PV 7** showed the high selectivity to **PPi** than other anions in 80/20 (%v/v) $CH_3CN/H_2O$ solution buffered with 10 mM HEPES at pH 6.4. The sensing selectivity is ascribed to the tuning of the distance between donor atoms of anion guests and their ability to encompass the $Cu^{2+}$-$Cu^{2+}$ distance within the cleft of (**$Cu_2$L1**). In addition, the preorganization of calix[4]arene in the cone conformation and steric hindrance of two bulky tripodal amine moieties are important factors to control the $Cu^{2+}$-$Cu^{2+}$ distance. Thus far, the remaining weak point of **PPi** detections using IDA approach is that the method cannot discriminate **PPi** from other phosphate containing anions effectively.

Therefore, the objectives of this research were,

1. To synthesize the new anthracene containing tripodal amine ligands **L2** and **L3** and their complexes with Cu(II) and Zn(II).
2. To investigate the recognition properties of the sensing ensembles toward anions and $\alpha$-amino acids under IDA strategy by changing indicators.
3. I expected that my synthesized coordination compounds could detect various types of anions and amino acids by using commercially available indicators.
4. I hoped that, by tuning proper indicators, my synthesized complexes can probably discriminate **PPi** from other phosphate containing anions under indicator displacement assay.

จุฬาลงกรณ์มหาวิทยาลัย
Chulalongkorn University

# CHAPTER III

# EXPERIMENTS

## 3.1 Instruments

Nuclear Magnetic Resonance (NMR) spectra were recorded in $CDCl_3$, $D_2O$ and $CD_3CN$ on a 400 MHz Bruker Ultra Shield AVANCE 400 spectrometer. The solid state structure was determined by X-ray crystallography using a Bruker APEX CCD diffractrometer (graphite monochromated Mo-K$\alpha$ radiation with $\lambda$ = 0.71073 Å). The UV–Vis spectra were measured on a Hewlett Packard UV–Vis 8453 spectrophotometer. The ESI-MS mass spectra were recorded using a Bruker microTOF mass spectrometer. Square wave voltammetry was performed using an AUTOLAB PGSTAT 100 potentiostat. All electrochemical experiments carried out with a three-electrode cell comprising of a Pt working electrode, a counter electrode and a $Ag^+$/AgCl reference electrode at room temperature.

## 3.2 Chemical reagents

All the chemicals were reagent grade form Merck, Fluka and Aldrich. Solvents for synthesis (LABSCAN) were commercially purchased and purified by distillation and stored over molecular sieves 3 or 4 Å. $CH_3CN$ (LABSCAN) was analytical grade and used as received. Sterile water for injection was obtained from General Hospital Products Public Co., Ltd, (PathumThani, Thailand). Column chromatography operations were carried out on silica gel (Kieselegel 60, 0.063-0.200 nm, Merck) and alumina (aluminium oxide 90, 0.063-0.200 nm, Merck).

จุฬาลงกรณ์มหาวิทยาลัย
Chulalongkorn University

## 3.3 Synthesis and characterization of ligands L2 and L3

### 3.3.1 Preparation of (E)-1-(pyridin-2-yl)-N-(pyridin-2-ylmethylene) methanamine (a)

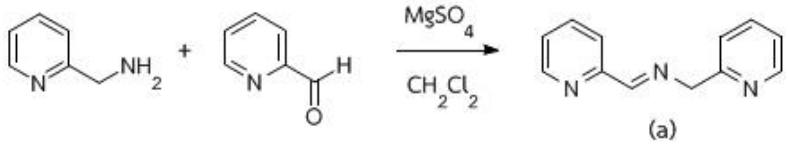


(a) **(3.1)**

To a suspension of anhydrous $MgSO_4$ (122 g, 183 mmol) in $CH_2Cl_2$ (30 mL) was added 2-pyridinecarboxaldehyde (3.96 g, 37 mmol) and 2-(aminomethyl) pyridine (4 g, 37 mmol). The mixture became warm and the color changed to yellow. After being stirred for 3 h at room temperature under nitrogen atmosphere, the suspension was filtered and washed with $CH_2Cl_2$ (150 mL), and the solvent was removed under vacuum. A yellow oil of (a) was obtained (7.3 g, quantitative yield)[76].

$^1$H NMR (400 MHz, $CDCl_3$, ppm): δ 8.67 (d, 1H, *J* = 3.6 Hz, Ar*H*), 8.58 (t, 2H, *J* = 3.6 Hz, Ar*H*), 8.10 (d, 1H, *J* = 7.6 Hz, Ar*H*), 7.76 (d, 1H, *J* = 1.6 Hz, Ar*H*), 7.67 (m, 1H, Ar*H*), 7.43 (d, 1H, *J* = 7.6 Hz, Ar*H*), 7.34 (m, 1H, Ar*H*), 7.19 (s, 1H, Ar*H*), 5.03 (d, 2H, *J* = 0.8 Hz, -C*H*$_2$-).

$^{13}$C NMR (100 MHz, $CDCl_3$, ppm): δ 163.94, 149.50, 149.37, 136.68, 136.55, 124.92, 122.38, 122.13, 121.49, 66.58.

### 3.3.2 Preparation of bis-pyridin-2-ylmethylamine (b)

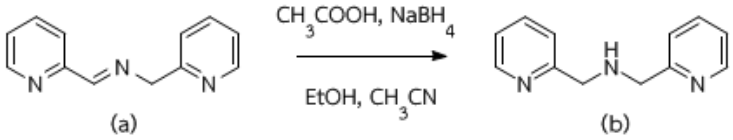


**(3.2)**

The imine **(a)** (4.02 g, 20 mmol) was dissolved in $CH_3CN$ (45 mL) and was cooled to -5 °C. Glacial acetic acid (1.47 mL, 25 mmol) was added in portions. To the resulting clear yellow solution was added $NaBH_4$ (3.78 g, 100 mmol) and EtOH (55 mL). After stirring for 18 h at room temperature, the reaction mixture was quenched with 12 M HCl (28 mL, 80 mmol) and heated at 60 °C for 2 h. The white precipitate was filtered. The filtrate was concentrated in vacuo and then redissolved in water (15 mL). The resulting yellow aqueous solution was basified by addition of solid NaOH pellets (12 g, 300 mmol) with efficient cooling. A red oil appeared immediately. It was extracted with diethyl ether (3 × 200 mL). The ether extracts were dried with anhydrous $Na_2SO_4$. After solvent removal, compound **(b)** was obtained (3.98 g, quantitative yield)[76].

$^1$H NMR (400 MHz, $CDCl_3$, ppm): δ 8.58 (m, 2H, Ar*H*), 7.66 (m, 2H, Ar*H*), 7.39 (d, 2H, *J* = 7.6 Hz, Ar*H*), 7.18 (m, 2H, Ar*H*), 4.00 (s, 4H, -C*H*$_2$-).

$^{13}$C NMR (100 MHz, $CDCl_3$, ppm): δ 159.63, 149.31, 136.51, 122.34, 121.99, 54.74.

### 3.3.3 Preparation of 2-[bis(2-pyridylmethyl)aminomethyl]nitrobenzene (c)

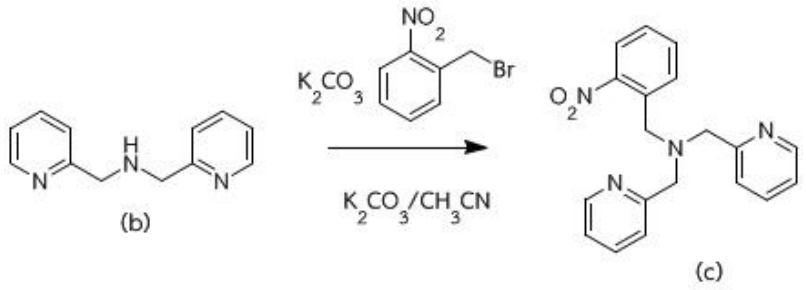


(3.3)

Amine **(b)** (3.86 g, 19.4 mmol), $K_2CO_3$ (20.8 g, 150 mmol), 2-nitrobenzylbromide (4.19 g, 419.4 mmol), and molecular sieves 3 Å (3.05 g) were mixed in 80 mL of $CH_3CN$ and stirred for 12 h under nitrogen atmosphere. The reaction mixture was filtered through Celite. After solvent removal, a brown oil was obtained. The oil was redissolved in $CH_2Cl_2$ (200 mL) and washed with water (3 × 300 mL). The organic extracts were dried with anhydrous $MgSO_4$. After solvent removal a dark oil of compound **(c)** was obtained (6.04 g, 93%)[77].

$^1$H NMR (400 MHz, $CDCl_3$, ppm): δ 8.52 (m, 2H, Ar*H*), 7.77 (t, 1H, *J* = 6.8 Hz, Ar*H*), 7.71 (s, 1H, Ar*H*), 7.65 (m, 1H, Ar*H*), 7.64 (d, 1H, *J* = 2 Hz, Ar*H*), 7.51 (d, 1H, *J* = 1.6 Hz, Ar*H*), 7.42 (d, 2H, *J* = 8 Hz, Ar*H*), 7.16 (m, 2H, Ar*H*), 4.09 (s, 2H, -C*H*$_2$-), 3.79 (s, 4H,-C*H*$_2$-).

$^{13}$C NMR (100 MHz, $CDCl_3$, ppm): δ 158.62, 148.92, 136.46, 134.38, 132.35, 131.39, 127.92, 124.31, 123.28, 122.13, 60.39, 55.87.

### 3.3.4 Preparation of 2-[bis(2-pyridylmethyl)aminomethyl]aniline (d)

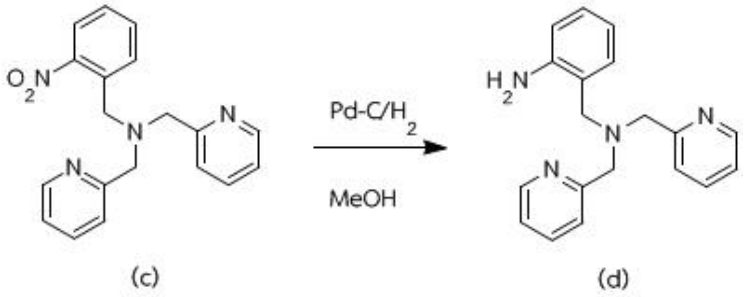


(c) (d) **(3.4)**

Pd-C (0.3 g) and nitro compound **(c)** (3 g, 8.97 mmol) were mixed in 150 mL of MeOH and stirred under a hydrogen atmosphere for 24 h. The reaction mixture was filtered through Celite to give a dark oil of **(d)** after solvent removal (2.73 g, quantitative yield)[77].

$^{1}$H NMR (400 MHz, $CDCl_3$, ppm): δ 8.55 (m, 2H, Ar*H*), 7.63 (m, 2H, Ar*H*), 7.39 (d, 2H, *J* = 7.6 Hz, Ar*H*), 7.15 (q, 2H, *J* = 5.2 Hz, Ar*H*), 7.07 (m, 2H, Ar*H*), 6.63 (t, 2H, *J* = 6.0 Hz, Ar*H*), 3.80 (s, 4H, -C$H_2$-), 3.66 (s, 2H, -C$H_2$-).

$^{13}$C NMR (100 MHz, $CDCl_3$, ppm): δ 159.10, 149.01, 147.01, 136.45, 131.18, 128.50, 123.53, 122.07, 117.22, 115.45, 60.14, 57.92.

### 3.3.5 Preparation of 9,10-bis(chloromethyl)anthracene (e)

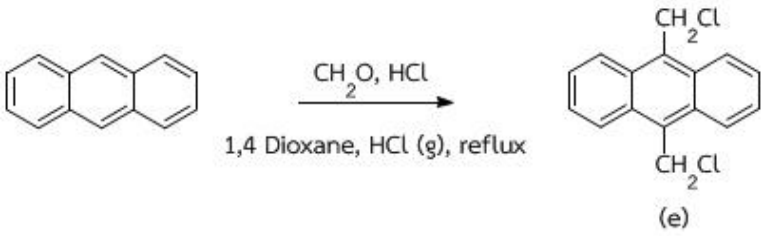


**(3.5)**

Anthracene (10.50 g, 58.90 mmol) and paraformaldehyde (11.25 g, 37.46 mmol) were dissolved in the mixture of 1,4-dioxane (90 mL) and concentrated HCl (15 mL). The reaction mixture was refluxed and stirred under HCl gas atmosphere for 3 h. The yellow precipitate was filtered and washed with 1,4-dioxane. Then, the crude product was recrystallized in hot 1,4-dioxane to give yellow needle crystal (8.7 g,53%)[78].

$^{1}$H NMR (400 MHz, $CDCl_3$, ppm): δ 8.41 (q, 4H, *J* = 3.6 Hz, Ar*H*), 7.69 (q, 4H, *J* = 3.6 Hz, Ar*H*), 5.64 (s, 4H, -C$H_2$-).

$^{13}$C NMR (100 MHz, $CDCl_3$, ppm): δ 130.23, 129.77, 126.73, 124.35, 38.82

จุฬาลงกรณ์มหาวิทยาลัย
Chulalongkorn University

### 3.3.6 Preparation of anthracene-9,10-dicarboxaldehyde (f)

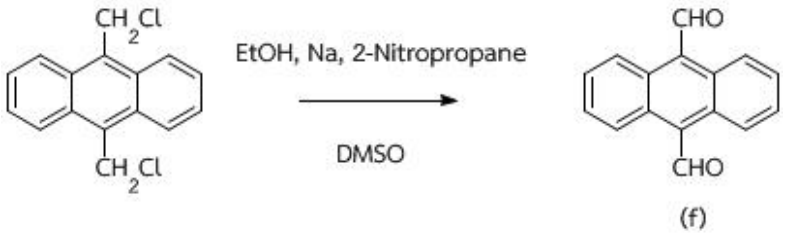


**(3.6)**

9,10-Bis(chloromethyl)anthracene (2 g, 7.27 mmol) was dissolved in DMSO 40 mL. The mixture of 2-nitropropane (2.40 mL) and sodium (0.4 g, 17.39 mmol) in EtOH (24 mL) was added in portions. The reaction mixture was stirred under nitrogen atmosphere for 3 h and was cooled to -4 °C for 2 h. The deep orange precipitate was filtered and washed with water and dried in a dessicator to give an orange product (0.8 g, 47%)[78].

$^{1}$H-NMR (400 MHz, $CDCl_3$, ppm): δ 11.52 (s, 2H, -C*H*O), 8.74 (q, *J* = 3.6 Hz, 4H, Ar*H*), 7.72 (q, *J* = 3.6 Hz, 4H, Ar*H*)

$^{13}$C-NMR (100 MHz, $CDCl_3$, ppm): δ 194.27, 131.69, 129.12, 128.35, 124.21

จุฬาลงกรณ์มหาวิทยาลัย
Chulalongkorn University

### 3.3.7 Preparation of (*N*,*N*'*E*,*N*,*N*'*E*)-*N*,*N*'-(anthracene-9,10-diylbis(methan-1-yl-1-ylidene))bis(2-((bis(pyridin-2-ylmethyl)amino)methyl)aniline) (h)

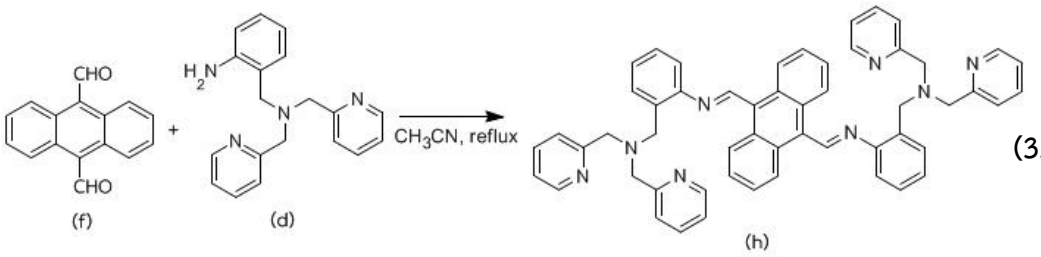


(3.7)

A mixture of 2-[bis(2-pyridylmethyl)aminomethyl]aniline (**d**) (1.93 g, 6.34 mmol) and 9,10-diformylanthracene (**f**) (0.64 g, 2.73 mmol) was dissolved in anhydrous $CH_3CN$ (50 mL) in a round bottom flask. The reaction mixture was refluxed under nitrogen for 12 h. After the solvent was removed, the product was obtained as a dark solid (**h**) (quantitative yield).

ESI-MS (positive mode); 807.3913 $[M+H]^+$.

จุฬาลงกรณ์มหาวิทยาลัย
Chulalongkorn University

### 3.3.8 Preparation of ligand L2

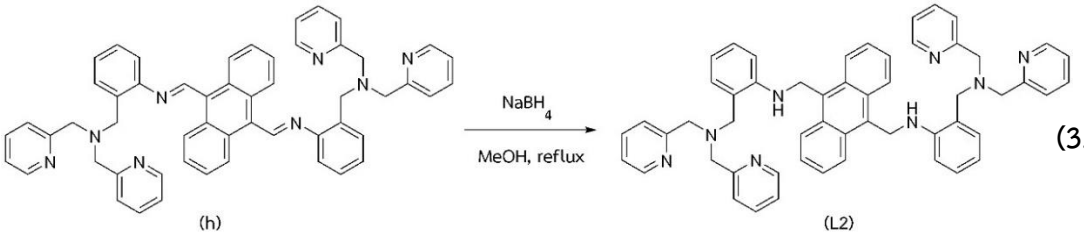


(3.8)

The crude imine (**h**) was dissolved in MeOH (100 mL) and the solution was cooled to -5 °C. Subsequently, $NaBH_4$ (4.18 g, 110 mmol) was added to the brown solution, and the mixture was refluxed for 12 h under nitrogen atmosphere. After the mixture was cooled to room temperature, water (150 mL) was added and the mixture was evaporated to remove MeOH. The residue was dissolved in $CH_2Cl_2$ (150 mL) and the organic layer was washed with water (3×100 mL), dried with anhydrous $MgSO_4$, filtered and the solvent was removed. The light yellow solid of ligand **L2** was obtained after recrystallization of the crude product in MeOH (0.90 g, 41%).

$^1$H-NMR (400 MHz, $CDCl_3$, ppm): δ 8.45 (q, *J* = 3.6 Hz, 4H, Ar*H*), 8.03 (d, *J* = 4.4 Hz, 4H, Ar*H*), 7.58 (q, *J* = 3.6 Hz, 4H, Ar*H*), 7.38 (t, *J* = 8 Hz, 2H, Ar*H*), 7.18 (d, *J* = 7.2 Hz, 2H, Ar*H*), 7.10 (d, *J* = 8 Hz, 2H, Ar*H*), 6.73 (m, 10H, Ar*H*), 6.51 (d, *J* = 7.6 Hz, 4H, Ar*H*), 6.33 (s, 2H, -N*H*-), 5.28 (s, 4H, -C$H_2$-), 3.59 (s, 4H, -C$H_2$-), 3.52 (s, 8H, -C$H_2$-).

$^{13}$C-NMR (100 MHz, $CDCl_3$, ppm): δ 158.43, 148.58, 148.05, 135.79, 131.43, 131.01, 130.89, 129.00, 126.13, 125.51, 122.55, 122.24, 121.96, 121.44, 116.69, 109.63, 60.35, 58.50, 40.96.

ESI-MS (positive mode); 811.4281 $[M+H]^+$.

Elemental analysis calculated for $C_{54}H_{50}N_8$: C, 79.97; H, 6.21; N, 13.82; found C, 79.89; H, 6.16; N, 13.87.

### 3.3.9 Preparation of (*E*)-*N*-(anthracen-9-ylmethylene)-2-((bis(pyridin-2-ylmethyl)amino)methyl)aniline (g)

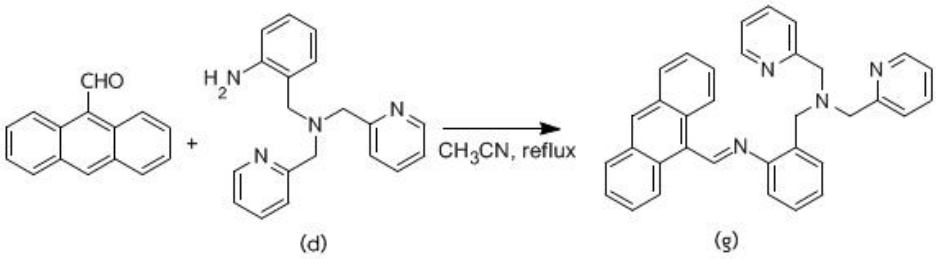


(d) (g) **(3.9)**

2-[bis(2-pyridylmethyl)aminomethyl]aniline (**d**) (1.41 g, 4.65 mmol) and 9-anthracenaldehyde (0.96 g, 6.47 mmol) were dissolved in anhydrous $CH_3CN$ (150 mL) in a round bottom flask. The reaction mixture was refluxed under nitrogen atmosphere for 24 h. The reaction mixture was concentrated in vacuo to give a brown oil product of (E)-N-(anthracen-9-ylmethylene)-2-((bis(pyridine-2-ylmethyl)amino)methyl)aniline in quantitative yield.

ESI-MS (positive mode, m/z): $[M+H]^+$ = 493.24

จุฬาลงกรณ์มหาวิทยาลัย
Chulalongkorn University

### 3.3.10 Preparation of ligand L3

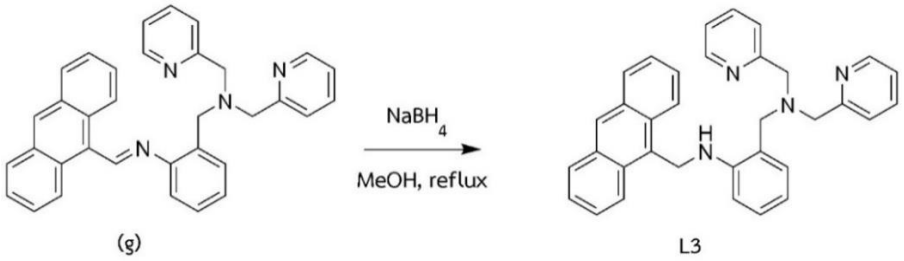


(3.10)

The brown oil of product **(g)** (0.64 g, 1.29 mmol) was dissolved in $CH_3OH$. The solution was treated with $NaBH_4$ (0.57 g, 15.48 mmol) in small portions at 0 °C and subsequently refluxed for 16 h under nitrogen atmosphere. At room temperature, water (50 mL) was added into the mixture, and the solvent was concentrated in vacuo. The organic layer was dried over anhydrous $MgSO_4$ and the solvent was removed under reduced pressure giving a red-brown oil. A mixture of $CH_3OH$ and diethyl ether was added to the oil and the product **L3** was obtained as a bright yellow solid (0.35 g, 55%).

$^1$H NMR (400 MHz, $CDCl_3$, ppm): δ 8.60 (s, 2H, Ar*H*), 8.28 (d, *J* = 8.8 Hz, 2H, Ar*H*), 8.15 (d, *J* = 8.4 Hz, 2H, Ar*H*), 8.04 (d, *J* = 4.0 Hz, 2H, Ar*H*), 7.57 (d, *J* = 7.2 Hz, 2H, Ar*H*), 7.50 (m, 2H, Ar*H*), 7.06 (s, 2H, Ar*H*), 6.74 (q, *J* = 4.0 Hz, 2H, Ar*H*), 6.62 (m, 2H, Ar*H*), 6.44 (d, *J* = 8.0 Hz, 2H, Ar*H*), 6.09 (s, 1H, -N*H*-), 5.15 (s, 2H, -C$H_2$-NH-), 3.56 (s, 2H, -C$H_2$-), 3.50 (s, 2H, -C$H_2$-).

$^{13}$C NMR (100 MHz, $CDCl_3$, ppm): δ 158.44, 148.46, 148.07, 135.90, 131.65, 131.42, 130.94, 129.98, 129.05, 129.05, 127.70, 126.34, 125.26, 124.79, 122.48, 121.77, 121.47, 116.57, 109.56, 58.51, 40.59.

ESI-MS (positive mode, m/z): $[M+H]^+$ = 495.2563.

The elemental analysis calculated for $C_{34}H_{30}N_4$: C, 82.56; H, 6.11; N, 11.33; found C, 82.49; H, 6.16; N, 11.45.

### 3.4 Synthesis and characterization of metal complexes of Cu(II) and Zn(II) with ligand L2 and L3

#### 3.4.1 Preparation of dinuclear complex $Cu_2L2$

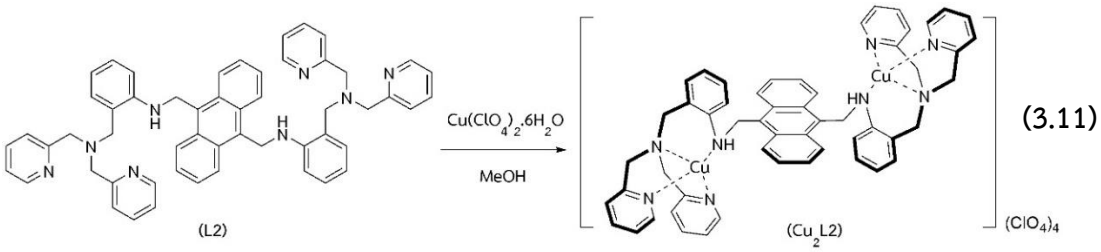


(3.11)

The methanolic solution of $Cu(ClO_4)_2.6H_2O$ (50 mg, 0.13 mmol) was added to the ethanolic suspension of **L2** (32.4 mg, 0.04 mmol) the color of solution changed to deep green immediately. Then, the mixture was refluxed under nitrogen for 12 h. After cooling to room temperature the green solid precipitate was filtered and washed with $CH_2Cl_2$ and MeOH to obtain **$Cu_2L2$** (48.1 mg, 90%).

ESI-MS (positive mode, m/z): $[M + 3ClO_4]^+$ = 1235.0554

Elemental analysis calcd for $C_{54}H_{50}Cl_4Cu_2N_8O_{16}$: C, 48.55; H, 3.77; N, 8.39; found C, 48.49; H, 3.76; N, 8.42.

### 3.4.2 Preparation of dinuclear complex $Zn_2L2$

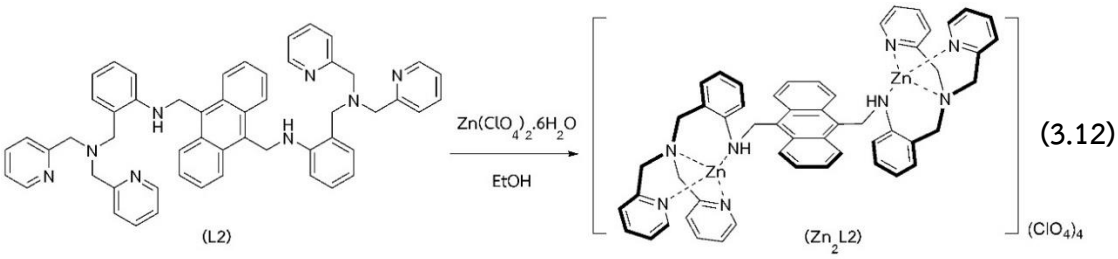


(3.12)

The ethanolic solution of $Zn(ClO_4)_2.6H_2O$ (37.2 mg, 0.1 mmol) was added to the ethanolic suspension of **L2** (24.3 mg, 0.03 mmol) and the color of solution changed to yellow immediately. Then, the yellow solution was refluxed under nitrogen for 12 h. After cooling to room temperature, the yellow solids were precipitated, filtered and washed with $CH_2Cl_2$ and MeOH to obtain **$Zn_2L2$** (35.4 mg, 88%).

$^1$H-NMR (400 MHz, 20% (v/v) $D_2O/CD_3CN$, ppm): δ 8.70 (bs, 4H, Ar*H*), 7.87 (bm, 8H, Ar*H*), 7.48 (bm, 4H, Ar*H*), 7.34 (bs, 8H, Ar*H*), 7.20 (d, *J* = 7.6 Hz, 2H, Ar*H*–NH–), 6.75 (t, *J* = 7.6 Hz, 2H, Ar*H*–NH–), 6.25 (t, *J* = 7.6 Hz, 2H, Ar*H*–NH–), 5.27 (bd, *J* = 7.6 Hz, 2H, Ar*H*–NH–) 4.98 (bs, 4H, Ar–NH–C$H_2$–), 4.29 (m, 12H, Ar–C$H_2$–).

$^{13}$C-NMR (100 MHz, 20% (v/v) $D_2O/CD_3CN$, ppm): δ 154.76, 147.63, 141.88, 140.97, 133.37, 129.79, 129.09, 128.72, 127.15, 126.23, 125.80, 124.93, 124.56, 124.34, 124.00, 59.02, 27.84, 45.11.

ESI-MS (positive mode); 1236.2163 $[M+3ClO_4^-]^+$.

Elemental analysis calculated for $C_{54}H_{50}Cl_4N_8O_{16}Zn_2.H_2O.CH_2$-$Cl_2$: C, 45.79; H, 3.77; N, 7.77; found C, 45.66; H, 3.76; N, 7.93.

### 3.4.3 Preparation of mononuclear complex CuL3

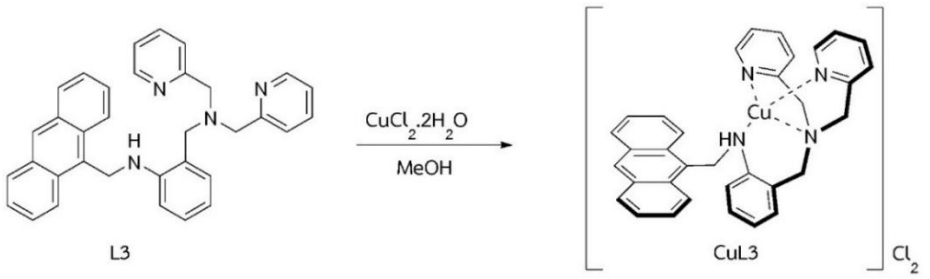


(3.13)

The methanolic solution of $CuCl_2.2H_2O$ (24 mg, 0.14 mmol) in methanol (5 mL) was added to the suspension of methanolic solution of **L3** (50 mg, 0.10 mmol) giving the deep green solution. The resulting deep green solution was allowed to stand at room temperature. After 1 week, green cubic-shaped X-ray diffraction quality single crystals of compound **CuL3** appeared (85 mg, 73%).

MALDI-TOF MS: [**CuL3+Cl**]$^+$, m/z = 592.833

Elemental analysis calcd for $C_{34}H_{30}Cl_2CuN_4$ : C, 64.91; H, 4.81; N, 8.91; found C, 64.60 ; H,4.86 ; N, 8.50.

จุฬาลงกรณ์มหาวิทยาลัย
Chulalongkorn University

### 3.4.4 Preparation of mononuclear complex ZnL3

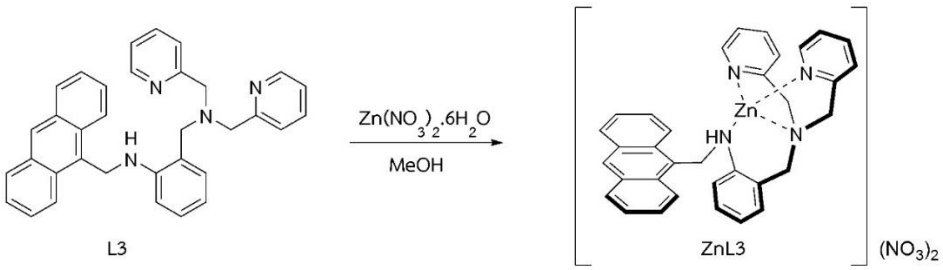


**(3.14)**

The methanolic solution of $Zn(NO_3)_2.6H_2O$ (41 mg, 0.14 mmol) in methanol (5 mL) was added to thr suspension of methanolic solution of **L3** (50 mg, 0.10 mmol) giving a yellow solution. The resulting solution was allowed to stand at room temperature. Compound **ZnL3** precipitated as a yellow solid (48 mg, 70%).

$^1$H NMR (400 MHz, $CDCl_3$, ppm): δ 8.63 (d, *J* = 4.4 Hz, 2H, Ar*H*), 8.58 (s, 1H, Ar*H*), 8.13 (t, *J* = 8.0 Hz, 4H, ArH), 8.57 (m, 4H, Ar*H*), 7.41 (t, *J* = 8.0 Hz, 1H, Ar*H*), 7.47 (m, 4H, Ar*H*), 7.14 (d, *J* = 8.0 Hz, 1H, Ar*H*), 6.94 (d, *J* = 7.6 Hz, 1H, Ar*H*), 6.87 (d, J = 7.2 Hz, 1H, Ar*H*), 6.65 (d, *J* = 7.2 Hz, 2H, Ar*H*), 5.17 (d, *J* = 4.8 Hz, 2H, -C$H_2$-), 4.42 (d, *J* = 15.6 Hz, 2H, -C$H_2$-), 3.95 (d, *J* = 15.6 Hz, 2H, -C$H_2$-), 3.82 (s, 1H, -N*H*-), 3.57 (s, 2H, -C$H_2$-).

$^{13}$C NMR (100 MHz, $CDCl_3$, ppm): δ 153.83, 148.58, 147.34, 140.09, 134.31, 131.44, 130.70, 130.43, 129.29, 128.33, 127.99, 127.34, 125.64, 124.81, 123.90, 123.24, 119.63, 118.40, 115.31, 56.30, 50.61, 42.18.

MALDI-TOF MS: [**ZnL3**+3$NO_3$]$^-$, m/z = 744.081

Elemental analysis calcd for $C_{34}H_30N_6O_6Zn$: C, 59.70; H, 4.42; N, 12.29; found C, 59.71; H,4.48; N, 12.28.

## 3.5 Screening tests for selective sensing of anions and α-amino acids sensing

### 3.5.1 Screening tests of indicators for selective PPi sensing

For the colorimetric detection of **PPi** anion, a solution of each indicator (400 μM, 0.1 mL) in 80/20 (% v/v) acetonitrile/aqueous solutions buffered at pH 7.4 with HEPES was added into a solution of **$Zn_2$L2** 20 μM (2 mL) in the same solvent system. Subsequently, 300 μL of tetrabutylammonium salts of anions (1 mM) was then added to the sensing ensemble. The resulting mixtures were allowed to stand for 5 min and subjected to UV–vis spectroscopic measurements. Photographs were taken by a digital camera (Canon EOS 7D with Tamron 17-50 mm F2.8 lens).

### 3.5.2 Screening tests of indicators for selective histidine sensing

Stock solutions (1 mM) of α-amino acids were prepared in 80/20 (% v/v) acetonitrile/aqueous solutions buffered at pH 7.4 with HEPES. A stock solution of each receptor (20 μM) and indicator (400 μM) were prepared in 80/20 (%v/v) acetonitrile/aqeous solutions buffered at pH 7.4 with HEPES. For colorimetric detection of histidine, a solution of each indicator was added into a solution of each complex. Subsequently, 300 μL of α-amino acids (1 mM) was then added to the as-prepared ensemble. The resulting mixtures were allowed to stand for 5 min and subjected to UV-vis spectroscopic measurements. Photographs were taken by a digital camera (Canon EOS 7D with Tamron 17-50 mm F2.8 lens).

จุฬาลงกรณ์มหาวิทยาลัย
Chulalongkorn University

## 3.6 UV-vis titrations under indicator displacement assay

### 3.6.1 UV-vis titrations under indicator displacement assay for PPi detection

All spectrometric titrations were performed in 80/20 (% v/v) acetronitrile/ aqueous solutions buffered at pH 7.4 with HEPES (10 mM) in quarzt cuvettes. Titrations were carried out by adding aliquots of a 400 μM (10 μL) solution of complex solution to a 20 μM (2 mL) of each indicator by a syringe. After each addition, the absorption

spectra of the indicator solution were recorded. Similar titration experiments were performed with **PPi**. In a typical titration, aliquots solution of **PPi** 400 μM (10 μL) were added to a 20 μM (2 mL) of 1:1 or 1:2 ensemble solution of [**$Zn_2$L2:MTB]**. The ensemble formation constants and the apparent competitive binding constants are calculated using SPECFIT32 program.

### 3.6.2 UV-vis titrations under indicator displacement assay for histidine detection

All spectrophotometric titrations were performed in 80/20 (%v/v) acetonitrile/aqueous solutions buffered at pH 7.4 with HEPES (10 mM) in quartz cuvettes. Titrations were carried out by adding aliquots of a 400 μM (10 μL) solution of the complex solution to a 20 μM (2 mL) of each indicator by a syringe. After each addition, the absorption spectra of the indicator solution were recorded. Similar titration experiments were performed with **His**. In a typical titration, aliquots solution of **His** 1 mM (10 μL) were added to a 20 μM (2 mL) of 1:1 ensemble solution of [**ML•PAR**]. The ensemble formation constants and the apparent competitive binding constants are calculated using SPECFIT32 program.

จุฬาลงกรณ์มหาวิทยาลัย
Chulalongkorn University

## 3.7 NMR titration experiments

Generally, all reagents in NMR titration experiments were prepared in 80% $CD_3CN/D_2O$. For **PPi** titration, aliquots of **$Zn_2$L2** 0.05 M (5 μL) were added into the 0.5 mL solution of the **PPi** (5 mM) by a syringe. For **MTB** titration, aliquots of **MTB** 0.05 M (5 μL) were added into the 0.5 mL solution of the **$Zn_2$L2** by a syringe. For **MTB** displacement titrations, aliquots of **PPi** were added into the 0.5 mL solution of 1:1 and 1:2 ensemble (5 mM) solution of **[$Zn_2$L2:MTB]**, respectively. Subsequently, $^{1}H$ or $^{31}P$ NMR spectra were then recorded.

For histidine detection, a 5 mM solution of **ZnL3** in 50/50 (%v/v) $CD_3CN/D_2O$ 0.5 mL was prepared in NMR tubes. A 0.05 M stock solution of **His** guest molecules in

50/50 (%v/v) $CD_3CN/D_2O$ was prepared in a small vial. The solution of **His** was added into the NMR samples (0 - 4 equivalents).

### 3.8 Tolerances limit study by UV-Visible spectrophotometry

A solution of **PAR** indicator 800 μM (0.1 mL) in 20% (v/v) water/acetonitrile solutions buffered at pH 7.4 with HEPES was added into a solution of **ZnL3** 20 μM (2 mL) in the same solvent system. Subsequently, 300 μL of **His** (1 mM) was then added to the as-prepared ensemble. After that, each interfering anion was added to the ensemble solution. The resulting mixtures were allowed to stand still for 5 min and subjected to UV-vis spectroscopic measurements. The tolerance level was defined as the maximum amount of the interfering species producing an error of ± 5% in **His** determination.

### 3.9 Urine samples preparation for histidine detection under indicator displacement assay

Human urine samples were collected from healthy adult volunteers. The urine samples were diluted 100-fold directly with 80% (v/v) acetonitrile/aqueous solutions buffered at pH 7.4 with HEPES. Then 10 μL of diluted sample was added to the 10 mL of 20 μM [**CuL3·PAR**] ensemble. The quantification of histidine and the absorption recovery with 10, 20 and 30 μM spiked amounts of histidine were done by a standard addition method.

จุฬาลงกรณ์มหาวิทยาลัย
Chulalongkorn University

# CHAPTER IV
# RESULTS AND DISCUSSION

## 4.1 Synthesis and characterization of ligands L2 and L3

### 4.1.1 Synthesis and characterization of L2

Ligand **L2** was straightforwardly synthesized in a moderate yield (41%) by a Schiff base condensation reaction between tripodal amine (**d**) and 9,10-diformyl anthracene (**f**) in refluxing acetonitrile and followed by in situ reduction using $NaBH_4$ in refluxing methanol (Scheme 1).

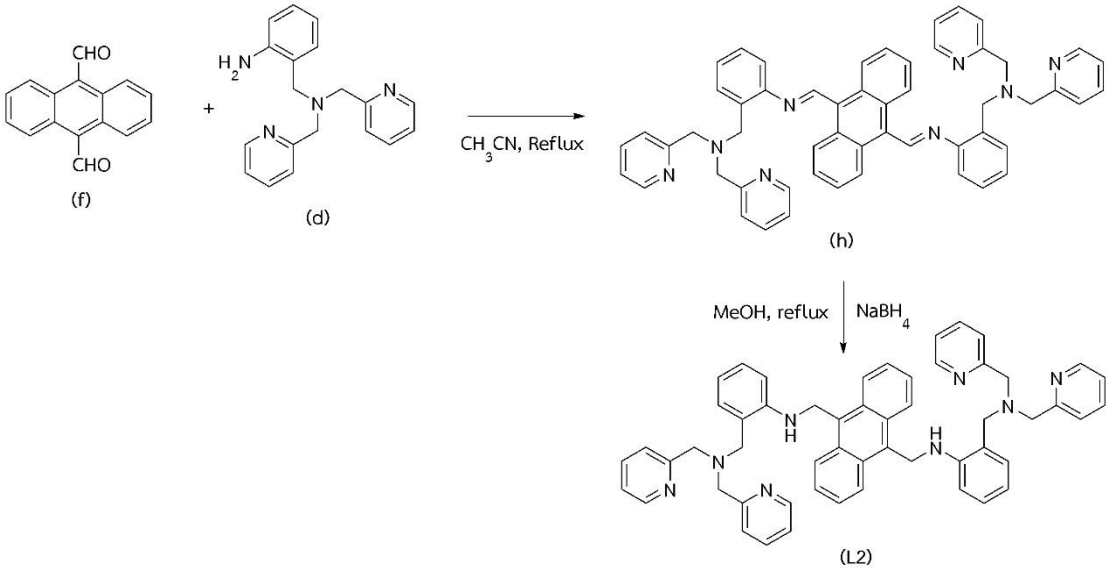


**Scheme 1**. The synthetic pathway for ligand **L2**

Ligand **L2** was characterization by various analytical methods. Firstly, $^1$H NMR spectrum of **L2** in $CDCl_3$, as shown in Figure 11. showed the singlet peak at chemical shift 3.52 ppm (8H) belongs to -C*H*$_2$- groups that connect to the pyridine rings. The singlet peak at chemical shift 3.59 ppm (4H) belongs to -C*H*$_2$- groups connecting to the benzene rings, other singlet peak at chemical shift 5.28 ppm (4H) belongs to -C*H*$_2$NH-

protons that connect to anthracene ring. The broad peak at chemical shift 6.33 ppm corresponds to NH protons. The $^{1}$H-NMR spectrum also showed signals for the protons of the pyridine rings (4H) in a low field region at chemical shift 8.45 ppm. HRMS-ESI (positive mode) mass spectrum showed the parent peak at m/z = 811.4281 corresponding to a singly charged molecular ion of [**L2**+H]$^{+}$ as shown in Figure 12. In addition**,** the doubly charged species of [**L2**+2H]$^{2+}$ was also observed at *m/z* 406.2193. The elemental analysis result agrees well with the proposed structure.

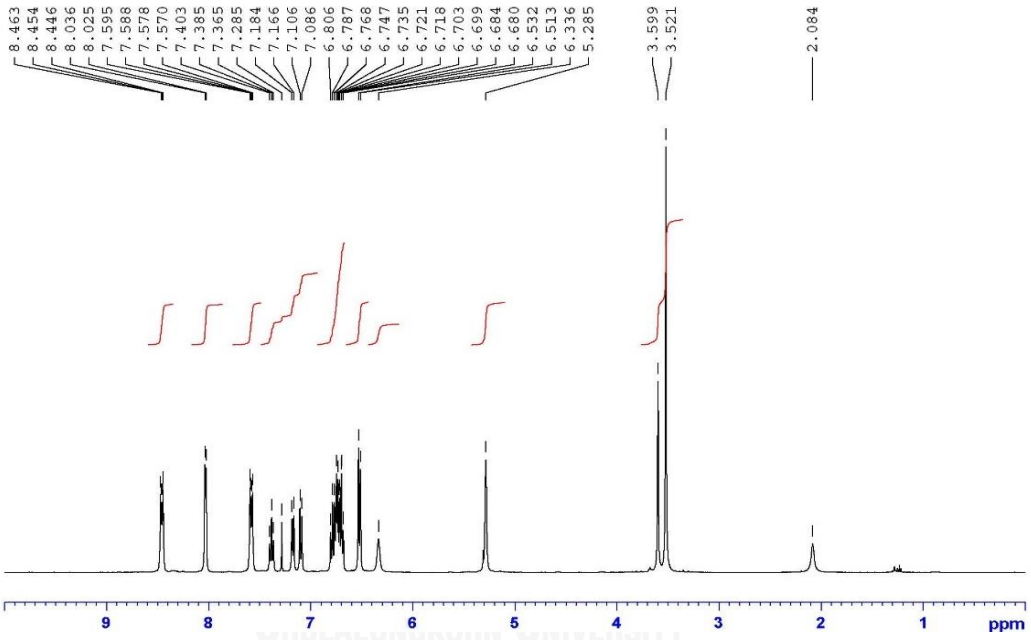


**Figure 11**. $^{1}$H NMR spectrum of ligand **L2** in $CDCl_3$

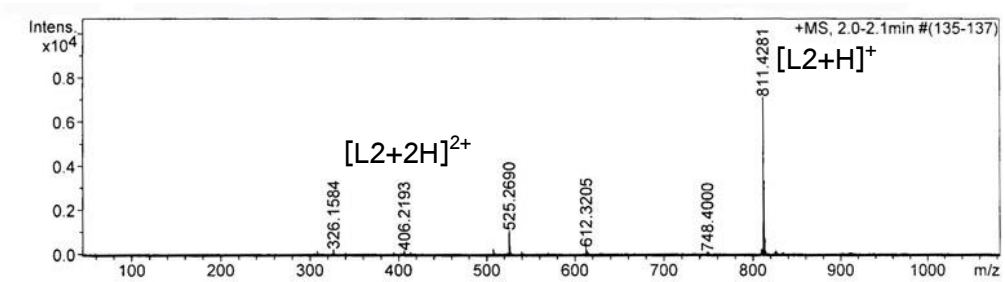


**Figure 12**. Mass spectrum of ligand **L2**

### 4.1.2 Synthesis and characterization of ligand L3

Ligand **L3** was straightforwardly synthesized in a moderate yield (55%) by a Schiff base condensation reaction between tripodal amine (**d**) and 9-anthracene aldehyde in refluxing acetonitrile and followed by in situ reduction using $NaBH_4$ in refluxing methanol (Scheme 2).

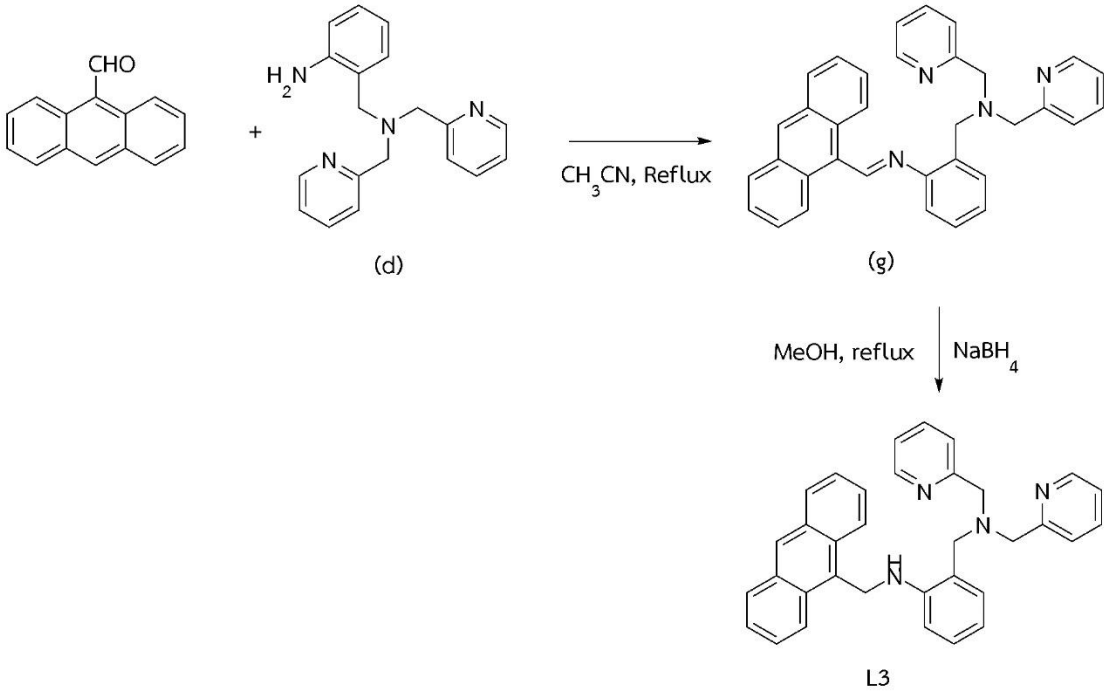


CHULALONGKORN UNIVERSITY

**Scheme 2.** The synthetic pathway for ligand **L3**

Ligand **L3** was characterization by standard analytical techniques. The $^1$H NMR spectrum of **L3** in $CDCl_3$ (Figure 13) showed the singlet peak at chemical shift 3.50 ppm (4H) belongs to -$CH_2$- groups that connect to the pyridine rings. The singlet peak at chemical shift 3.56 ppm (2H) belongs to -$CH_2$- groups connecting to the benzene rings, other singlet peak at chemical shift 5.13 ppm (2H) belongs to -$CH_2$NH- protons that connect to anthracene ring. The broad peak at chemical shift 6.09 ppm corresponds to NH protons. The $^1$H-NMR spectrum also showed signals for the protons of the

pyridine rings (2H) in low field region at chemical shift 8.60 ppm. HRMS-ESI (positive mode) mass spectrum showed the parent peak at m/z = 495.2563 corresponding to the singly charged molecular ion of [**L3**+H]$^+$, as shown in Figure 14. The elemental analysis result agrees well with the proposed structure.

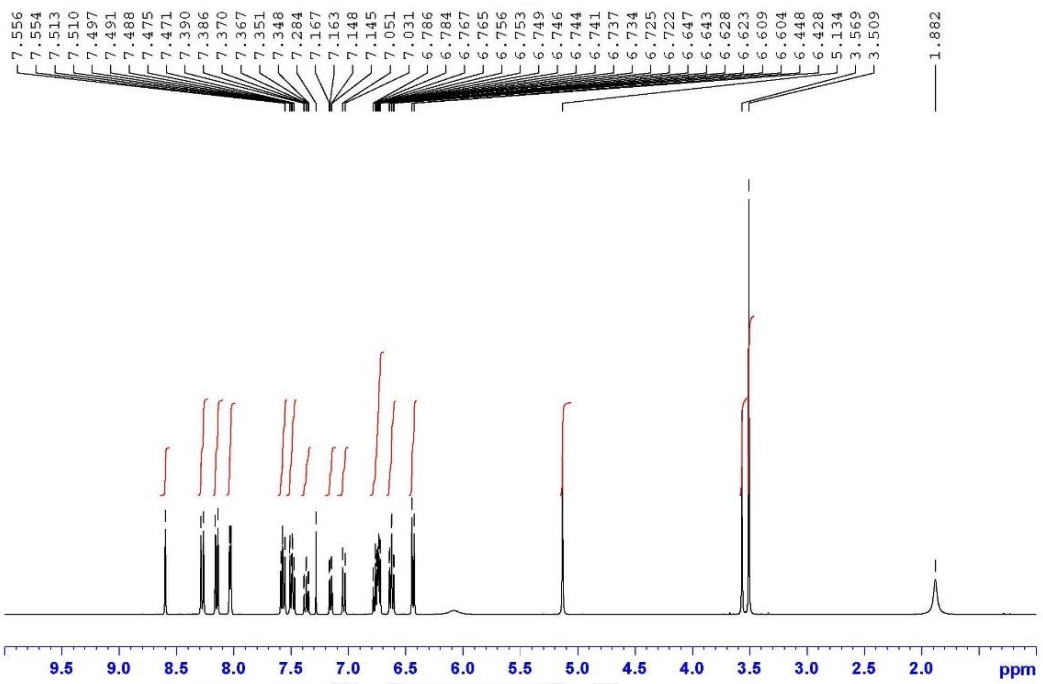


**Figure 13**. $^1$H NMR spectrum of ligand **L3** in $CDCl_3$

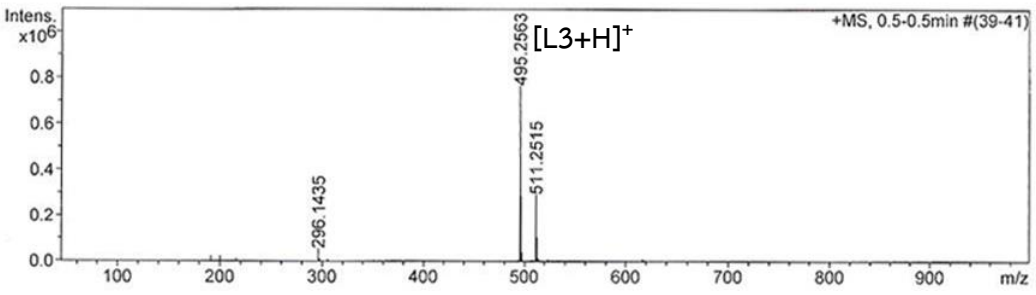


**Figure 14**. Mass spectrum of ligand **L3**

The suitable single crystal of **L3** has grown in MeOH and crystallized in the space group P-1. The intramolecular hydrogen bonding between the NH amine and tertiary nitrogen atom with a N(1)-N(2) distance of 3.026(3) Å with hydrogen bond angle of 137(3)° was found in the crystal structure, Figure 15. This result agreed with the $^{1}$H-NMR spectrum of **L3** in $CDCl_3$ in which the NH amine proton was observed in the downfield region ($\delta$ = 6.09 ppm). It revealed that the preorganization of **L3** was controlled by the intramolecular hydrogen bond.

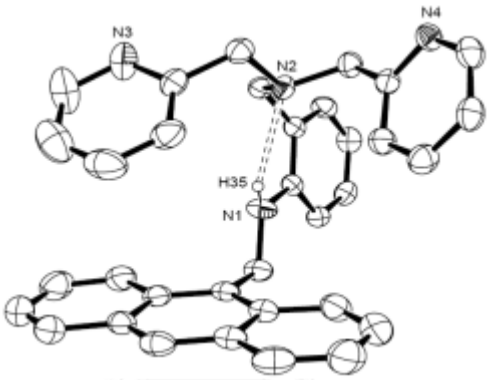


**Figure 15**. ORTEP plot of ligand **L3**

จุฬาลงกรณ์มหาวิทยาลัย

## 4.2 Synthesis and characterization of dinuclear complexes $Cu_2L2$ and $Zn_2L2$ and mononuclear complexes CuL3 and ZnL3

### 4.2.1 Synthesis and characterization of $Cu_2L2$

The dinuclear copper(II) complex, **$Cu_2L2$**, was synthesized by refluxing $Cu(ClO_4)_2.6H_2O$ with ligand **L2** in methanol and obtained as deep green precipitated in 90% yield. Then**,** it was characterized by mass spectrometry technique and C/H/N analysis technique. HRMS-ESI (positive mode) mass spectrum, as shown in Figure 16, showed a molecular ion at m/z = 1235.0554 related to [**$Cu_2L2$** + $3ClO_4$]$^{+}$. Moreover**,** the doubly charged species of [**L2**+$2ClO_4$]$^{2+}$ was also observed at m/z = 569.2438. The elemental analysis result agrees well with the proposed structure.

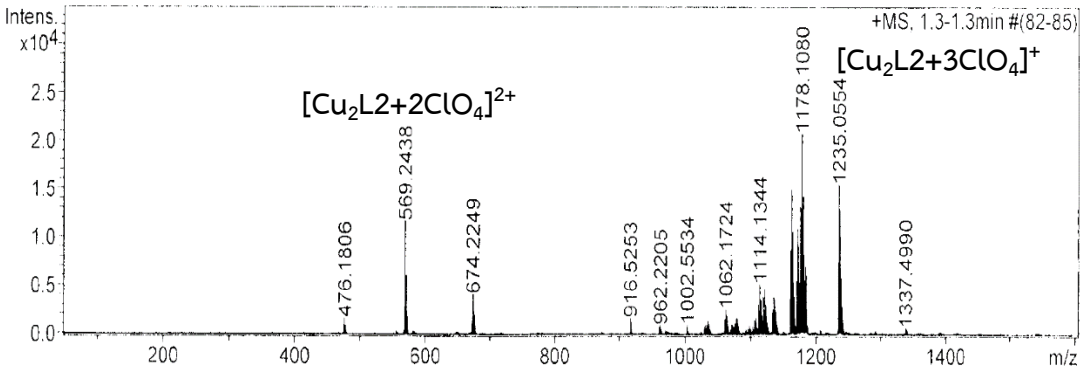


**Figure 16**. Mass spectrum of dinuclear complex **$Cu_2$L2**

### 4.2.2 Synthesis and characterization of $Zn_2$L2

The dinuclear zinc(II) complex, **$Zn_2$L2**, was readily obtained by refluxing $Zn(ClO_4)_2 \cdot 6H_2O$ with ligand **L2** in ethanol in 88% yield. The **$Zn_2$L2** complex was characterized by standard analytical methods. The $^1$H NMR spectrum of **$Zn_2$L2** in 20% $D_2O/CD_3CN$ showed rather broad signals (Figure 17), compared to that of the free ligand **L2**. A multiplet signal of methylene protons of the two pyridine groups and the amine groups appeared at 4.29 ppm. The aromatic protons of the aryl rings connecting to the amine group appeared at more upfield positions compared to that of **L2**, probably due to the coordination of the N atom to the Zn(II) center. I proposed that **L2** behaved as a tetradentate ligand to coordinate Zn(II) using 4 N atoms of the tripodal amine unit[77]. HRMS-ESI (positive mode) mass spectrum showed a molecular ion at m/z = 1236.2163 related to [**$Zn_2$L2** + $3ClO_4$]$^+$ as shown in Figure 18. The elemental analysis result agrees well with the proposed structure.

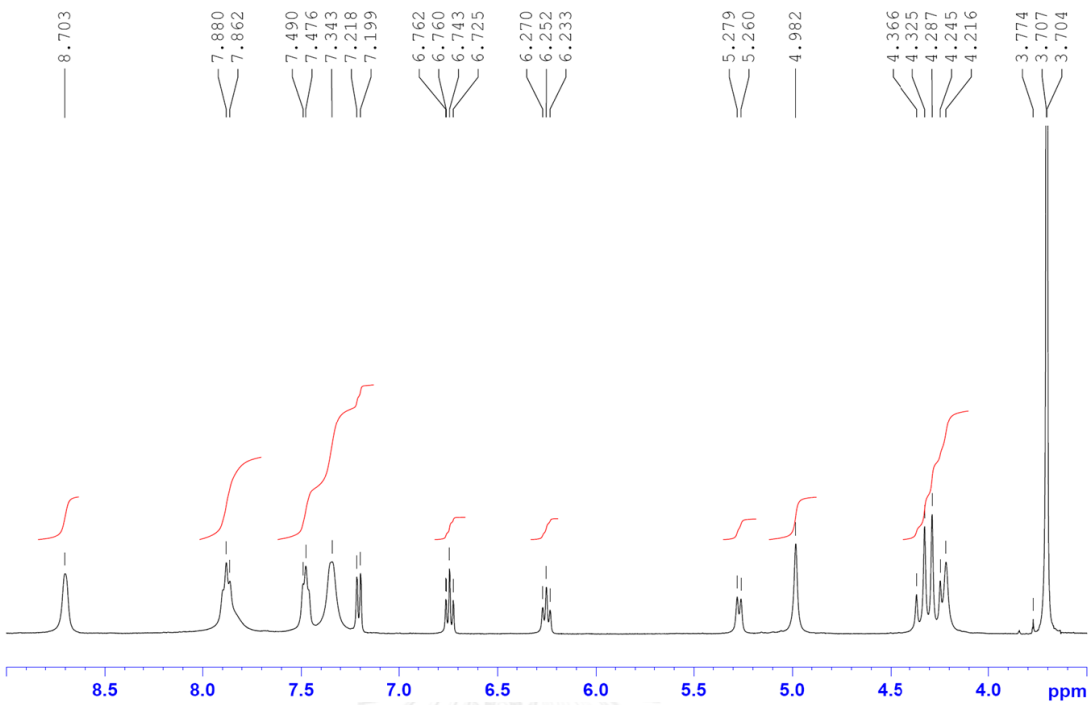


**Figure 17**. $^{1}H$ NMR spectrum of complex **$Zn_2L2$** in 20% $D_2O/CD_3CN$

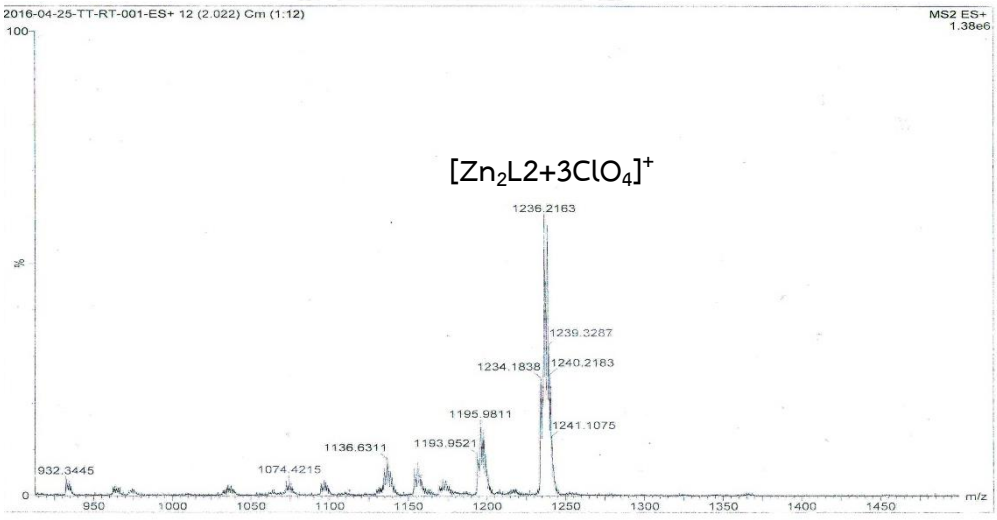


**Figure 18**. Mass spectrum of complex **$Zn_2L2$**

### 4.2.3 Synthesis and characterization of CuL3

The mononuclear copper(II) complex **$Cu_2$L3** was synthesized using a straight forward method from the reaction of copper(II) chloride salts with the methanolic solutions of the ligand **L3** and obtained as deep green solid in 73% yield. MALDI-TOF mass spectrum shown in Figure 19, reveals the formation of **CuL3** found at m/z = 592.833 for [**CuL3-Cl**]$^+$. The suitable single crystal of **CuL3** was obtained after recrystallized in MeOH. An ORTEP plot of **CuL3** is shown in Figure 20. The geometry around the copper(II) center is best described as tetragonal structure with chloride ion, tertiary nitrogen atom and two nitrogen atoms of pyridine rings occupying the equatorial coordination sites, and the secondary amine nitrogen atom together with the chloride ion in the axial positions. Due to pseudo Jahn–Teller effect, the **CuL3** complex shows an elongated axis along the axial Cu–N(1) and Cu-Cl(2) with bond distances of 2.541(2) Å and 2.791 (3) Å, respectively.These bond distances are larger than those of equatorial ones; Cu-Cl(1) 2.273 (2) Å, Cu-N(2), 2.068 (2) Å, Cu-N(3) 2.019 (2) Å and Cu-N(4) 2.012 (2) Å.

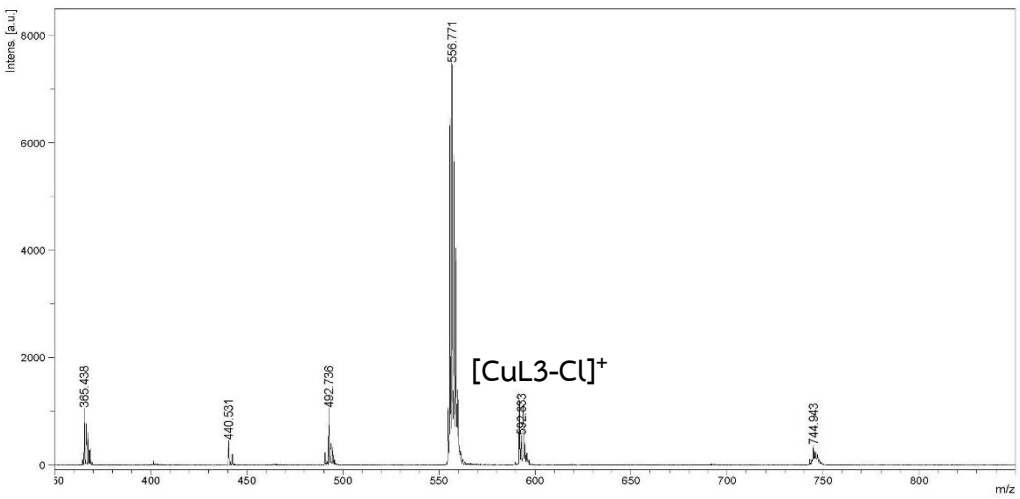


**Figure 19**. Mass spectrum of mononuclear complex **CuL3**

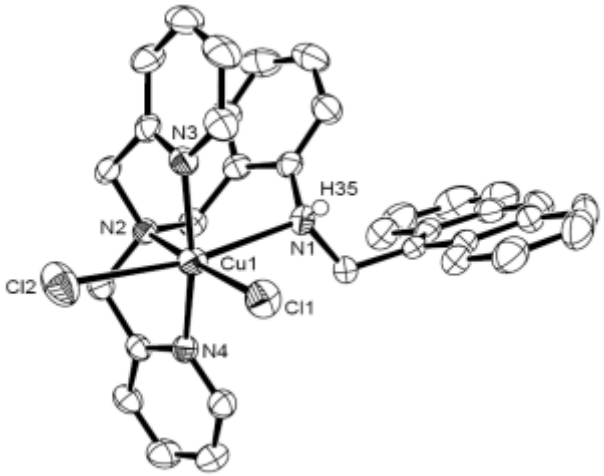


**Figure 20**. ORTEP plot of mononuclear complex **CuL3**

### 4.2.4 Synthesis and characterization of ZnL3

The **ZnL3** was easily synthesized by refluxing $Zn(NO_3)_2.6H_2O$ with ligand **L3** in methanol to give yellow compound product in 70% yield. I have tried to grow the single crystal of **ZnL3**. However, the crystal is not good enough to collect the X-ray data. Compared to the crystal structure of **CuL3**, I expected that upon $Zn^{2+}$ coordination at the tripodal amine unit the intramolecular hydrogen bond between NH-N was broken. Notably, $^1H$ NMR spectrum of **ZnL3** could confirm my expectation, Figure 21. The result showed that the NH amine proton of **ZnL3** was shifted upfield ($\Delta\delta$ = 2.27 ppm) compared to free **L3**. It should be noted that the four methylene protons of tripodal amine unit in **ZnL3** appear as a pair of doublets (AB system) at 4.42 and 3.95 ppm with $J$ = 15.6 Hz. The resonances from the protons proximal to the Zn(II) centers show a downfield shift, while protons that are distant from the metal centers show an upfield shift. This implies that the electronic environment of protons on the same methylene carbon is not identical upon coordination of $Zn^{2+}$. MALDI-TOF mass spectrum shown in Figure 22 showed the parent peak at m/z = 744.081 corresponding to the singly charged molecular ion [**ZnL3**+$3NO_3$]$^-$. Elemental analysis result agrees well with the proposed structure.

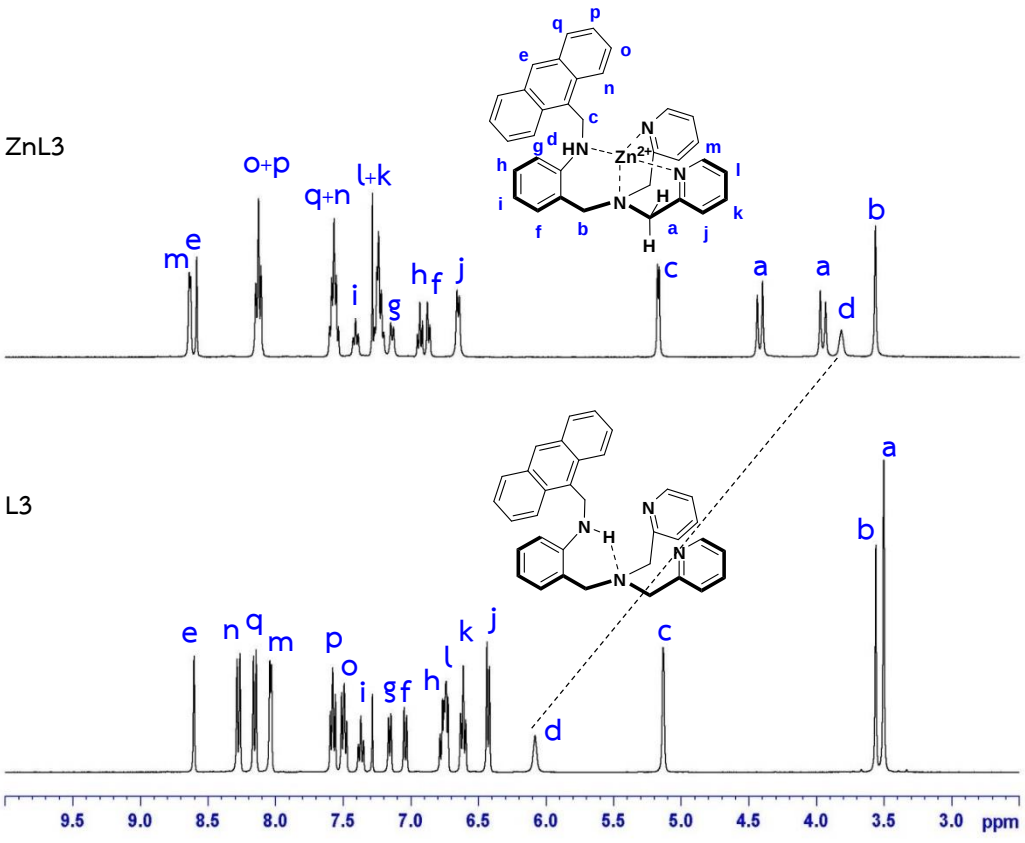


**Figure 21**. Comparison of $^{1}H$ NMR spectra of ligand **L3** and mononuclear complex **ZnL3** in $CDCl_3$

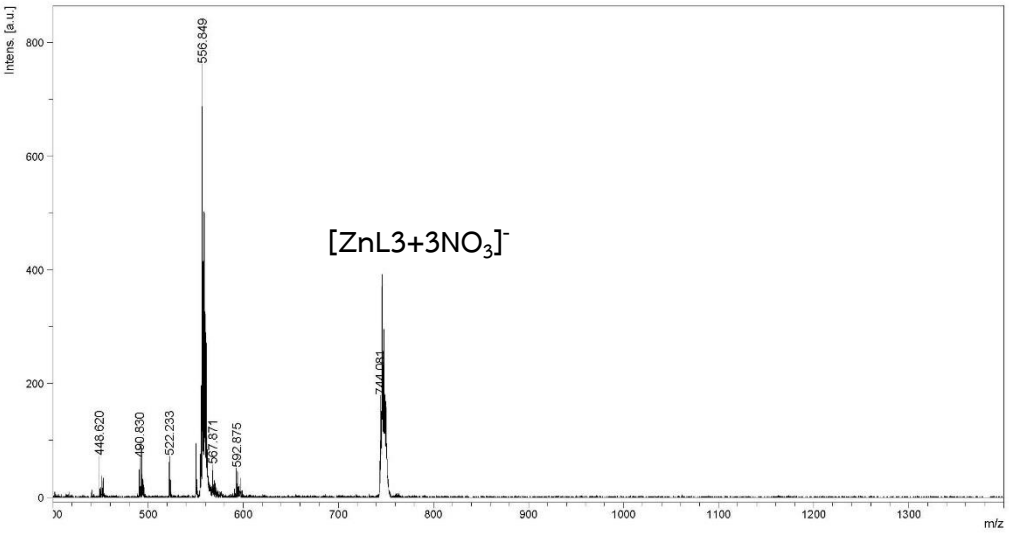


**Figure 22**. Mass spectrum of mononuclear complex **ZnL3**

## 4.3 Sensing of PPi under an indicator displacement assay

### 4.3.1 Screening tests of indicators for selective PPi sensing

I first tested the anion sensing capabilities of the receptor **$Zn_2$L2** by using an indicator displacement assay. In this study, 4 commercial dyes (Figure 23), pyrocatechol violet (**PV**), bromopyrogallol red (**BPG**), methylthymol blue (**MTB**) and xylenol orange (**XO**), which were complexometric indicators for the determination of metal ions were employed[79-81]. I prepared both 1:1 and 1:2 receptor to indicator ratios in 20% (v/v) water–acetonitrile solution buffered at pH 7.4 with HEPES to screen the sensing abilities toward **PPi** over other anions.

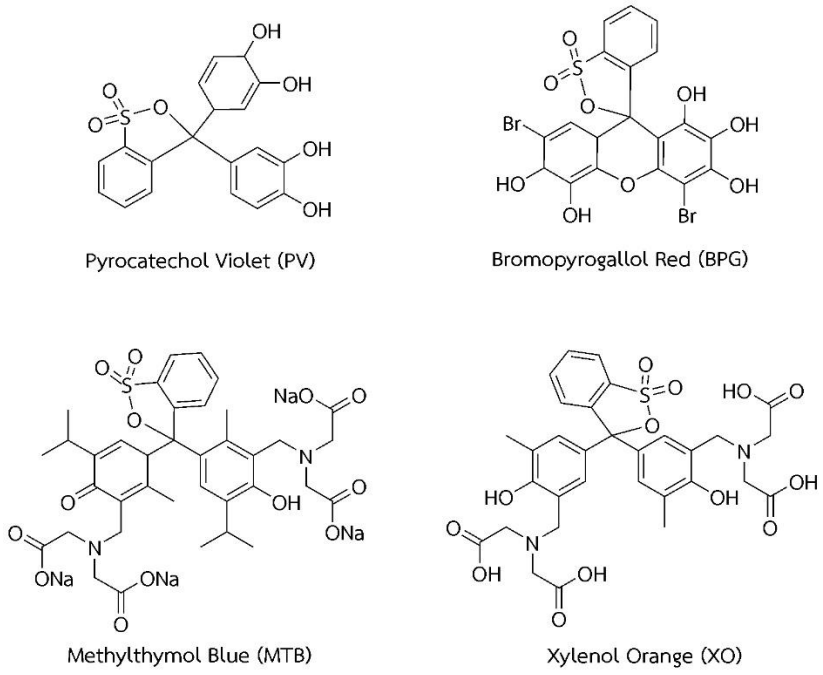


**Figure 23**. Structures of indicators employed in **PPi** sensing under the IDA studies.

After the addition of various anions (7.5 equivalents of tetrabutylammonium salts) to four ensemble solutions, I found that only the **[$Zn_2$L2·MTB]** ensemble was able to discriminate **PPi** from other anions as indicated by a color change from blue to purple shown in Figure 24, and giving the same result with [**$Cu_2$L2·MTB]** ensemble

(Figure S36). However, the **PV**– and **BPG–$Zn_2$L2** ensembles responded to all phosphate containing anions because the color of the corresponding ensembles was converted to the color of the free indicators. In the case of the **XO–$Zn_2$L2** ensemble, there were no significant changes upon addition of all anions. Therefore, the anions were not able to dislodge the **XO** indicator. Both **MTB** and **XO** have a similar core structure, they differ only in the bulky substituents on the rings. I expect that the binding affinity of the **$Zn_2$L2**–indicator ensemble must play an important role in the displacement of the indicator by an anion. Compared to dinuclear Zn(II)–DPA receptors which could undergo IDA using the indicator **PV**[50, 82, 83], my **$Zn_2$L2** needed a different indicator due to the change in coordination chemistry around the Zn(II) center.

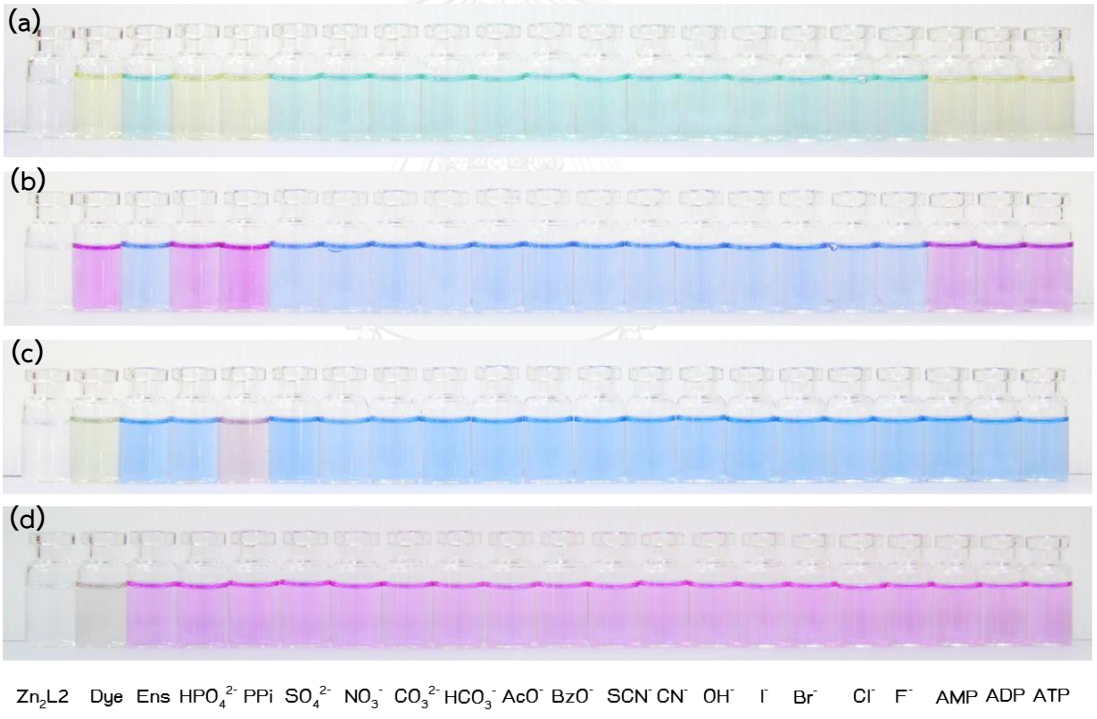


**Figure 24**. Color changes of the **$Zn_2$L2**-based (20 μM, 2 mL) ensembles (Ens) with various indicators (Dye) (400 μM, 0.2 mL) at a 1:2 receptor to indicator ratio (a) **PV**, (b) **BPG**, (c) **MTB** and (d) **XO** in the presence of various anions (1 mM, 0.3 mL) in 80/20 (%v/v) acetonitrile/aqueous solution buffered at pH 7.4 with HEPES.

### 4.3.2 Binding studies of $Zn_2L2$ with PPi by $^1H$ and $^{31}P$ NMR spectroscopy

The binding properties of **$Zn_2L2$** with **PPi** was studied by $^1H$ and $^{31}P$ NMR spectroscopy as well as UV-vis spectrophotometry. Upon adding portions of **PPi** (in 20% $D_2O/CD_3CN$) to the solution of **$Zn_2L2$**, the $^1H$ NMR spectrum of the **$Zn_2L2$** starts broaden indicating a fluxional behaviour (Figure 25). When 2 equivalents of **PPi** is added, the spectrum becomes resolved. All protons can be assigned by the HMQC technique. Interestingly, in the absence of **PPi** the aromatic proton *a* of the dinuclear complex **$Zn_2L2$** appears in a higher magnetic field region, at $\delta$= 5.3 ppm, probably due to the shielding effect of the ring current of the aromatic anthracene ring. Upon addition of **PPi**, the proton a disappears from the NMR spectrum and reappears in a more downfield region. The aromatic protons *b* and *c* move downfield and the methylene protons e and *f* move upfield. Therefore, protons on the aromatic ring A generally move significantly while protons *g, i, j* and *k* on the aromatic ring B move to a lesser extent. The proton *h* of the methylene linkage between anthracene and the tripodal amine unit, functioning as a pivot of the movement, stays sharp upon addition of **PPi**. The results imply that the aromatic ring A probably moves away from the anthracene moiety upon the binding of **PPi** to the Zn(II) center.

จุฬาลงกรณ์มหาวิทยาลัย
Chulalongkorn University

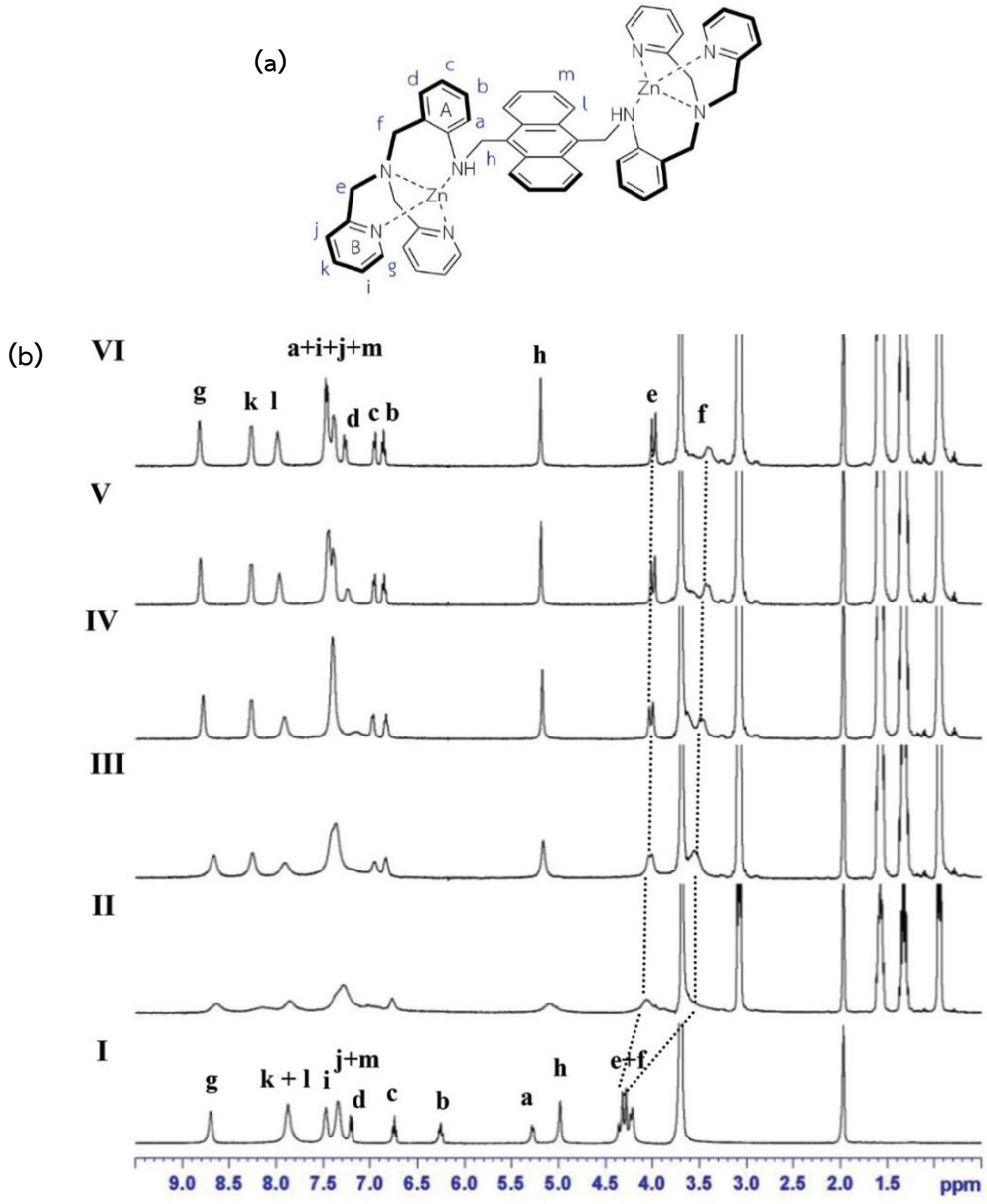


**Figure 25**. (a) structure of dinuclear complex **$Zn_2$L2** (b) $^1$H NMR spectra of (I) free **$Zn_2$L2**, (II) **$Zn_2$L2** + **PPi** 0.5 equiv., (III) **$Zn_2$L2** + **PPi** 1.0 equiv., (IV) **$Zn_2$L2** + **PPi** 1.5 equiv., (V) **$Zn_2$L2** + **PPi** 2.0 equiv. And (VI) **$Zn_2$L2** + **PPi** 2.5 equiv. in 20% $D_2O/CD_3CN$.

$^{31}$P NMR titrations of **$Zn_2$L2** in 20% $D_2O/CD_3CN$ with portions of **PPi** were carried out and the spectra are shown in Figure 26. The free **PPi** has a signal at −6.0 ppm. It can be clearly seen that adding up to 1.0 equivalent of **PPi** to the solution of **$Zn_2$L2** gave a single broad peak at −3.0 ppm due to the formation of a complex between an equivalent amount of **$Zn_2$L2** and **PPi** concomitant with the disappearance of the signal at −6.0 ppm. The single peak at −3.00 ppm implied that two P atoms in **PPi** bound **$Zn_2$L2** are magnetically equivalent. Upon adding more than 1 equivalents of **PPi** a signal at a more upfield position appears in the spectrum. After the addition of 4 equivalent of **PPi**, this peak shifts to a more downfield position, close to that of the signal of free **PPi** and the signal at −3.0 ppm becomes more resolved.

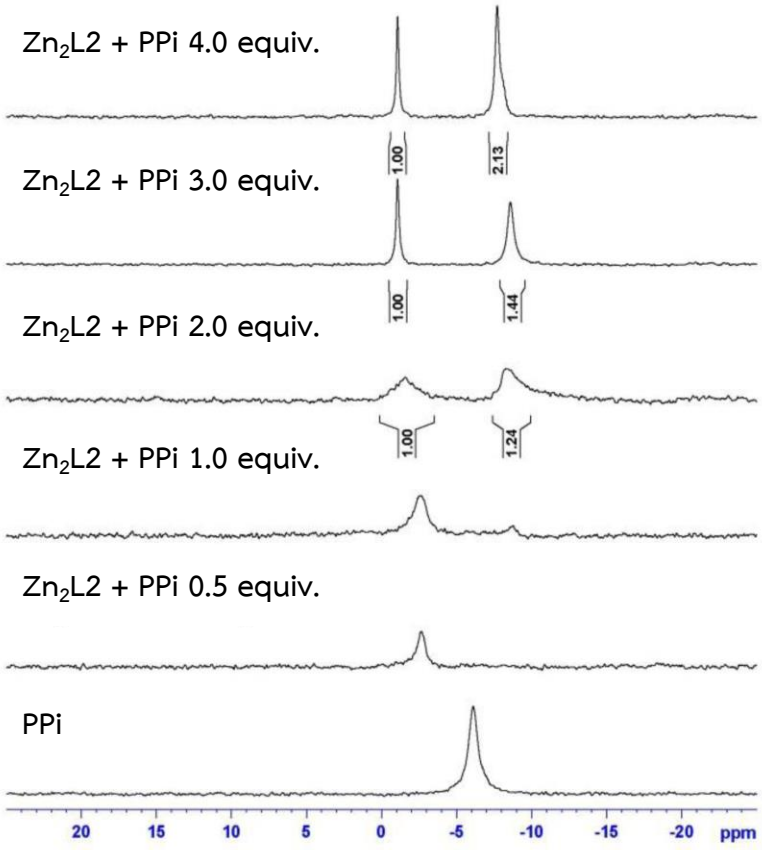


**Figure 26**. $^{31}$P NMR spectra of **$Zn_2$L2** (5 mM) upon addition of various concentrations of **PPi** (0.05 M) in 80/20 (%v/v) $CD_3CN/D_2O$.

The best way to obtain the exact structure of the **$Zn_2$L2–PPi** complex is from the crystal structure determination. However, I cannot obtain a suitable crystal of the complex for X-ray crystallography, probably due to the mixed solvent system ($H_2O/CH_3CN$) used in the preparation of the complex. Based on the several binding modes of **PPi** toward the metal center reported previously[84], the density functional theory (DFT) calculations of a possible complex of **$Zn_2$L2** and **PPi** in 1:1 and 2:2 fashions were carried out to find the most stable structure instead. According to computer simulations, the 1:1 complex model was not possible due to too much strain in the molecule of the 1:1 **PPi**-bound **$Zn_2$L2** complex. However, six conformers of dimeric 2:2 species represented as 2**$Zn_2$L2**·2**PPi** were found and their energies were calculated (Table S2 and Figure S37 – S42 in the appendix). All optimized structures were obtained by DFT calculations using the B3LYP/LANL2DZ level of theory[85-87] performed with the GAUSSIAN09 program. The most stable structure of 2**$Zn_2$L2**·2**PPi** is shown in Figure 27. The dimeric species is composed of two **$Zn_2$L2** and two **PPi** units forming a tetranuclear Zn(II) complex with **PPi** as bridging ligands. Two oxygen atoms on each phosphorus of **PPi** coordinated to one $Zn^{2+}$ ion, the same as the structure reported by Hong et al[34]. Interestingly, the calculated structure showed a high symmetry structure of the **PPi** units. This agreed with the result from the $^{31}$P NMR spectroscopy where the two phosphorous atoms in **PPi** appeared as a singlet peak the in $^{31}$P NMR spectrum. In addition, the calculated structure is also relevant to the signals that appeared in the $^{1}$H NMR spectrum shown in Figure 25. The calculated dimeric structure is similar to the structure of the **PPi** bound-dinuclear Zn(II) complex reported by Lee et al[88].

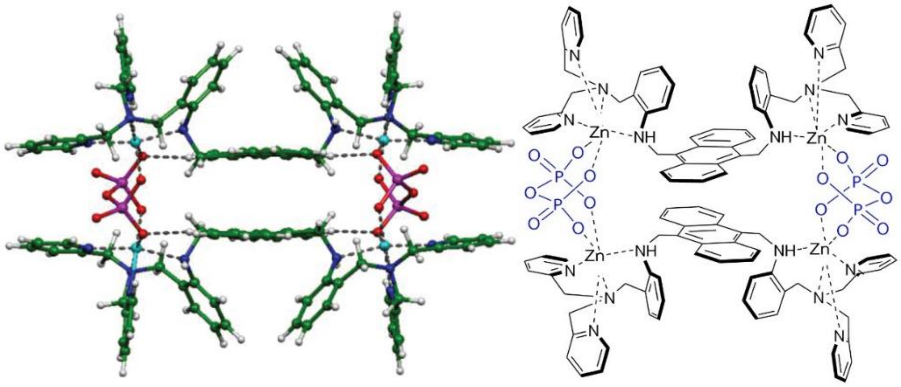

**Figure 27**. The most stable DFT-calculated structure of the dimeric 2:2 species, 2**$Zn_2$L2**·2**PPi** complex.

### 4.3.3 Binding studies of dinuclear complex $Zn_2$L2 with MTB and displacement studies with PPi using $^1$H NMR spectroscopy

Upon addition of portions of **MTB** (in 80/20 (%v/v) $CD_3CN/D_2O$) to the solution of **$Zn_2$L2**, $^1$H NMR spectra were obtained and are shown in Figure 28. The $^1$H NMR spectrum of **$Zn_2$L2** starts to broaden after adding portions of **MTB** and is too complicated to assign each proton signal. However, it can be clearly seen that upon adding more than 1 equivalent of **MTB** to **$Zn_2$L2**, the peak due to free **MTB** emerges in the spectrum.

Chulalongkorn University

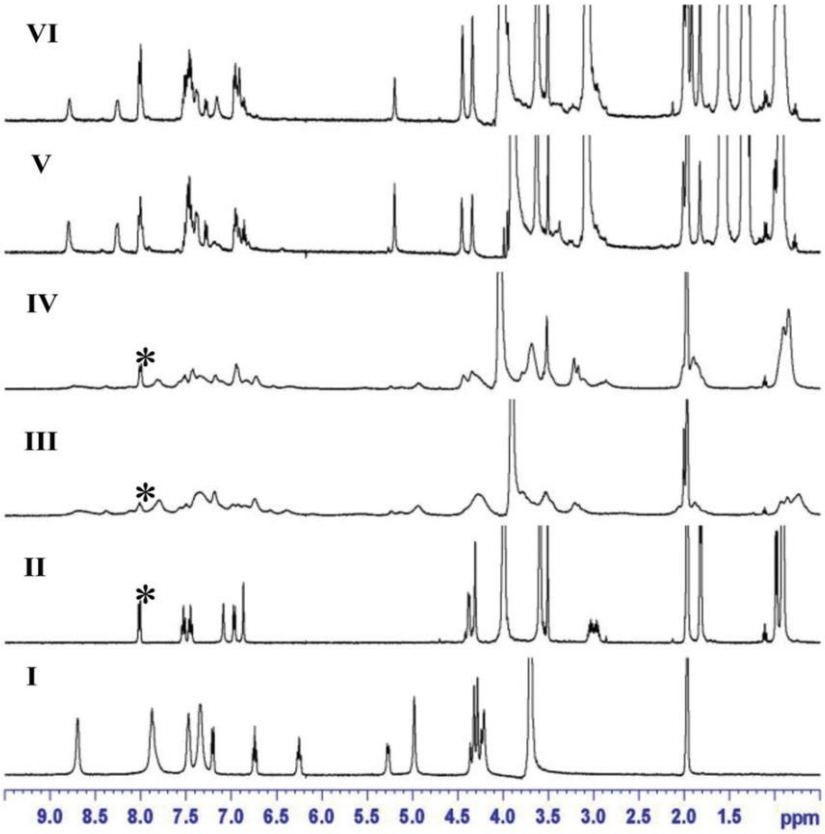


**Figure 28.** $^{1}$H NMR titration spectra of (I) free **$Zn_2$L2** (5 mM), (II) **MTB**, (III) **$Zn_2$L2·MTB**, (IV) **$Zn_2$L2**·2**MTB**, (V) **$Zn_2$L2·MTB** + 2.0 equiv. of **PPi** and (VI) **$Zn_2$L2**·2**MTB** + 2.0 equiv. of **PPi** in 80/20 (%v/v) $CD_3CN$ /$D_2O$, where * is the residue of free **MTB** present in the ensemble.

Therefore, $^{1}$H NMR titrations of 1:1 and 1:2 ensembles of **$Zn_2$L2** and **MTB** with **PPi** were carried out in 80/20 (%v/v) $CD_3CN/D_2O$ (Figure S43 and S44 in the appendix). The spectra were too complicated to clearly assign the signal to particular protons. Interestingly, after more than 1 equivalent of **PPi** was added, the spectra of both 1:1 and 1:2 ensembles became very similar and were almost the same as those observed for the 1:1 species of **$Zn_2$L2·PPi** shown in Figure 25. $^{31}$P NMR titrations of the 1:1 and 1:2 ensembles of **$Zn_2$L2** and **MTB** with **PPi** in 80/20 (%v/v) $CD_3CN/D_2O$ (Fig. S45 and S46 in the appendix) gave almost identical spectra to the results shown in Figure 26.

These results confirm that **MTB** can be replaced by **PPi**, and most of the final species are **PPi** bound **$Zn_2$L2**.

### 4.3.4 Studies of $Zn_2$L2–indicator ensembles by UV-vis spectrophotometry

From the above results, I can clearly see that the new **$Zn_2$L2** complex can be used to detect **PPi** selectively. Therefore, I studied the binding behaviors in aqueous solution using UV-vis spectrophotometry. To understand the sensing phenomenon of my ensembles, I had to determine the ensemble formation constants (log **β**) by employing the SPECFIT32 program. Typically, an experiment was carried out by the titration of **$Zn_2$L2** to a solution of each indicator. The addition of 0 to 0.4 equivalent of **$Zn_2$L2** to a solution of **MTB**, resulted in a bathochromic shift of the absorption around 450 nm to 530 nm (Figure 29a) and the color changed from pale green to violet (Figure 29c, vials no. i–v), visible to the naked eye. Subsequently, increasing the amount of **$Zn_2$L2** to the ensemble solutions, caused the bathochromic shift of the absorption at 530 nm to 600 nm and finally the blue color was observed (Figure 29c, vials no. vi–xi). The UV-vis spectrum at 600 nm was completely saturated around 1.3 equivalents of **$Zn_2$L2**.

จุฬาลงกรณ์มหาวิทยาลัย
Chulalongkorn University

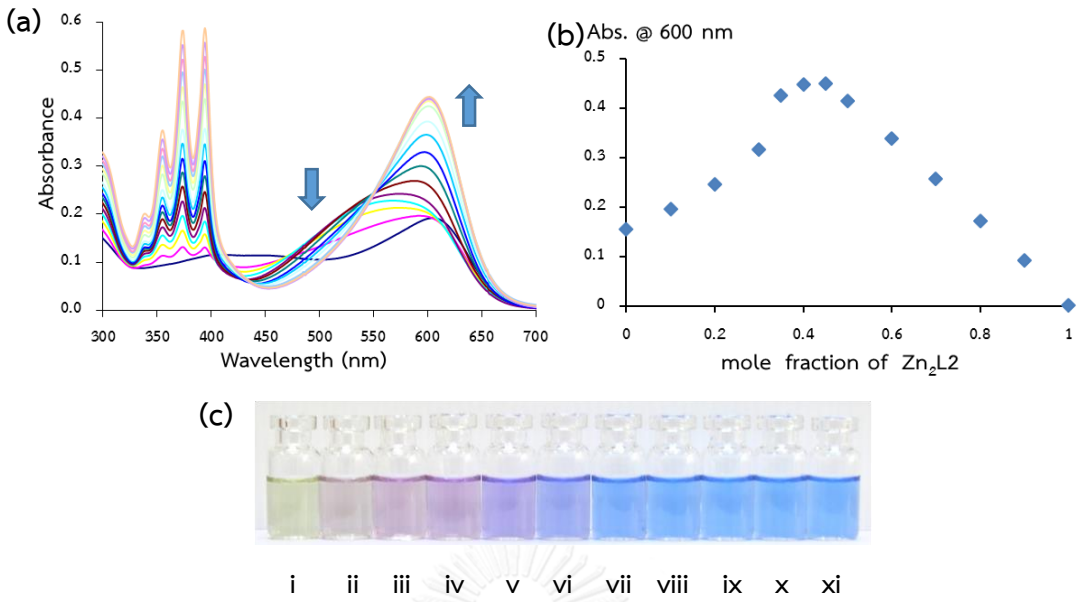


**Figure 29.** (a) UV-vis spectra obtained by the addition of **$Zn_2$L2** (400 μM) to a solution of **MTB** (20 μM), inset: Job's plot analysis of the **MTB**-based ensemble and (b) color changes upon increasing the amount of **$Zn_2$L2** (400 μM) to the **MTB** (20 μM) solution: (i) free **MTB**, (ii) 0.1 equiv., (iii) 0.2 equiv., (iv) 0.3 equiv., (v) 0.4 equiv., (vi) 0.5 equiv., (vii) 0.6 equiv., (viii) 0.7 equiv., (ix) 0.8 equiv., (x) 0.9 equiv. and (xi) 1.0 equiv.

จุฬาลงกรณ์มหาวิทยาลัย
Chulalongkorn University

The results showed that two species were formed during the titration. From the concentration profile, upon addition of **$Zn_2$L2** to the **MTB** solution, a complex of 1:2 species of **[$Zn_2$L2·2MTB]** was present in a maximum abundance of 15% at 10 μM of **$Zn_2$L2**. On further addition of **$Zn_2$L2**, a 1:1 species of **[$Zn_2$L·MTB]** could form in 80% abundance, which was much higher than that of the **[$Zn_2$L2·2MTB]** species, Figure 30. The presence of two co-existing ensemble species (1:1 and 1:2) agreed well with the Job's plot analysis of the ensembles (Figure 29b) and the unresolved $^1$H NMR spectra shown in Figure 28.

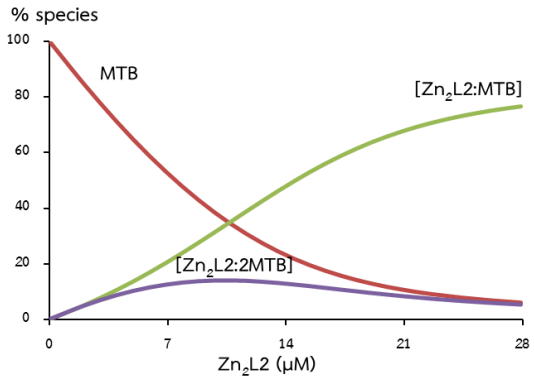


**Figure 30**. Concentration profiles of the species present at equilibrium in the UV-vis titration of **MTB**-base ensemble, where % is referred to the total concentration of **MTB**.

Ensembles of **$Zn_2$L2** and **PV**, **BPG** as well as **XO** were also studied by UV-vis spectrophotometry, and their absorption spectra are shown in Figure S38 –S40 in the appendix. Stepwise formation constants of all ensembles calculated by SPECFIT32 are tabulated in Table 1. The results showed that two species were formed during the titration. Upon addition of **$Zn_2$L2** to the indicator (**I**) solution, the 1:2 **$Zn_2$L2**·2**I** species occurred because the concentration of **I** was much higher than that of **$Zn_2$L2** at the beginning of titration. Further addition of **$Zn_2$L2** would yield the **$Zn_2$L2·I** species. Therefore, the **$Zn_2$L2·I** would exist in high concentration at the end of titrations. The presence of two co-existing ensemble species of those three indicators (1:1 and 1:2) agreed well with the Job's plots (Figure S47– S49 in the appendix).

**Table 1**. Stepwise ensemble formation constants (log **β**) between **$Zn_2$L2** and the indicators

| | **log $\beta_1$** | **log $\beta_2$** |
|---|---|---|
| **PV** | 3.98 ± 0.38 | 8.43 ± 0.22 |
| **BPG** | 4.76 ± 0.26 | 9.14 ± 0.26 |
| **MTB** | 6.05 ± 0.16 | 10.80 ± 0.32 |
| **XO** | 7.72 ± 0.18 | 13.48 ± 0.28 |

**XO** showed the highest binding constant (log $\beta_1$) to the **$Zn_2$L2** receptor compared to **PV**, **BPG** and **MTB** suggesting that **XO** could sit in the ensemble cleft with the strongest interactions with **$Zn_2$L2**. The log $\beta_1$ of **MTB** to **$Zn_2$L2** was lower than that of **XO**. Presumably, the two bulky isopropyl groups of **MTB**, giving the more steric hindrance than **XO**, decreased the binding affinity of **MTB** to the **$Zn^{2+}$** metal ions. For **PV** and **BPG** indicators, log $\beta_1$ values were smaller than that of **XO** and **MTB** suggesting that their structural scaffolds were less suitable for coordinating to the two metal centers in **$Zn_2$L2**.

จุฬาลงกรณ์มหาวิทยาลัย
Chulalongkorn University

### 4.3.5 PPi sensing studies by UV-vis spectrophotometry

The screen test of my IDA system suggests that **MTB** was the best indicator to be replaced solely by **PPi**. In addition, results from the NMR and UV-vis studies suggest that upon the addition of excess **MTB** to **$Zn_2$L2**, both 1:1 and 1:2 **[$Zn_2$L2·MTB]** were formed with the former most dominant in solution. To investigate the sensing ability of **PPi** under IDA experiments, the chemosensing ensembles were prepared by mixing **$Zn_2$L2** and the **MTB** indicator in a 1:2 molar ratio in 80/20 (%v/v) acetonitrile/aqueous solution buffered at pH 7.4 with HEPES. The displacement of indicators by anions was carried out by the addition of various anions to those ensemble solutions. Subsequently, colorimetric changes as well as the UV-visible spectra changes were examined. Upon addition of various anions (as tetrabutylammonium salts, 7.5

equivalents) to the **[$Zn_2$L2·MTB]** based ensemble solutions, only **PPi** could turn the color from blue to violet, while other anions did not give rise to either changes in the UV-vis spectra or in color. These results suggest that those anions did not interfere with the **PPi** sensing. Indeed, the lack of interference may be due to the fact that the binding affinities of the other anions with **$Zn_2$L2** are weaker than that of **MTB** with **$Zn_2$L2**. The results suggested that **MTB** possessed an appropriate affinity to **$Zn_2$L2** to facilitate such a selective response to **PPi**.

The addition of **PPi** 0–3 equivalents to the 1:2 base ensemble of [**$Zn_2$L2·2MTB]** led to the hypsochromic shift corresponding to the disappearance of the absorption band of the ensemble at 600 nm and the appearance of a new absorption band around 530 nm. The UV-vis spectrum at 530 nm was completely saturated at 3 equivalents of **PPi** (Figure 31a). In addition, the color of the ensemble turned from blue to violet. The apparent competitive binding constants of **PPi** with [**$Zn_2$L2·MTB]** in the displacement assay were determined by SPECFIT32 to be log $\beta_1$ = 8.97 ± 0.28 and log $\beta_2$ = 10.79 ± 0.28 corresponding to [**$Zn_2$L2·2PPi**] and [**2$Zn_2$L2·2PPi**], respectively (Figure 31b). The presence of the [**2$Zn_2$L2·2PPi**] species at the end of titration agreed well with the most stable structure shown in Figure 27 obtained from DFT calculations. It should be noted that, the observed violet color in the **PPi** competition experiments was similar to the color observed in the ensemble formation experiments (see Figure 29c, vial no. iii).

จุฬาลงกรณ์มหาวิทยาลัย
Chulalongkorn University

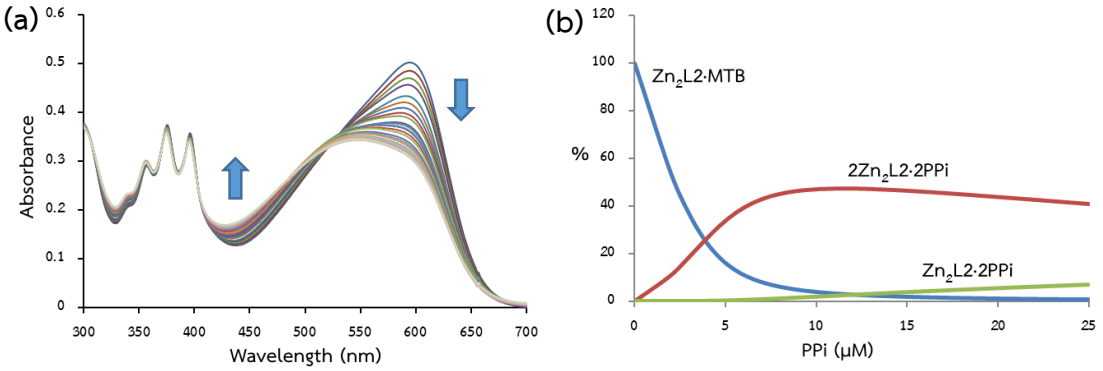


**Figure 31**. (a) UV-vis spectra obtained for the addition of **PPi** (1 mM) to a 1:2 ensemble solution of **$Zn_2$L2** and **MTB** (20 μM) and (b) concentration profiles of the species present at equilibrium in the UV-vis titration of **PPi** displaced [**$Zn_2$L2·MTB**] ensemble.

### 4.3.6. Studies of interferences and limit of detection

To further explore the effective applications of the [**$Zn_2$L2·MTB**] ensemble, the competition experiments were also measured. As shown in Figure 32a, even in the presence of a large excess of other competitive anions, no obvious interference with the detection of **PPi** was observed. These results clearly indicated that the [**$Zn_2$L2·MTB**] ensemble was useful for selectively sensing **PPi** even under competition from other related anions, which would fulfill the purpose of real-time monitoring. In addition, the detection limit of the absorption changes calculated on the basis of $3\sigma/K$ was 0.3 μM[89] (Figure 32b).

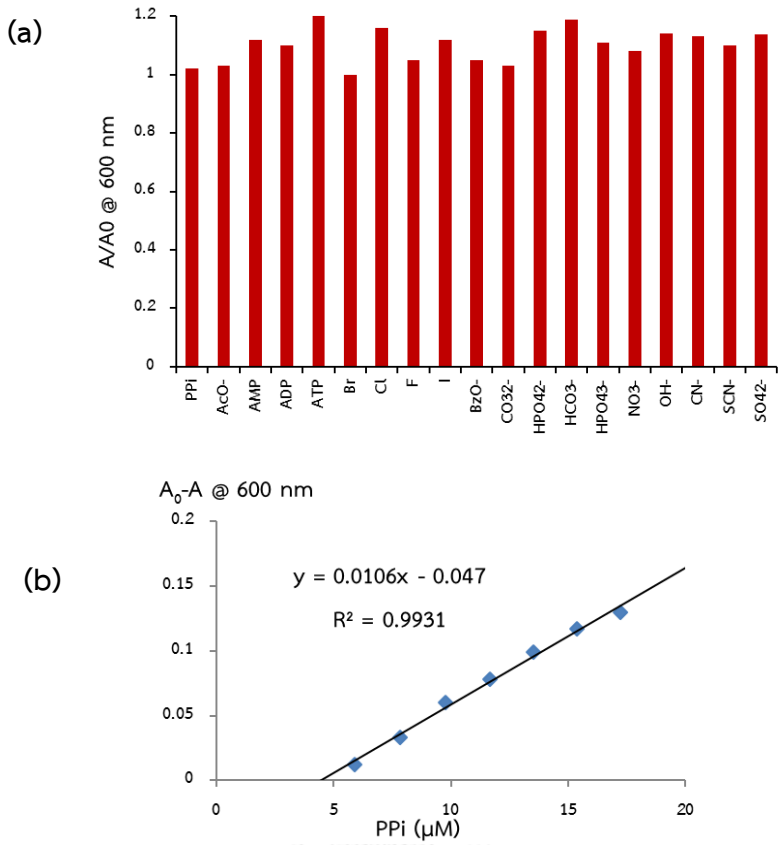


**Figure 32**. (a) Sensing of **PPi** in the presence of competitive anions (7.5 equivalents) in 80/20 (%v/v) acetonitrile/aqueous solution buffered at pH 7.4 with 10 mM HEPES (b) Calibration curve for detection of **PPi** using [**MTB·$Zn_2$L2**] ensemble.

## 4.4 Sensing of histidine under an indicator displacement assay

### 4.4.1 Sensing abilities studies of Zn2L2 based ensemble towards α-amino acids

From the previous results I found that [**Zn2L2•MTB**] ensemble could be used as metal complex-based IDA receptor for **PPi**. Consequently, I have tried to use **$Zn_2$L2** for selective detection of **α**-amino acids under IDA strategy in human urine sample. After addition of various 1 mM of 20 amino acids (10 equivalent) to [**$Zn_2$L2•MTB**] ensembles (20 μM) solutions, the results showed that [**$Zn_2$L2•MTB**] ensemble seems

to detect **His** selectively. However, **His** could not replace the Zn-bound **MTB** completely (Figure 33b). Presumably, the dicarboxylate indicator **MTB** is not an appropriate indicator in this system.

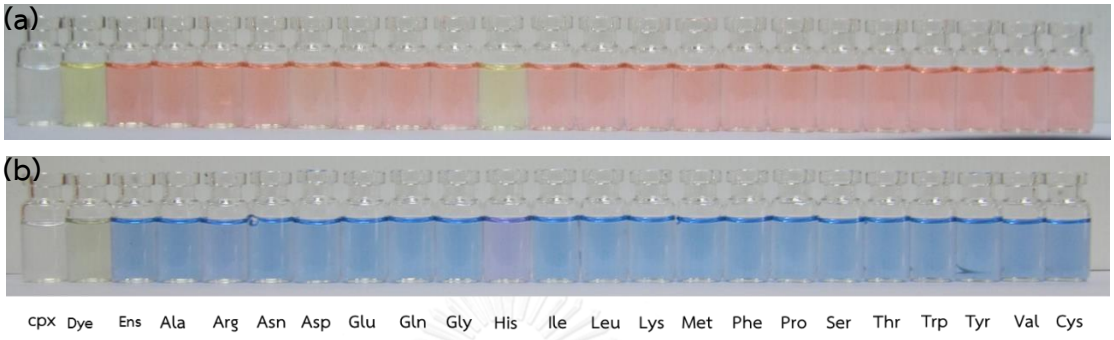


**Figure 33**. Color changes of (a) **[$Zn_2$L2·PAR]** and (b) **[$Zn_2$L2·MTB]** ensembles (20 μM) in the presence of various amino acids (1 mM) in 80/20 (%v/v) $CH_3CN/H_2O$ buffered at pH 7.4 with HEPES.

Then, a commercially available dye 4-(2-pyridylazo)resorcinol (**PAR**) having azo and -OH functional groups which is already known to be used as complexometric indicator for metal ion determination was chosen[43, 46, 90-94]. I envisaged that the **PAR** based ensemble with **$Zn_2$L2** complex should give the promising results in which **His** could replace **$Zn_2$L2**-bound **PAR** from its ensemble with the color change from red color of ensemble to the yellow color of the free **PAR** (Figure 33a), indicating the expected displacement of the indicator. Therefore, **PAR** is a suitable indicator for **His** under IDA condition. Indeed, the lack of interference stems from the fact that the binding constants of other amino acids with **$Zn_2$L2** complex are weaker than that of the ensemble of **$Zn_2$L2** and **PAR**. Therefore, to understand the interactions between **$Zn_2$L2** complex receptors with **PAR**, UV-vis spectrophotometry has been employed to study.

The addition of **$Zn_2$L2** to the yellow solution of **PAR** resulting in the bathochromic shift of absorption at $\lambda_{max}$ 400 nm of free **PAR** to 510 nm of ensemble,

being attributed to charge transfer in the ensemble. The absorption at 510 nm was saturated at 1.2 equivalent of **$Zn_2$L2**, Figure 34a. The ensemble formation constants (log **β**) were calculated to be 4.33 ± 0.4 and 10.67 ± 0.04 corresponding to [**$Zn_2$L2•PAR**] and [**$Zn_2$L2•2PAR**] species respectively, Figure 34b showed that [**$Zn_2$L2•2PAR**] is the dominated species in the solution. The presence of 1:2 ratio of **$Zn_2$L2** and **PAR** could be confirmed by Job's plot analysis, Figure 34c. By quantitative titration of a 1 mM solution of **His** in 20 μM of [**$Zn_2$L2•2PAR**] ensemble, the original absorption at 503 nm diminished as **His** was added, and a new absorption at 400 nm appeared (Figure S50 in appendix), responsible for the color change from red to yellow. It is implied that the bound **PAR** in the [**$Zn_2$L2•2PAR**] could be replaced by the added **His**. However, amino acids could behave as monodentate or polydentate ligand[95], the ternary complex of [**$Zn_2$L2•2His**] should be obtained in the displacement experiments. From this result, I expect that the ensemble between mononuclear complex analogue of **$Zn_2$L2**, **ZnL3**, and **PAR** could be exploited as chemosensing ensemble for **His** under IDA strategy.

จุฬาลงกรณ์มหาวิทยาลัย
Chulalongkorn University

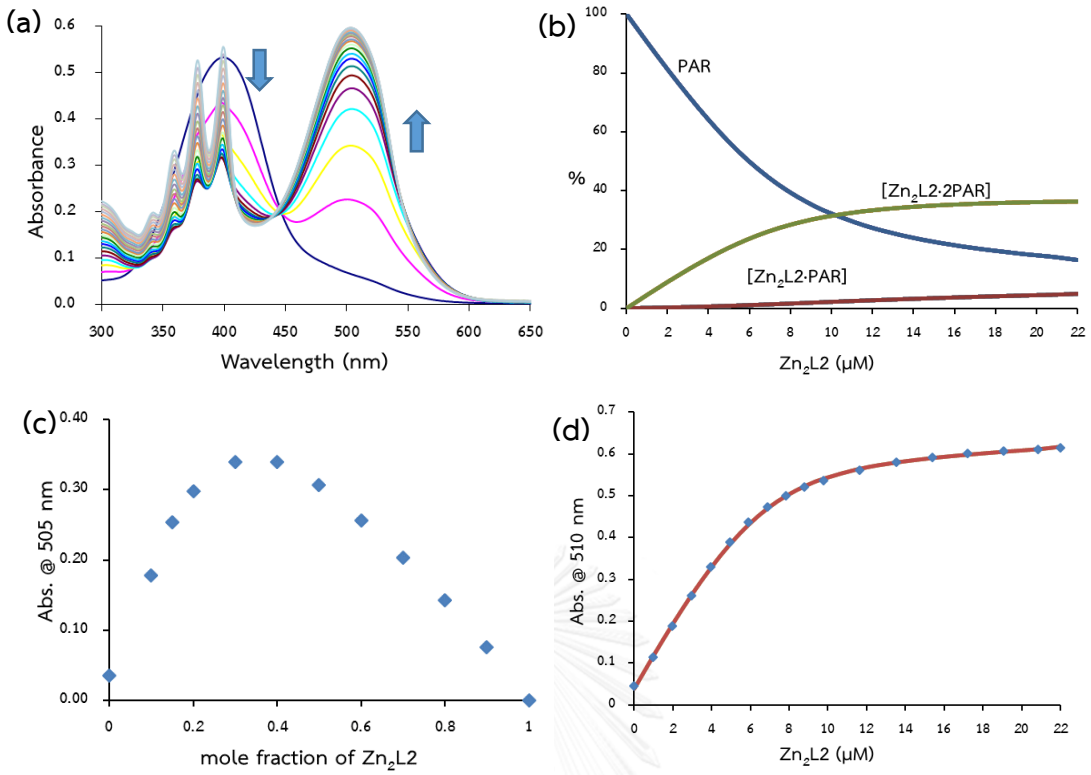


**Figure 34**. (a) UV/vis titration spectra obtained by addition of **$Zn_2$L2** (400 μM) to a solution of **PAR** (20 μM) (b) concentration profiles of the species present at equilibrium in the UV-vis titration of **[$Zn_2$L2·PAR]** base ensemble, where % is referred to the total concentration of **PAR** (c) Job's plot analysis in HEPES buffered pH 7.4 in 80/20 (% v/v) acetonitrile/aqueous solution and (d) A plot of absorption against concentration of **$Zn_2$L2** titrated in **PAR**. The red solid line is nonlinear least-squares fittings of the titration profiles using SPECFIT32 program.

### 4.4.2 Sensing abilities studies of ZnL3 based ensemble towards α-amino acids

Consequently, to test my hypothesis the sensing ensemble of **ZnL3** with **PAR** indicator was prepared in HEPES buffered pH 7.4 in 80/20 (% v/v) acetonitrile/aqueous solution. The sensing ability studies of this ensemble towards amino acids have been carried out in a similar fashion to [**$Zn_2$L2•2PAR**] ensemble. As I expected, the

mononuclear ensemble could discriminate **His** from the other amino acids similar to the dinuclear **$Zn_2$L2** ensemble (Figure 35c). Therefore, I decided to study the potential application of mononuclear **ZnL3** as **His** naked-eye sensor in biological fluid According to the UV-visible titration results in Figure 35a, the log **β** of **ZnL3** with **PAR** was calculated to be 6.85 ± 0.2 corresponding to 1:1 species of [**ZnL3•PAR**]. The sensing properties of [**ZnL3•PAR**] toward **His** was investigated by spectrophotometric titration.

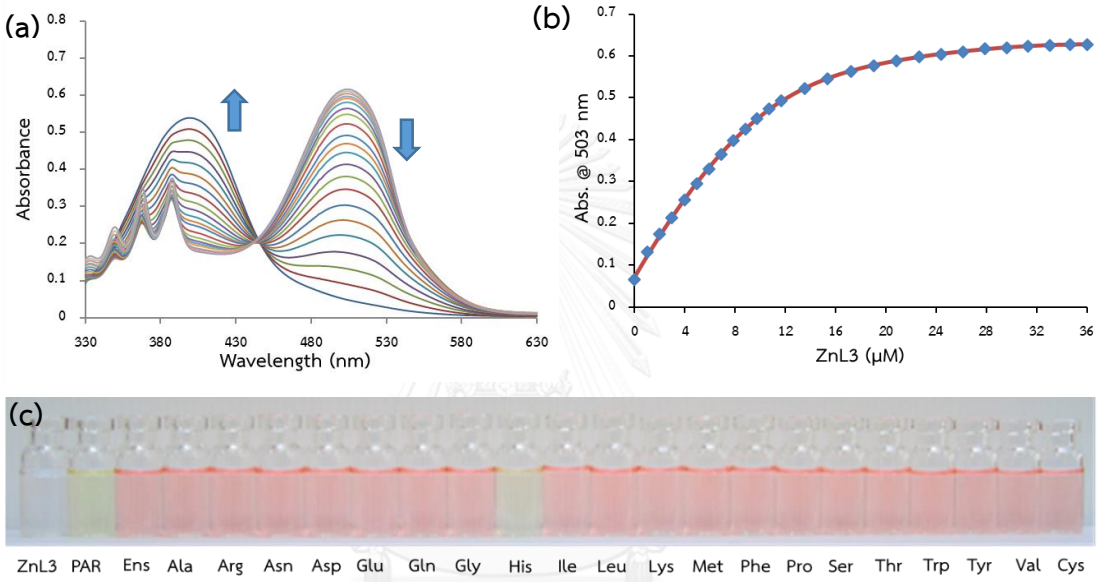


**Figure 35.** (a) UV/vis spectra obtained by addition of **ZnL3** (400 μM) to a solution of **PAR** (20 μM) in HEPES buffered pH 7.4 in 80/20 (% v/v) acetonitrile/aqueous solution (b) a plot of absorption against concentration of **ZnL3** titrated in **PAR**. The red solid line is nonlinear least-squares fittings of the titration profiles using SPECFIT32 program and (c) color changes of **[ZnL3·PAR]** ensemble (20 μM) in the present of various amino acids (12.5 equiv.).

The competition between **His** and the bound **PAR** was studied using UV-visible titrations. The addition of increasing amount of **His** 1 mM to a 20 μM solution of [**ZnL3•PAR**] results in significant changes in the absorption at 503 nm of the ensemble decreased concomitant with increasing in the absorption intensity at 400 nm of the

free **PAR**. The absorption at 400 nm was saturated at 10 equivalents of **His**, Figure S52 in the appendix. The color change from red to yellow was observed under IDA approach in which the log **β** of the complex [**ZnL3•His**] species was 6.92 ± 0.40. Moreover, the UV-visible for **His** titration also demonstrates that [**ZnL3•PAR**] has a detection limit toward **His** of 0.8 μM. The formation of ternary complex was further supported by HRMS, where solution of **ZnL3** was prepared in the presence His **1.2** equiv. The results from these measurements also demonstrated the molecular ion peak at m/z = 712.2373 which assigned to the complex of [**ZnL3•His**] species, Figure S53 in appendix.

I next investigated the formation of complex of [**ZnL3•His**] by using $^{1}$H-NMR titration experiments in 50/50 (%v/v) $D_2O/CD_3CN$. $^{1}$H NMR spectra recorded in the **[ZnL3•His**] system by varying the **ZnL3**-to-**His** ratio containing the coordination mode of the **ZnL3** as shown in Figure 36. Obviously, all of the observed signals are broadened. This phenomenon refers to the presence of ternary complex of [**ZnL3•His**], which are in relatively slow (intermediate) mutual exchange with each other and with the free **His**. The methylene protons of tripodal amine at **δ** around 4.6 – 4.9 ppm shifted upfield and overlapped to the proton signals of the added **His**, while all of the aromatic protons in **ZnL3** except aromatic protons *a* and *b* also shifted upfield. All the signal variations of the protons suggested that their chemical circumstances have been changed due to the coordination between **His** and $Zn^{2+}$ in **ZnL3** receptor. In addition, due to the low solubility of L3 in 50% $CD_3CN/D_2O$, therefore the removal of $Zn^{2+}$ from **L3** by **His** which would lead to observe in the precipitation of **L3** in the solution. Notably, upon increasing concentration of **His** to 4.0 equivalents no evidence of the solid of free **L3** precipitated. It indicates that **His** does not displace $Zn^{2+}$ from **L3** in the solution in this system, and the ternary complex of [**ZnL3•His**] still exists in the solution.

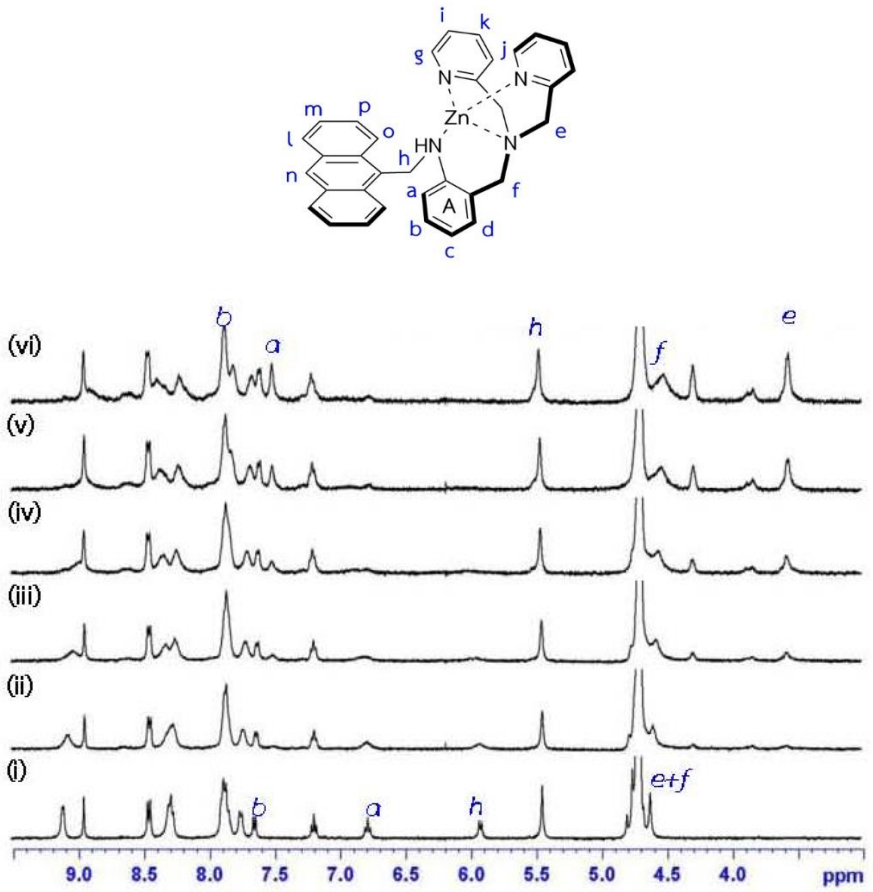


**Figure 36**. $^{1}$H NMR spectra of **ZnL3** (5 mM) upon addition of various concentrations of **His** (0.05 M) in 50% (v/v) $D_2O/CD_3CN$; (i) free **ZnL3**, (ii) **ZnL3** + **His** 0.2 equiv., (iii) **ZnL3** + His 0.4 equiv., (iv) **ZnL3** + **His** 0.6 equiv., (v) **ZnL3** + **His** 0.8 equiv. and (vi) **ZnL3** + **His** 1.0 equiv.

### 4.4.3 DFT Calculations of the adduct structure between ZnL3 and His

It is already known there are three binding modes of **His** to coordinate to metal ions.; (i) N,N- or histamine like structure[96], (ii) N,N,/O-[97] and (iii) N,O- or glycine like structure[98]. Therefore, the density functional theory (DFT) calculations of a possible complex of coordination of **His** to **ZnL3** were carried out to find the most stable structure. Three conformers of 1:1 **ZnL3**:**His** were found and their energies were calculated (Table S1 and Figure S54-S56 in appendix). All optimized structures were

obtained by DFT calculations using the B3LYP/LANL2DZ[85-87] level of theory performed with the GAUSSIAN09 program. All of calculated ternary structure showed that ligand **L3** behaves as a tridentate ligand in which **His** coordinated to $Zn^{2+}$ in **ZnL3** in both N,N,O- and N,O- fashions. The most stable structure of ternary complex of [**ZnL3•His**] is shown in Figure 37, in which the environment around $Zn^{2+}$ could be ascribed to a trigonal bipyramidal structure in which **His** coordinated to $Zn^{2+}$ in glycine like structure. The formation of 1:1 adduct agrees well with the result from the HRMS. In addition, the calculated structure is related to the signals that appeared in $^{1}$H-NMR spectrum that discussed so far.

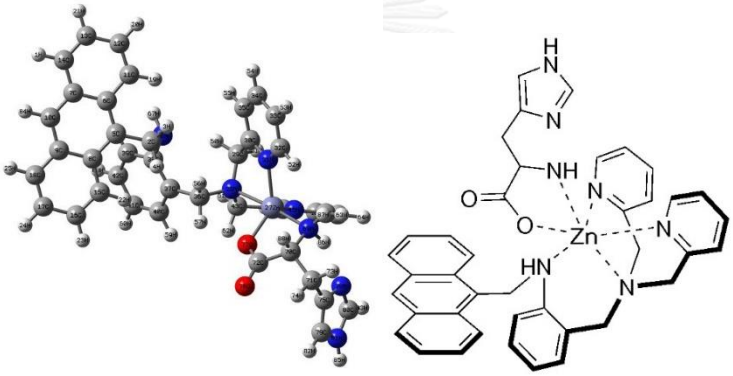


**Figure 37.** The most stable DFT-calculated structure of complex of [**ZnL3•His**].

### 4.4.4 His sensing studies by [ZnL3•PAR] ensemble in biological samples

For a practical application of **[ZnL3•PAR]** ensemble for **His** sensing in biological samples, some key issues should be taken into consideration. The interference of coexisting anions should be excluded. After the addition of 8 equivalents of anions to the [**ZnL3•PAR**] ensembles, it was found that [**ZnL3•PAR**] ensemble responded to all of phosphate containing anions because the red color of the corresponding ensembles was converted to the yellow color of the free **PAR** indicators as shown in Figure 38 (**[$Zn_2$L2•PAR]** ensemble giving the same result with **[ZnL3•PAR]** as shown in Figure S51). Therefore, [**ZnL3•PAR**] ensemble might not be proper to be used as

chemosensing ensemble for detect **His** in the real sample. Moreover, it is implied that the ensemble formation constant of **PAR** with **ZnL3** is weaker than that of the coexisting anions. The tolerance level was defined as the maximum amount of the interfering species producing an error of ±5% in His determination. The study was performed by analyzing 30 μM of **His** solution containing concomitant anions in different concentrations. The experiment results demonstrated that 2 μM **PPi**, 3 μM **ADP** and **ATP**, 7 μM $HPO_4^{2-}$ and 20 μM **AMP** could interfere with determination of **His** using the [**ZnL3•PAR**] ensemble system.

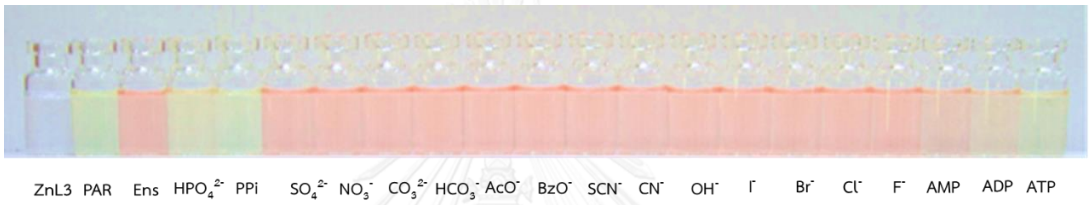


**Figure 38**. Color changes of [**ZnL3•PAR**] ensemble (20 μM) in the present of various anions in 10 mM HEPES buffered pH 7.4 in 80/20 (% v/v) acetonitrile/ aqueous solution.

According to the stability constants along Irving-William series, $Cu^{2+}$ ion shows the highest complex formation constants compared to the other first row transition metal series. Thus, it might be possible that the $Cu^{2+}$ complex with **L3**, **CuL3**, might be able to be a good candidate to detect **His** in real sample.

### 4.4.5 Sensing abilities studies of CuL3 based ensemble towards α-amino acids

So far, copper(II) complexes have been utilized as metal based indicator displacement assay chemosensor for amino acids[99]. Most of these reported showed a significant selectivity towards **His**. Therefore, I expected that the mononuclear **CuL3** might be applied as a suitable IDA receptor for **His**. Therefore, the chemosensing

ensemble of **CuL3** with **PAR** indicator was prepared and the sensing abilities towards **α**-amino acid and anions were investigated. Interestingly, I found that the proposed ensemble could discriminate **His** from the other amino acid completely in which the red color of ensemble turned to yellow color of free **PAR**, Figure 39a. Moreover, there was no observable color change noticeable upon mixing of **[CuL3·PAR]** ensemble with any anions indicated that anions could not replace the bound **PAR** from the coordination sphere of the ensemble as depicted in Figure 39b. The log **β** of **CuL3** with **PAR** was found to be 7.18 ± 0.5 corresponding to [**CuL3•PAR**] species by UV-visible titration, Figure S57 in appendix. It should be mentioned that log **β** of [**CuL3•PAR**] is higher than that of [**ZnL3•PAR**]. Therefore, [**CuL3•PAR**] ensemble is suitable for determination of His in human urine sample rather than [**ZnL3•PAR**] ensemble. Notably, the addition of other amino acids did not alter the initial absorption spectrum of the ensemble [**CuL3•PAR**] significantly, Figure 39c. From these absorption spectral studies, it is clear that the chemosensing ensemble [**CuL3•PAR**] shows a very high selective sensing affinity for **His** even in the presence of other amino acids. Thus, the ensemble [**CuL3•PAR**] can be used as a selective naked-eye sensor for **His** over other competing amino acids and anions in various environmental and biological systems.

จุฬาลงกรณ์มหาวิทยาลัย
Chulalongkorn University

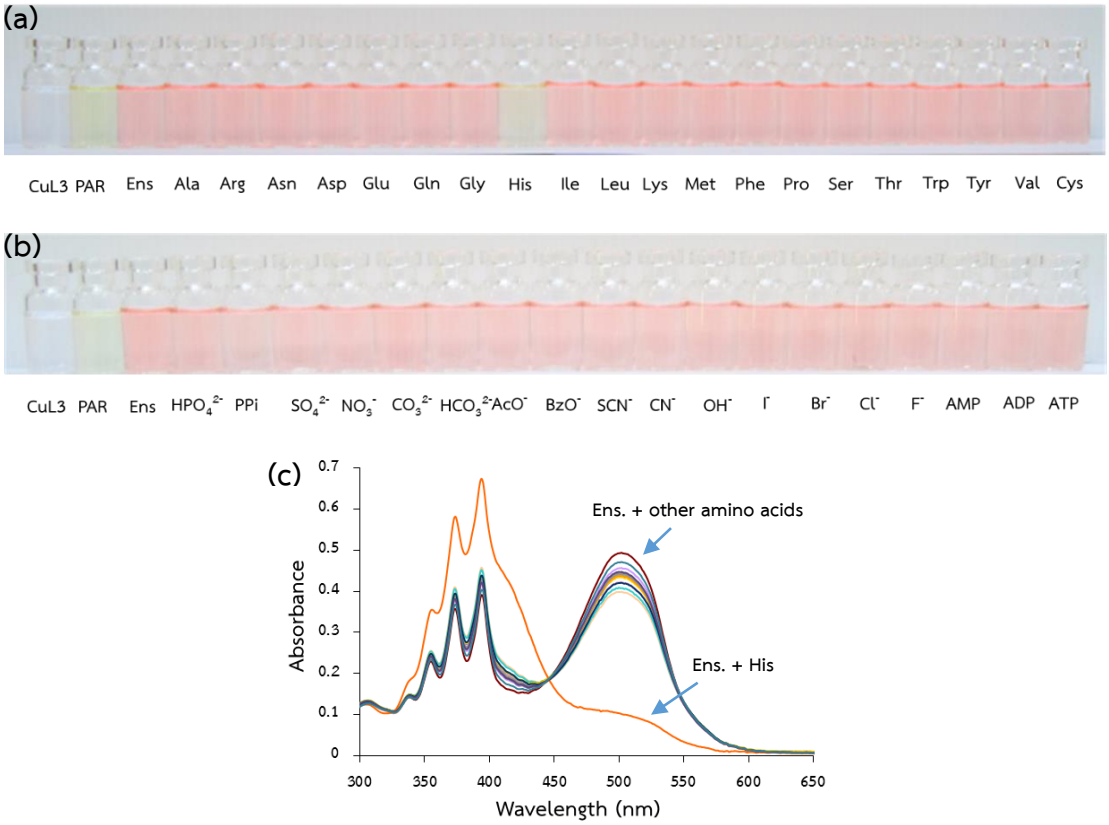


**Figure 39**. (a) color changes of **[CuL3·PAR]** ensemble (20 μM) in the present of various amino acids (12 equiv.) (b) color changes of [**CuL3·PAR]** ensemble (20 μM) in the presence of various anions (12 equiv.) and (c) UV–vis spectra obtained by addition of various amino acids (7.5 equiv) to [**CuL3•PAR**] (20 μM) ensemble in 10 mM HEPES buffered pH 7.4 in 80/20 (% v/v) acetonitrile/aqueous solution.

It is well known that the binding constants of **His** with $Cu^{2+}$ is very high (log K = 18.1)[100], therefore **His** might extract $Cu^{2+}$ ion from **CuL3** to release both free **L3** and **PAR** to the solution resulting in the yellow color of free **PAR**. In order to understand the sensing mechanism of **CuL3** towards **His**, I obtained the square wave voltammetry (SWV) of $CuCl_2$ and **CuL3** complex in the presence of **His**. Indeed, I are attempted to study the electrochemical behavior of **His** sensing under displacement assay by using my sensing ensemble. However, the experiments could not perform

due to the solubility problem of HEPES buffer. Therefore, the study of electrochemical behaviour of **CuL3** with **His** using square wave voltammetry was carried out in 20/80 (%v/v) acetonitrile/aqueous solution with 0.1 M $NaNO_3$ as supporting electrolyte. It was found that upon increasing concentration of **His** to 0.3 equivalents the pale yellow solids occurred in the solution. Figure 40 gives the SWVs of $Cu^{2+}$ and **CuL3** upon treatment with 3 equivalents of **His**. Because the SWV waves of **CuL3** after treating with His are similar to those of $Cu^{2+}$ with **His**, it indicates that $Cu^{2+}$ center is being pulled from the **L3** ligand to yield Cu(**His**)$_2$ species. The Cu (II/I) redox couple of **CuL3** occurs at -0.15 V and the more cathodic reduction wave appears at -0.70 V which is assigned to the Cu (I/0) couple[101]. Compared to redox couple of $Cu^{2+}$ in $CuCl_2$, the potential at -0.05 V and -0.70 V corresponding to the redox couples of Cu (II/I) and Cu (I/0), respectively. The addition of stoichiometric amounts of **His** to a solution of **CuL3** changed the voltammogram to that of [Cu(**His**)$_2$]. Moreover, $^1$H-NMR spectrum of a resulting solid precipitated during the electrochemical studies was identical to that of free ligand **L3**, Figure S58 in appendix. This result confirmed that $Cu^{2+}$ was removed from the **CuL3** complex and free **L3** was regenerated in presence of **His**.

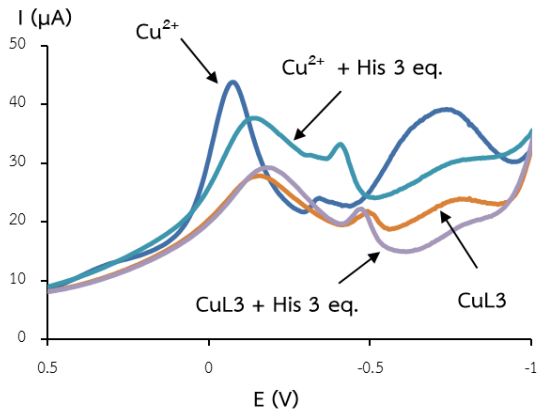


**Figure 40**. Square wave voltammograms of $Cu^{2+}$ and **CuL3** in the presence of **His** 3 equivalents scan rate 100 mV/s.

In addition, the ligand displacement of **His** with [**CuL3•PAR**] ensemble was studied by UV-visible titrations. Upon titration of **His** (1 mM) solution to the [**CuL3•PAR**] (20 μM) ensemble caused the color of the solution gradually changed from red to yellow while the absorption peak at 510 nm decreased but the absorption peak at 400 nm increased as shown in Figure 41. The UV-vis spectrum at 400 nm of was completely saturated around 7.5 equivalents of **His**. According to the results from electrochemical studies, it should be noted that the selective naked-eye detection of **His** by [**CuL3•PAR**] ensemble achieved on the ligand displacement between **His** and the bound **PAR** as well as ligand **L3**. As the binding constant for the interaction of $Cu^{2+}$ and **His** is 102 orders of magnitude larger than that of the interaction of $Cu^{2+}$ and **PAR**, the formation of [Cu(**His**)$_2$] is highly favorable.

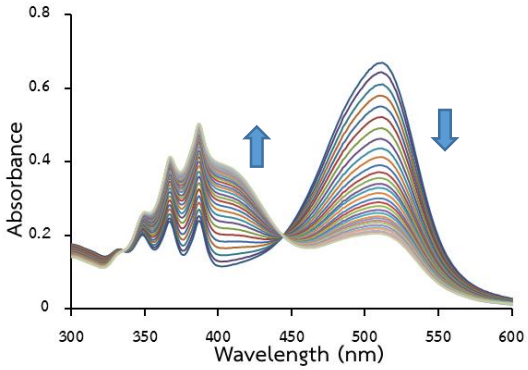


Chulalongkorn University

**Figure 41**. UV-Visible spectra obtained by addition of **His** (1 mM) to an ensemble solution of [**CuL3•PAR**] ensemble (20 μM), in HEPES buffered pH 7.4 in 80/20 (% v/v) acetonitrile/aqueous solution.

### 4.4.6 Analytical Performance for His detection

To collaborate the practical appliacability of [**CuL3•PAR**] ensemble as a selective naked-eye sensor for **His** under ligand displacement strategy, I carried out a competitive UV-visible study with other competing amino acids. As shown in Figure 42, even in the presence of large excess of other competitive amino acids, no obvious

interference with the detection of **His** was observed. These results clearly indicated that the [**CuL3•PAR**] ensemble was useful for selectively sensing **His** even the presence of such potential interfering amino acids.

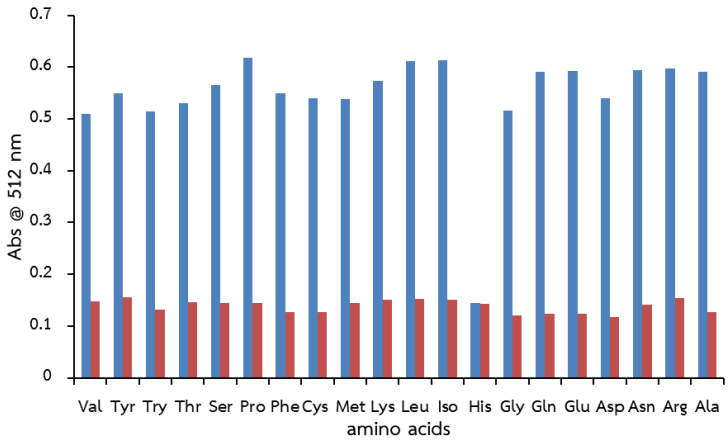


**Figure 42**. Absorption response of [**CuL3•PAR**] ensemble 20 μM to various amino acids in HEPES buffered pH 7.4 in 80/20 (% v/v) acetonitrile/aqueous solution. The blue bars represent the absorption of [**CuL3•PAR**] in the presence of amino acids 12.5 equivalents. The red bars represent the change of the absorption that occurs upon the subsequent addition of **His** to the various amino acids to the solution of [**CuL3•PAR**]. The intensities were recorded at 512 nm.

In order to further testify the potential of the newly developed chemosensing ensemble for the detection of **His** in real samples, I employed the proposed [**CuL3•PAR**] ensemble to determination **His** in human urine sample by standard addition method. To evaluate the sensitivity of the system for detecting **His** under displacement conditions, the absorbance at 510 nm of [**CuL3•PAR**] ensemble is monitored as a function of the **His**. It is clearly seen that with the increase of **His** concentration, the absorbance decrease gradually. The absorption exhibits a good linear relationship with **His** in the concentration range from 0 μM to 80 μM. The regression equation is y = -0.0063x + 0.7123, where x is final concentration of **His** in

μM and y is absorbance at 510 nm, with a correlation coefficient of 0.9977, Figure 43. The limit of detection (3σ/k)[89] for **His** was 0.5 μM which is lower than that of [**ZnL3•PAR**] ensemble and this level of the detection limit is sufficient to sense **His** even in biological systems because the normal concentration of **His** in human urine sample is 130 mM and 2100 mM[4].

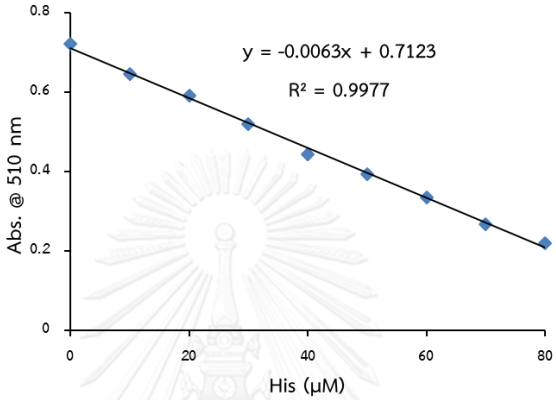


**Figure 43**. Calibration curve for detection of **His** using [**CuL3•PAR**] ensemble.

The relative standard deviation for 10 replicate detections of 10 μM **His** was 3.0%. The analytical utility of the [**CuL3•PAR**] ensemble for the analysis of **His** was tested using spiked **His** to urine sample. Table 2 showed the results obtained for the recoveries for spiking 10, 20 and 30 μM of **His** in urine samples range from 98.3% to 102.3% with a generally satisfactory precision. Therefore, it is feasible to apply the proposed sensor to quantitatively determine the concentration of **His** in urine samples.

**Table 2**. Analytical results for **His** in human urine samples.

| Sample | Concentration of **His** (μM) | | Recovery (%) |
|---|---|---|---|
| | Amount Added | Amount found [a] | |
| **Urine 1** | 10 | 9.80 ± 0.3 | 99.4 |
| **Urine 2** | 20 | 21.2 ± 0.5 | 98.3 |
| **Urine 3** | 30 | 29.2 ± 0.9 | 102.3 |

[a] Average for three determinations

จุฬาลงกรณ์มหาวิทยาลัย
Chulalongkorn University

# CHAPTER V

# CONCLUSIONS

In conclusion, two ligands based on anthracene platform containing tripodal amine units for accommodating metal ions were synthesized. Ditripodal amine ligand **L2** and monotripodal amine **L3** were obtained in 41% and 55% yields, respectively. Dinuclear copper(II) complex of ligand **L2** (**$Cu_2$L2**) and mononuclear copper(II) of ligand **L3** (**CuL3**) (Figure 44) can be obtained as green solids in 90% and 73% yields, respectively. In addition, dinuclear zinc(II) complex of ligand **L2** (**$Zn_2$L2**) and mononuclear zinc(II) complex of **L3** (**ZnL3**) (Figure 44) can be synthesized as yellow solids in 88% and 70% yields, respectively. The structures of all synthesized ligands and coordination compounds were fully characterized by NMR spectroscopy, mass spectrometry, elemental analysis and X-ray crystallography.

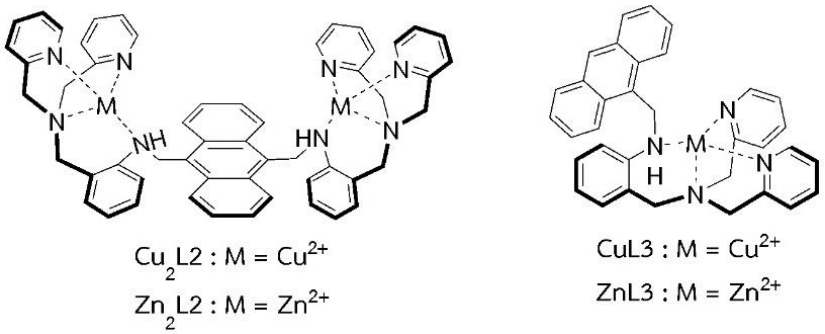


**Figure 44**. Structures of dinuclear complexes **$Cu_2$L2** and **$Zn_2$L2** and mononuclear complexes **CuL3** and **ZnL3**.

Sensing applications of **$Cu_2$L2**, **CuL3**, **$Zn_2$L2** and **ZnL3** as IDA receptors for anions and $\alpha$-amino acids were investigated. For sensing of anions under indicator displacement assay, I demonstrated for the first time that the tripodal amine dinuclear Zn(II) complex **$Zn_2$L2** could be used to discriminate **PPi** from other phosphate containing anions using **MTB** as the reporting indicator. Based on DFT calculations and

NMR data, the binding mode of **PPi** to **$Zn_2$L2** was the 2:2 complex species. It was found that the **MTB** indicator possessed suitable binding affinities with **$Zn_2$L2** compared to the previously reported **PV** indicator found in dinuclear Zn(II)–DPA systems resulting in the high discrimination between **PPi** and other phosphate containing anions. Therefore, the new [**$Zn_2$L2·MTB]** ensemble system could be used to detect **PPi** selectively with the detection limit of 0.3 μM in 80/20 (%v/v) acetonitrile/aqueous solution buffered at pH 7.4 with HEPES.

For sensing of α-amino acids under indicator displacement assay, the dinuclear **$Zn_2$L2** and mononuclear complexes **CuL3** and **ZnL3** were investigated as "naked-eye" sensor for histidine **(His)**. The [**$Zn_2$L2•PAR]** ensemble could be used to discriminate **His** from other amino acids. However, in the presence of the phosphate containing anions such as **PPi**, the [**$Zn_2$L2•PAR]** ensemble also responded to the phosphate containing anions. Moreover, mononuclear ensemble [**ZnL3•PAR]** showed that it could discriminate **His** from the other amino acids similar to the dinuclear [**$Zn_2$L2•PAR]** ensemble and all phosphate containing anions could interfere this system. Therefore, the mononuclear **CuL3** was used to detect **His** because $Cu^{2+}$ showed higher binding affinity to **His** than $Zn^{2+}$. It was found that the ensemble of **[CuL3·PAR]** showed highly selective sensing for **His** in urine samples in the presence of other amino acids and phosphate containing anions. The result from UV-vis spectrophotometry, square wave voltammetry and $^1$H-NMR experiments suggested that **His** displaced **PAR** and **L3** moieties from the $Cu^{2+}$ center. Therefore, the mononuclear ensemble **[CuL3·PAR]** could be used to detect **His** selectively with the detection limit of 0.5 μM in 80/20 (%v/v) acetonitrile/aqueous solution buffered at pH 7.4 with HEPES.

**Suggestions for future works**

Try to obtain the single crystals of complexes, ensembles and the product from the displacement conditions and try to apply all of receptors to detect other anions or importance biological molecules under the indicator displacement assay approach by modify structure of receptors or changing the indicators.

## REFERENCES


[1] Hargrove, A.E., Nieto, S., Zhang, T., Sessler, J.L., and Anslyn, E.V. Artificial Receptors for the Recognition of Phosphorylated Molecules. Chemical Reviews 111(11) (2011): 6603-6782.

[2] Meyers, R.A. Reviews in Cell Biology and Molecular Medicine. Encyclopedia of Molecular Cell Biology and Molecular Medicine 2 (2008): 1147-1151.

[3] Sullivan, D.J., Gluzman, I.Y., and Goldberg, D.E. Plasmodium Hemozoin Formation Mediated by Histidine-Rich Proteins. Science 271(5246) (1996): 219-222.

[4] Guo Nan, C., Xiao Ping, W., Jian Ping, D., and Hong Qing, C. A study on electrochemistry of histidine and its metabolites based on the diazo coupling reaction. Talanta 49(2) (1999): 319-330.

[5] Rao, M.L., Stefan, H., Scheid, C., Kuttler, A.D.S., and Froscher, W. Serum Amino Acids, Liver Status, and Antiepileptic Drug Therapy in Epilepsy. Epilepsia 34(2) (1993): 347-354.

[6] Kovach, P.M. and Meyerhoff, M.E. Development and application of a histidine-selective biomembrane electrode. Analytical Chemistry 54(2) (1982): 217-220.

[7] Kim, S.K., Lee, D.H., Hong, J.-I., and Yoon, J. Chemosensors for Pyrophosphate. Accounts of Chemical Research 42(1) (2009): 23-31.

[8] Liang, L.J., Zhao, X.J., and Huang, C.Z. Zn(ii) complex of terpyridine for the highly selective fluorescent recognition of pyrophosphate. Analyst 137(4) (2012): 953-958.

[9] Yang, S., Feng, G., and Williams, N.H. Highly selective colorimetric sensing pyrophosphate in water by a NBD-phenoxo-bridged dinuclear Zn(ii) complex. Organic & Biomolecular Chemistry 10(29) (2012): 5606-5612.

[10] Hamad, M. and Klein, J.R. Phenotypic and functional heterogeneity of murine intestinal intraepithelial lymphocytes defined by cell density: implications for route of differentiation and responsiveness to proliferation induction. Immunology 82(4) (1994): 611-616.

[11] Nyren, P., Pettersson, B., and Uhlen, M. Solid Phase DNA Minisequencing by an Enzymatic Luminometric Inorganic Pyrophosphate Detection Assay. Analytical Biochemistry 208(1) (1993): 171-175.

[12] Ronaghi, M., Karamohamed, S., Pettersson, B., Uhlén, M., and Nyrén, P. Real-Time DNA Sequencing Using Detection of Pyrophosphate Release. Analytical Biochemistry 242(1) (1996): 84-89.

[13] Kawasaki, M., Li, P., and Yamamoto, H. Enantioselective O-Nitroso Aldol Reaction of Silyl Enol Ethers. Angewandte Chemie International Edition 47(20) (2008): 3795-3797.

[14] Tateda, N., Matsuhisa, K., Hasebe, K., Kitajima, N., and Miura, T. High-performance liquid chromatographic method for rapid and highly sensitive determination of histidine using postcolumn fluorescence detection with o-phthaldialdehyde. Journal of Chromatography B: Biomedical Sciences and Applications 718(2) (1998): 235-241.

[15] Zhang, L.-Y. and Sun, M.-X. Determination of histamine and histidine by capillary zone electrophoresis with pre-column naphthalene-2,3-dicarboxaldehyde derivatization and fluorescence detection. Journal of Chromatography A 1040(1) (2004): 133-140.

[16] Inoue, T. and Kirchhoff, J.R. Electrochemical Detection of Thiols with a Coenzyme Pyrroloquinoline Quinone Modified Electrode. Analytical Chemistry 72(23) (2000): 5755-5760.

[17] Amini, M.K., Shahrokhian, S., and Tangestaninejad, S. PVC-Based Mn(III) Porphyrin Membrane-Coated Graphite Electrode for Determination of Histidine. Analytical Chemistry 71(13) (1999): 2502-2505.

[18] Kurzą tkowska, K., Shpakovsky, D., Radecki, J., Radecka, H., Jingwei, Z., and Milaeva, E. Iron (III) porphyrin bearing 2,6-di-tert-butylphenol pendants deposited onto gold electrodes for amperometric determination of l-histidine. Talanta 78(1) (2009): 126-131.

[19] Shahlaei, M., Gholivand, M.B., and Pourhossein, A. Simultaneous Determination of Tyrosine and Histidine by Differential Pulse Cathodic Stripping Voltammetry

Using H-point Standard Addition Method in Tap and Seawater. Electroanalysis 21(22) (2009): 2499-2502.

[20] Razi, S.S., Ali, R., Srivastava, P., Shahid, M., and Misra, A. An azo based colorimetric probe for the detection of cysteine and lysine amino acids and its real application in human blood plasma. RSC Advances 4(33) (2014): 16999-17007.

[21] De Santis, G., Fabbrizzi, L., Licchelli, M., Poggi, A., and Taglietti, A. Molecular Recognition of Carboxylate Ions Based on the Metal–Ligand Interaction and Signaled through Fluorescence Quenching. Angewandte Chemie International Edition in English 35(2) (1996): 202-204.

[22] Fabbrizzi, L., et al. Fluorescent molecular sensing of amino acids bearing an aromatic residue. Journal of the Chemical Society, Perkin Transactions 2 (11) (2001): 2108-2113.

[23] Fabbrizzi, L., Francese, G., Licchelli, M., Perotti, A., and Taglietti, A. Fluorescent sensor of imidazole and histidine. Chemical Communications (6) (1997): 581-582.

[24] Wu, P. and Yan, X.-P. $Ni^{2+}$-modulated homocysteine-capped CdTe quantum dots as a turn-on photoluminescent sensor for detecting histidine in biological fluids. Biosensors and Bioelectronics 26(2) (2010): 485-490.

[25] Azath, I.A. and Pitchumani, K. Flavone modified-$\beta$-cyclodextrin as a highly selective and efficient fluorescent chemosensor for $Cu^{2+}$ ions and l-histidine. Sensors and Actuators B: Chemical 188 (2013): 59-64.

[26] Huang, Z., Du, J., Zhang, J., Yu, X.-Q., and Pu, L. A simple and efficient fluorescent sensor for histidine. Chemical Communications 48(28) (2012): 3412-3414.

[27] Kruppa, M., Mandl, C., Miltschitzky, S., and König, B. A Luminescent Receptor with Affinity for N-Terminal Histidine in Peptides in Aqueous Solution. Journal of the American Chemical Society 127(10) (2005): 3362-3365.

[28] Martínez-Máñez, R. and Sancenón, F. Fluorogenic and Chromogenic Chemosensors and Reagents for Anions. Chemical Reviews 103(11) (2003): 4419-4476.

[29] Wiskur, S.L., Ait-Haddou, H., Lavigne, J.J., and Anslyn, E.V. Teaching Old Indicators New Tricks. Accounts of Chemical Research 34(12) (2001): 963-972.

[30] Nguyen, B.T. and Anslyn, E.V. Indicator–displacement assays. Coordination Chemistry Reviews 250(23–24) (2006): 3118-3127.

[31] Han, M.S. and Kim, D.H. Naked-Eye Detection of Phosphate Ions in Water at Physiological pH: A Remarkably Selective and Easy-To-Assemble Colorimetric Phosphate-Sensing Probe. Angewandte Chemie International Edition 41(20) (2002): 3809-3811.

[32] Hanshaw, R.G., Hilkert, S.M., Jiang, H., and Smith, B.D. An indicator displacement system for fluorescent detection of phosphate oxyanions under physiological conditions. Tetrahedron Letters 45(47) (2004): 8721-8724.

[33] Fabbrizzi, L., Marcotte, N., Stomeo, F., and Taglietti, A. Pyrophosphate Detection in Water by Fluorescence Competition Assays: Inducing Selectivity through the Choice of the Indicator. Angewandte Chemie International Edition 41(20) (2002): 3811-3814.

[34] Lee, J.H., Park, J., Lah, M.S., Chin, J., and Hong, J.-I. High-Affinity Pyrophosphate Receptor by a Synergistic Effect between Metal Coordination and Hydrogen Bonding in Water. Organic Letters 9(19) (2007): 3729-3731.

[35] Morgan, B.P., He, S., and Smith, R.C. Dizinc Enzyme Model/Complexometric Indicator Pairs in Indicator Displacement Assays for Inorganic Phosphates under Physiological Conditions. Inorganic Chemistry 46(22) (2007): 9262-9266.

[36] Kim, S.Y. and Hong, J.-I. Dual signal (color change and fluorescence ON–OFF) ensemble system based on bis(Dpa-CuII) complex for detection of PPi in water. Tetrahedron Letters 50(17) (2009): 1951-1953.

[37] Tang, L., Li, Y., Zhang, H., Guo, Z., and Qian, J. A new chemosensing ensemble for fluorescent recognition of pyrophosphate in water at physiological pH. Tetrahedron Letters 50(49) (2009): 6844-6847.

[38] Watchasit, S., Kaowliew, A., Suksai, C., Tuntulani, T., Ngeontae, W., and Pakawatchai, C. Selective detection of pyrophosphate by new tripodal amine calix[4]arene-based Cu(II) complexes using indicator displacement strategy. Tetrahedron Letters 51(26) (2010): 3398-3402.

[39] McCleskey, S.C., Metzger, A., Simmons, C.S., and Anslyn, E.V. Competitive indicator methods for the analysis of citrate using colorimetric assays. Tetrahedron 58(4) (2002): 621-628.

[40] Schmuck, C. and Schwegmann, M. A naked-eye sensing ensemble for the selective detection of citrate-but not tartrate or malate-in water based on a tris-cationic receptor. Organic & Biomolecular Chemistry 4(5) (2006): 836-838.

[41] Fabbrizzi, L., Leone, A., and Taglietti, A. A Chemosensing Ensemble for Selective Carbonate Detection in Water Based on Metal–Ligand Interactions. Angewandte Chemie 113(16) (2001): 3156-3159.

[42] Aït-Haddou, H., Wiskur, S.L., Lynch, V.M., and Anslyn, E.V. Achieving Large Color Changes in Response to the Presence of Amino Acids: A Molecular Sensing Ensemble with Selectivity for Aspartate. Journal of the American Chemical Society 123(45) (2001): 11296-11297.

[43] Hortalá, M.A., Fabbrizzi, L., Marcotte, N., Stomeo, F., and Taglietti, A. Designing the Selectivity of the Fluorescent Detection of Amino Acids: A Chemosensing Ensemble for Histidine. Journal of the American Chemical Society 125(1) (2003): 20-21.

[44] Bonizzoni, M., Fabbrizzi, L., Piovani, G., and Taglietti, A. Fluorescent detection of glutamate with a dicopper(II) polyamine cage. Tetrahedron 60(49) (2004): 11159-11162.

[45] Buryak, A. and Severin, K. A Chemosensor Array for the Colorimetric Identification of 20 Natural Amino Acids. Journal of the American Chemical Society 127(11) (2005): 3700-3701.

[46] Folmer-Andersen, J.F., Lynch, V.M., and Anslyn, E.V. “Naked-Eye” Detection of Histidine by Regulation of CuII Coordination Modes. Chemistry – A European Journal 11(18) (2005): 5319-5326.

[47] Han, M.-S.K., Dong H. Visual Detection of Di-and Tri-phosphates in Aqueous Solution of Neutral pH. Bulletin of the Korean Chemical Society 25(8) (2004): 1151-1155.

Chulalongkorn University

[48] Atilgan, S. and Akkaya, E.U. A calixpyridinium–pyranine complex as a selective anion sensing assembly via the indicator displacement strategy. Tetrahedron Letters 45(50) (2004): 9269-9271.

[49] Swamy, K.M.K., Kwon, S.K., Lee, H.N., Shantha Kumar, S.M., Kim, J.S., and Yoon, J. Fluorescent sensing of pyrophosphate and ATP in 100% aqueous solution using a fluorescein derivative and Mn2+. Tetrahedron Letters 48(49) (2007): 8683-8686.

[50] Jang, H.H., Yi, S., Kim, M.H., Kim, S., Lee, N.H., and Han, M.S. A simple method for improving the optical properties of a dimetallic coordination fluorescent chemosensor for adenosine triphosphate. Tetrahedron Letters 50(46) (2009): 6241-6243.

[51] Amendola, V., Bergamaschi, G., Buttafava, A., Fabbrizzi, L., and Monzani, E. Recognition and Sensing of Nucleoside Monophosphates by a Dicopper(II) Cryptate. Journal of the American Chemical Society 132(1) (2010): 147-156.

[52] Zhang, T. and Anslyn, E.V. Using an Indicator Displacement Assay to Monitor Glucose Oxidase Activity in Blood Serum. Organic Letters 9(9) (2007): 1627-1629.

[53] Kruppa, M. and König, B. Reversible Coordinative Bonds in Molecular Recognition. Chemical Reviews 106(9) (2006): 3520-3560.

[54] Steed, J.W., Atwood, J. L. Supramolecular Chemistry. Buffins Lane, Chichester, West Sussex PO19 1UD, England: John Wiley & Sons. (2000).

[55] Fabbrizzi, L. and Poggi, A. Sensors and switches from supramolecular chemistry. Chemical Society Reviews 24(3) (1995): 197-202.

[56] Gawley, R.E., et al. Chemosensors for the Marine Toxin Saxitoxin. Journal of the American Chemical Society 124(45) (2002): 13448-13453.

[57] D. Beer, P., K. Hopkins, P., and D. McKinney, J. Cooperative halide, perrhenate anion-sodium cation binding and pertechnetate extraction and transport by a novel tripodal tris(amido benzo-15-crown-5) ligand. Chemical Communications (13) (1999): 1253-1254.

[58] Trapani, G., et al. Peripheral Benzodiazepine Receptor Ligand–Melphalan Conjugates for Potential Selective Drug Delivery to Brain Tumors. Bioconjugate Chemistry 14(4) (2003): 830-839.

[59] Lavigne, J.J. and Anslyn, E.V. Sensing A Paradigm Shift in the Field of Molecular Recognition: From Selective to Differential Receptors. Angewandte Chemie International Edition 40(17) (2001): 3118-3130.

[60] Suksai, C. and Tuntulani, T. Chromogenic anion sensors. Chemical Society Reviews 32(4) (2003): 192-202.

[61] Gunnlaugsson, T., Glynn, M., Tocci, G.M., Kruger, P.E., and Pfeffer, F.M. Anion recognition and sensing in organic and aqueous media using luminescent and colorimetric sensors. Coordination Chemistry Reviews 250(23–24) (2006): 3094-3117.

[62] Suksai, C., et al. A new heteroditopic receptor and sensor highly selective for bromide in the presence of a bound cation. Tetrahedron Letters 46(16) (2005): 2765-2769.

[63] Bowman-James, K. Alfred Werner Revisited: The Coordination Chemistry of Anions. Accounts of Chemical Research 38(8) (2005): 671-678.

[64] Schmidtchen, F.P. and Berger, M. Artificial Organic Host Molecules for Anions. Chemical Reviews 97(5) (1997): 1609-1646.

[65] Berger, M. and Schmidtchen, F.P. Zwitterionic Guanidinium Compounds Serve as Electroneutral Anion Hosts. Journal of the American Chemical Society 121(43) (1999): 9986-9993.

[66] Llinares, J.M., Powell, D., and Bowman-James, K. Ammonium based anion receptors. Coordination Chemistry Reviews 240(1–2) (2003): 57-75.

[67] Bazzicalupi, C., et al. Thermodynamics of Phosphate and Pyrophosphate Anions Binding by Polyammonium Receptors. Journal of the American Chemical Society 121(29) (1999): 6807-6815.

[68] Bondy, C.R. and Loeb, S.J. Amide based receptors for anions. Coordination Chemistry Reviews 240(1–2) (2003): 77-99.

[69] Gomez, D.E., Fabbrizzi, L., Licchelli, M., and Monzani, E. Urea vs. thiourea in anion recognition. Organic & Biomolecular Chemistry 3(8) (2005): 1495-1500.

[70] Anzenbacher Jr, P., Nishiyabu, R., and Palacios, M.A. N-confused calix[4]pyrroles. Coordination Chemistry Reviews 250(23–24) (2006): 2929-2938.

[71] Biesaga, M., Pyrzyńska, K., and Trojanowicz, M. Porphyrins in analytical chemistry. A review. Talanta 51(2) (2000): 209-224.

[72] Linton, B. and Hamilton, A.D. Formation of Artificial Receptors by Metal-Templated Self-Assembly. Chemical Reviews 97(5) (1997): 1669-1680.

[73] Metzger, A., Lynch, V.M., and Anslyn, E.V. A Synthetic Receptor Selective for Citrate. Angewandte Chemie International Edition in English 36(8) (1997): 862-865.

[74] Fabbrizzi, L., Leone, A., and Taglietti, A. A Chemosensing Ensemble for Selective Carbonate Detection in Water Based on Metal–Ligand Interactions. Angewandte Chemie International Edition 40(16) (2001): 3066-3069.

[75] Hu, M. and Feng, G. Highly selective and sensitive fluorescent sensing of oxalate in water. Chemical Communications 48(55) (2012): 6951-6953.

[76] Incarvito, C., et al. Bimetallic reactivity. Preparations, properties and structures of complexes formed by unsymmetrical binucleating ligands bearing 4- and 6-coordinate sites supported by alkoxide bridges. Journal of the Chemical Society, Dalton Transactions (23) (2001): 3478-3488.

[77] Burdette, S.C., Frederickson, C.J., Bu, W., and Lippard, S.J. ZP4, an Improved Neuronal $Zn^{2+}$ Sensor of the Zinpyr Family. Journal of the American Chemical Society 125(7) (2003): 1778-1787.

[78] Klanderman, B.H. Aldehyde Synthesis. A Study of the Preparation of 9,10-Anthracenedicarboxaldehyde and Other Aromatic Dialdehydes. The Journal of Organic Chemistry 31(8) (1966): 2618-2620.

[79] Benamor, M., Belhamel, K., and Draa, M.T. Use of xylenol orange and cetylpyridinium chloride in rapid spectrophotometric determination of zinc in pharmaceutical products. Journal of Pharmaceutical and Biomedical Analysis 23(6) (2000): 1033-1038.

[80] Ghasemi, J. and Seifi, S. β-Correction as a preprocessing method for partial least squares in simultaneous determination of zinc and lead. Talanta 63(3) (2004): 751-756.

[81] Steinberg, I.M., Lobnik, A., and Wolfbeis, O.S. Characterisation of an optical sensor membrane based on the metal ion indicator Pyrocatechol Violet. Sensors and Actuators B: Chemical 90(1–3) (2003): 230-235.

[82] Ngo, H.T., Liu, X., and Jolliffe, K.A. Anion recognition and sensing with Zn(ii)-dipicolylamine complexes. Chemical Society Reviews 41(14) (2012): 4928-4965.

[83] Surman, A.J., et al. A Pyrophosphate-Responsive Gadolinium(III) MRI Contrast Agent. Chemistry – A European Journal 17(1) (2011): 223-230.

[84] Ikotun, O.F., Marino, N., Kruger, P.E., Julve, M., and Doyle, R.P. Coordination complexes incorporating pyrophosphate: Structural overview and exploration of their diverse magnetic, catalytic and biological properties. Coordination Chemistry Reviews 254(7–8) (2010): 890-915.

[85] Becke, A.D. Density□functional thermochemistry. III. The role of exact exchange. The Journal of Chemical Physics 98(7) (1993): 5648-5652.

[86] Lee, C., Yang, W., and Parr, R.G. Development of the Colle-Salvetti correlation-energy formula into a functional of the electron density. Physical Review B 37(2) (1988): 785-789.

[87] Hay, P.J. and Wadt, W.R. Ab initio effective core potentials for molecular calculations. Potentials for the transition metal atoms Sc to Hg. The Journal of Chemical Physics 82(1) (1985): 270-283.

[88] Lee, H.N., et al. Pyrophosphate-Selective Fluorescent Chemosensor at Physiological pH: Formation of a Unique Excimer upon Addition of Pyrophosphate. Journal of the American Chemical Society 129(13) (2007): 3828-3829.

[89] Kar, C., Adhikari, M.D., Ramesh, A., and Das, G. NIR- and FRET-Based Sensing of $Cu^{2+}$ and $S^{2-}$ in Physiological Conditions and in Live Cells. Inorganic Chemistry 52(2) (2013): 743-752.

[90] Engström, E., Jönebring, I., and Karlberg, B. Assessment of a screening method for metals in seawater based on the non-selective reagent 4-(2-pyridylazo)resorcinol (PAR). Analytica Chimica Acta 371(2–3) (1998): 227-234.

[91] Asghari, A. and Mohammadi, B. Nano-alumina coated with sodium dodecyl sulfate and modified with 4-(2-Pyridylazo) resorcinol for extraction of heavy

metals in different matrixes. Journal of Industrial and Engineering Chemistry 20(3) (2014): 824-829.

[92] Liu, T., Li, G., Zhang, N., and Chen, Y. An inorganic–organic hybrid optical sensor for heavy metal ion detection based on immobilizing 4-(2-pyridylazo)-resorcinol on functionalized HMS. Journal of Hazardous Materials 201–202 (2012): 155-161.

[93] Tabata, M. and Tanaka, M. Mixed ligand complexes of copper(II)-4-(2-pyridylazo)resorcinol complex with unidentate ligands. Journal of Inorganic and Nuclear Chemistry 38(8) (1976): 1529-1532.

[94] Nonova, D. and Stoyanov, K. Extraction—spectrophotometric determination of copper(II) with 4-(2-pyridylazo)resorcinol and a long-chain quaternary ammonium salt. Analytica Chimica Acta 138 (1982): 321-328.

[95] Shimazaki, Y., Takani, M., and Yamauchi, O. Metal complexes of amino acids and amino acid side chain groups. Structures and properties. Dalton Transactions (38) (2009): 7854-7869.

[96] Harding, M.M. and Cole, S.J. The crystal structure of di(histidino)zinc pentahydrate. Acta Crystallographica 16(7) (1963): 643-650.

[97] Kretsinger, R.H., Cotton, F.A., and Bryan, R.F. The crystal and molecular structure of di-(l-histidine)-zinc(II) dihydrate. Acta Crystallographica 16(7) (1963): 651-657.

[98] Evertsson, B. The crystal structure of bis-l-histidinecopper(II) dinitrate dihydrate. Acta Crystallographica Section B 25(1) (1969): 30-41.

[99] Bryan, R.F., Greene, P.T., Stokely, P.F., and Wilson, E.W. Crystal and molecular structure of tris(glycinato)chromium(III) monohydrate, $Cr(C_2H_4NO_2)_3.H_2O$. Inorganic Chemistry 10(7) (1971): 1468-1473.

[100] Robert M. Smith, A.E.M. Critical Stability Constants : Amoino Acids. 1: New York, Plenum Press, 1976.

[101] Crutchley, R.J., Hynes, R., and Gabe, E.J. Five- and four-coordinate copper(II) complexes of 2,2'-bipyridine and phenylcyanamide anion ligands: crystal structures, cyclic voltammetry, and electronic absorption spectroscopy. Inorganic Chemistry 29(24) (1990): 4921-4928.

จุฬาลงกรณ์มหาวิทยาลัย
Chulalongkorn University

# APPENDIX

จุฬาลงกรณ์มหาวิทยาลัย
Chulalongkorn University

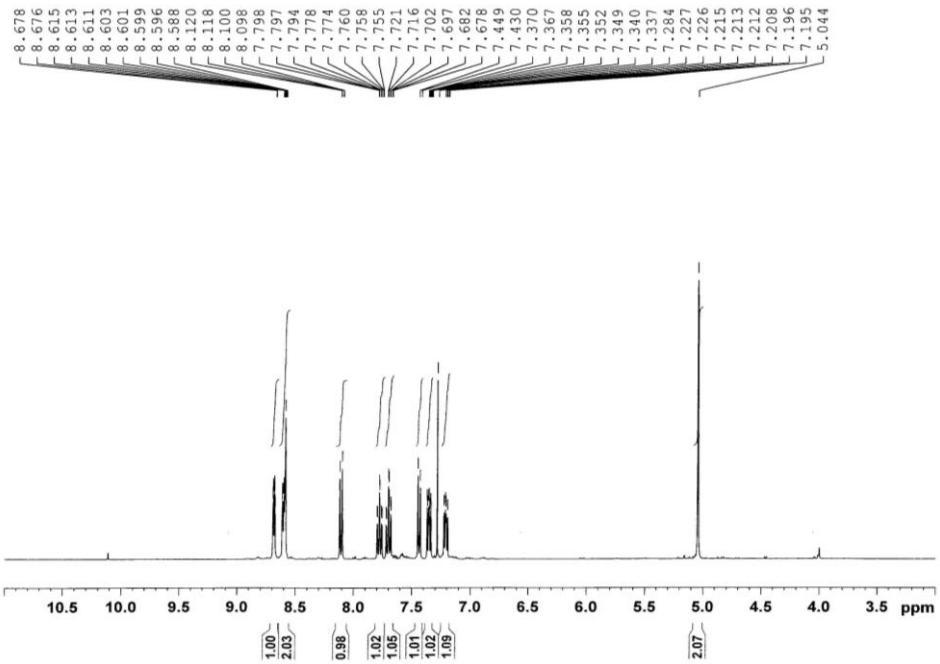


**Figure S1**. $^{1}H$ NMR spectrum of pyridin-2-ylmethypyridin-2-ylmethyleneamine ) **(a)** in $CDCl_3$

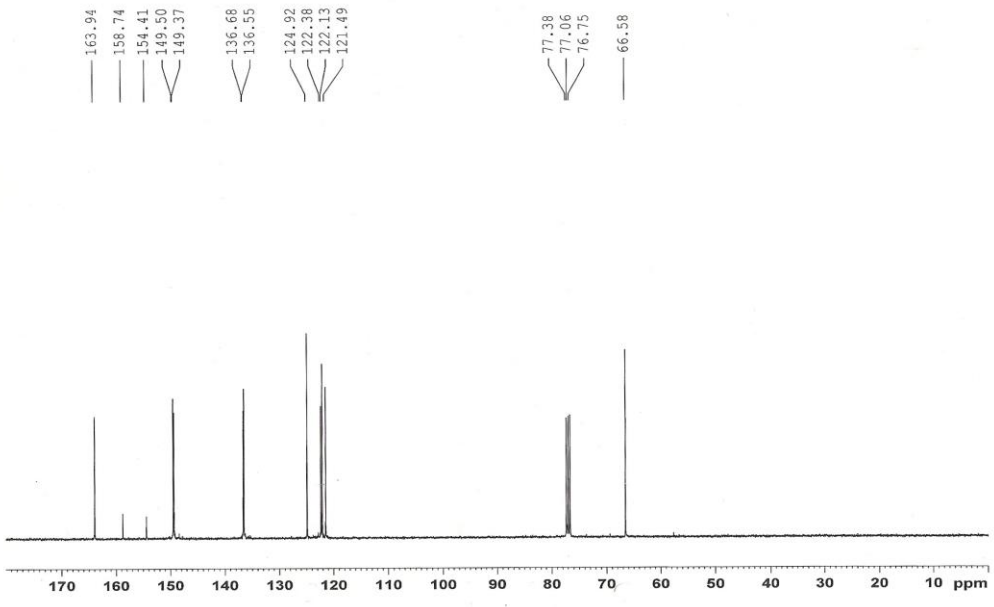


**Figure S2**. $^{13}C$ NMR spectrum of pyridin-2-ylmethypyridin-2-ylmethyleneamine (**a**) in $CDCl_3$

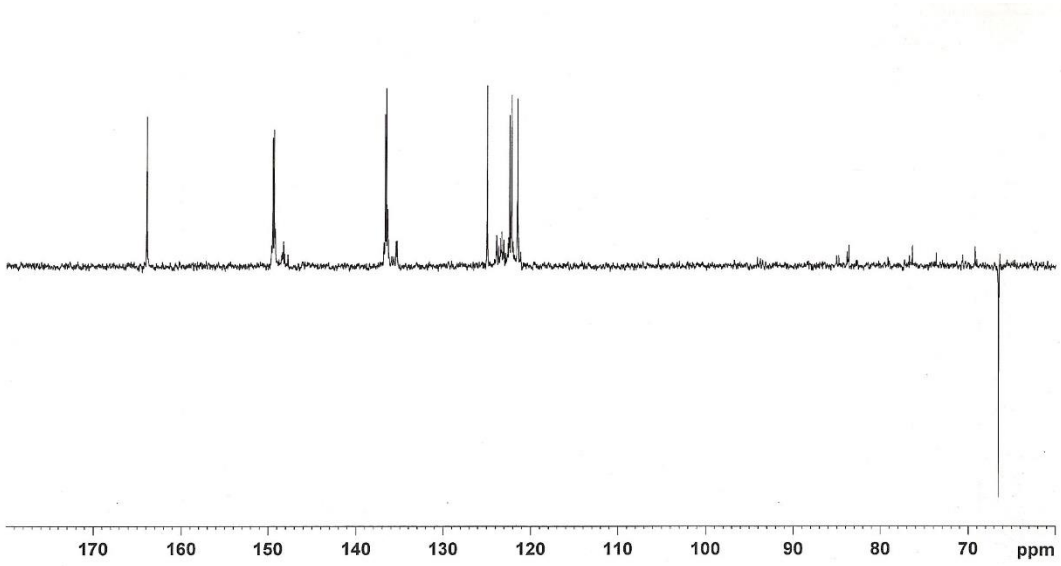


**Figure S3**. DEPT 135 NMR spectrum of pyridin-2-ylmethypyridin-2-ylmethyleneamine (**a**) in $CDCl_3$

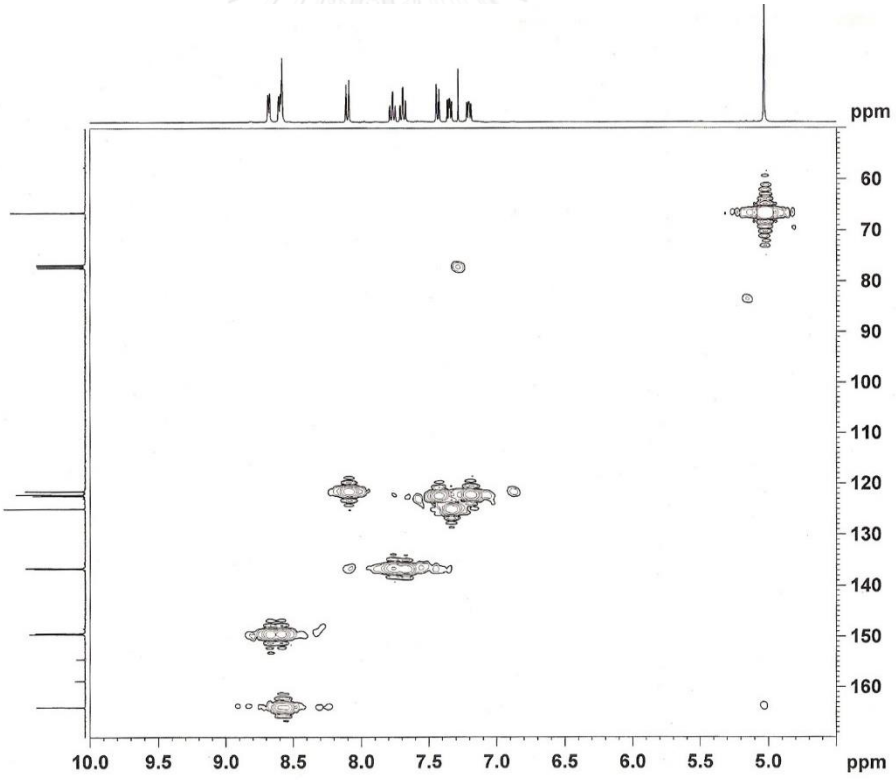


**Figure S4**. HMQC NMR spectrum of pyridin-2-ylmethypyridin-2-ylmethyleneamine (**a**) in $CDCl_3$

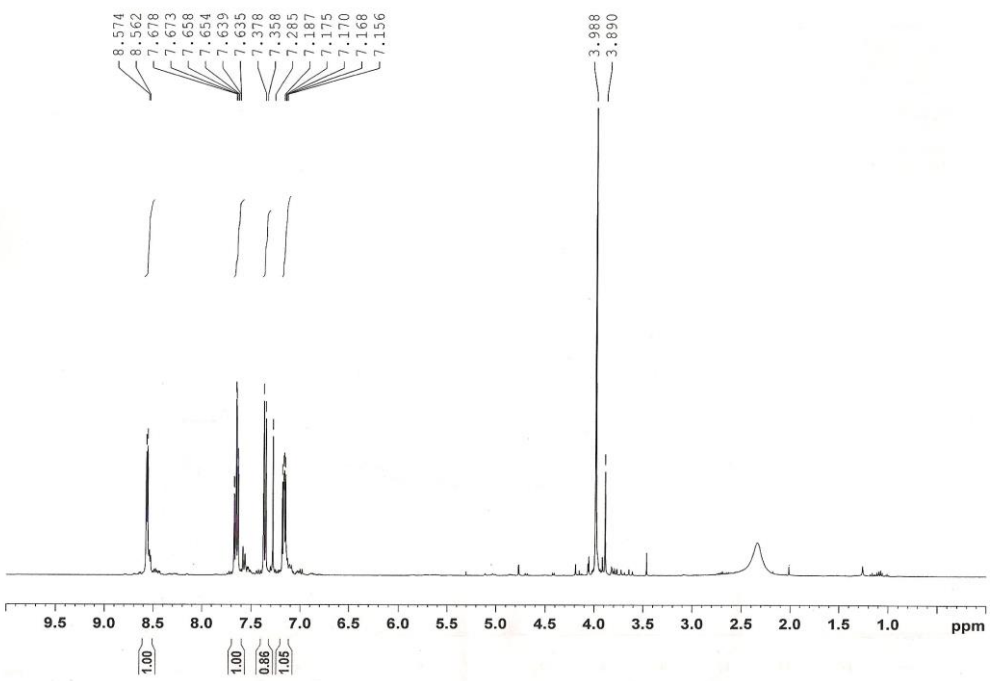


**Figure S5**. $^{1}H$ NMR spectrum of bis-pyridin-2-ylmethylamine (**b**) in $CDCl_3$

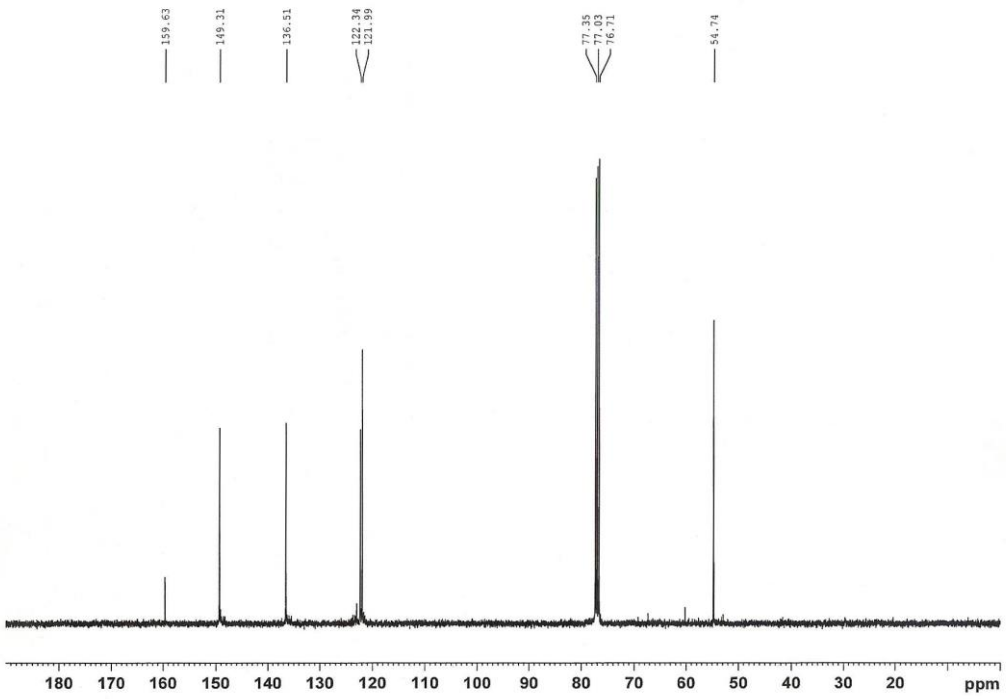


**Figure S6**. $^{13}C$ NMR spectrum of bis-pyridin-2-ylmethylamine (**b**) in $CDCl_3$

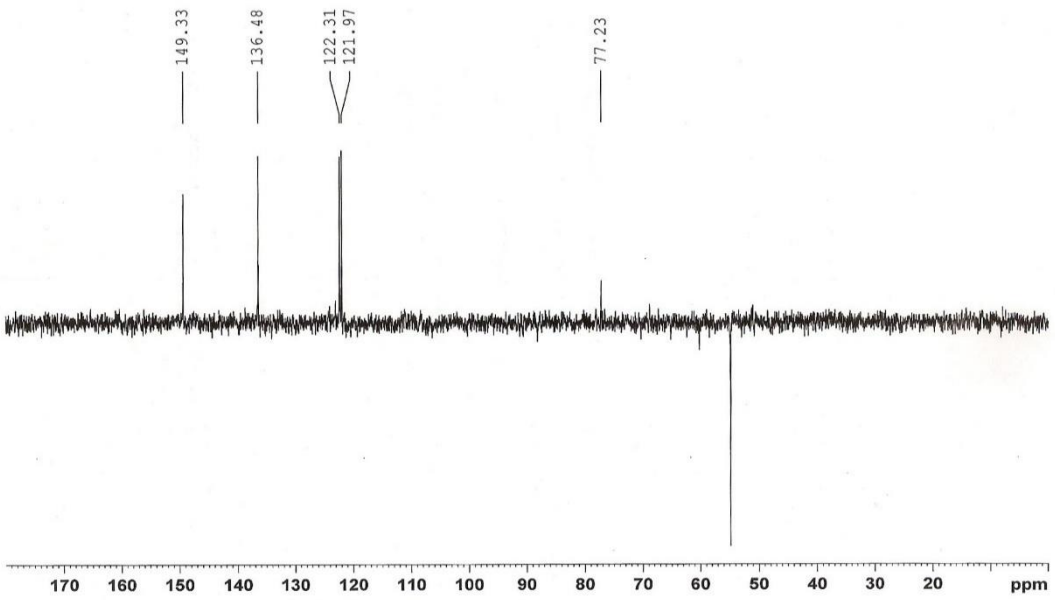


**Figure S7**. DEPT 135 NMR spectrum of bis-pyridin-2-ylmethylamine (**b**) in $CDCl_3$

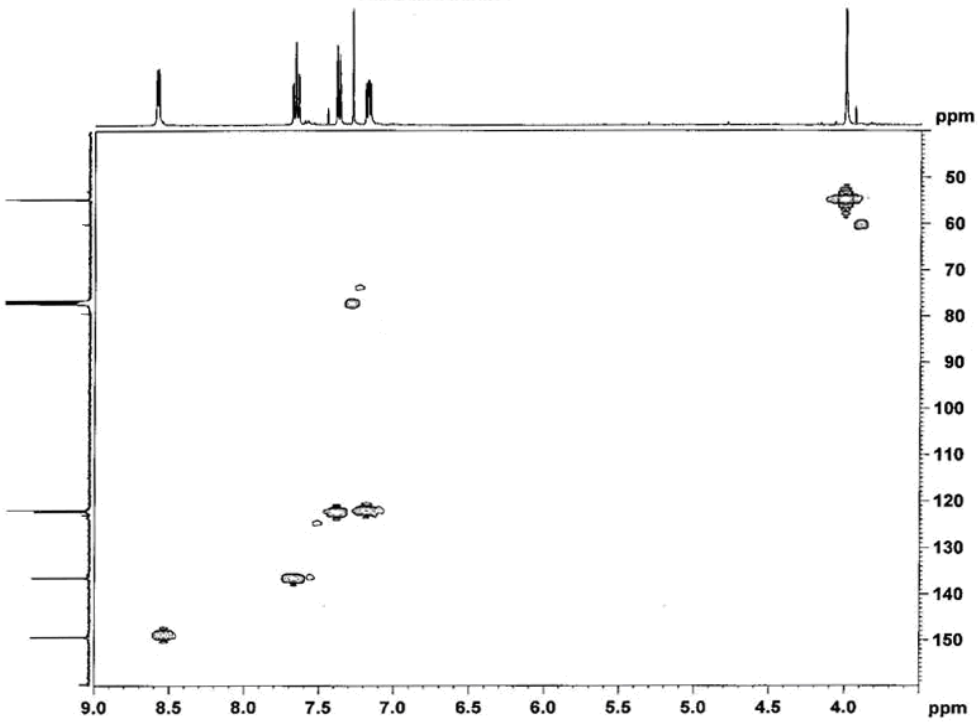


**Figure S8**. HMQC NMR spectrum of bis-pyridin-2-ylmethylamine (**b**) in $CDCl_3$

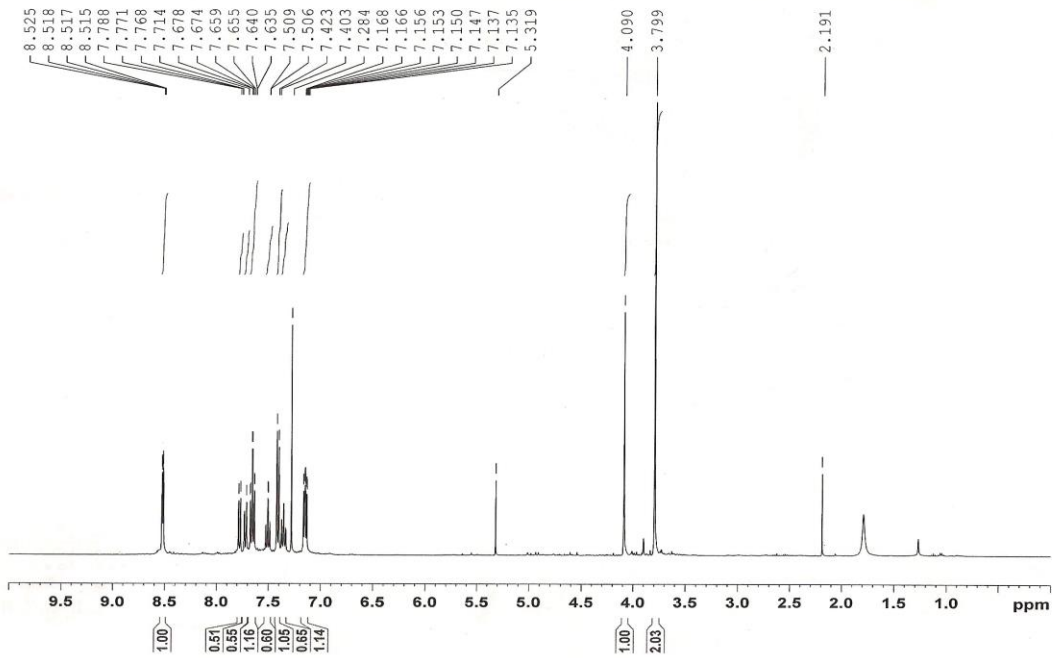


**Figure S9**. $^{1}$H NMR spectrum of 2-[bis(2-pyridylmethyl)aminomethyl]nitrobenzene (**c**) in $CDCl_3$

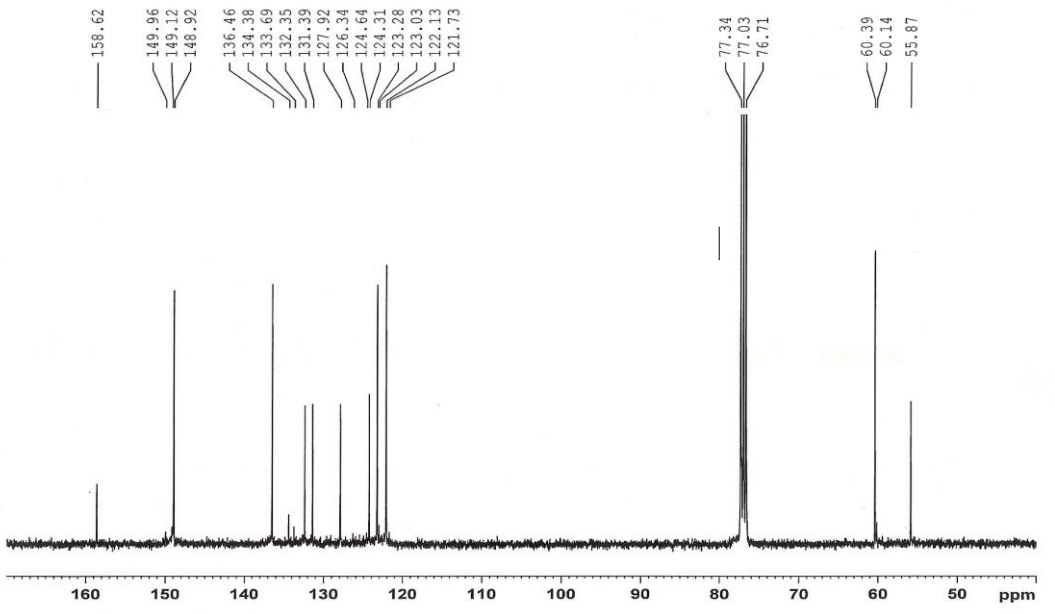


**Figure S10**. $^{13}$C NMR spectrum of 2-[bis(2-pyridylmethyl)aminomethyl]nitrobenzene (**c**) in $CDCl_3$

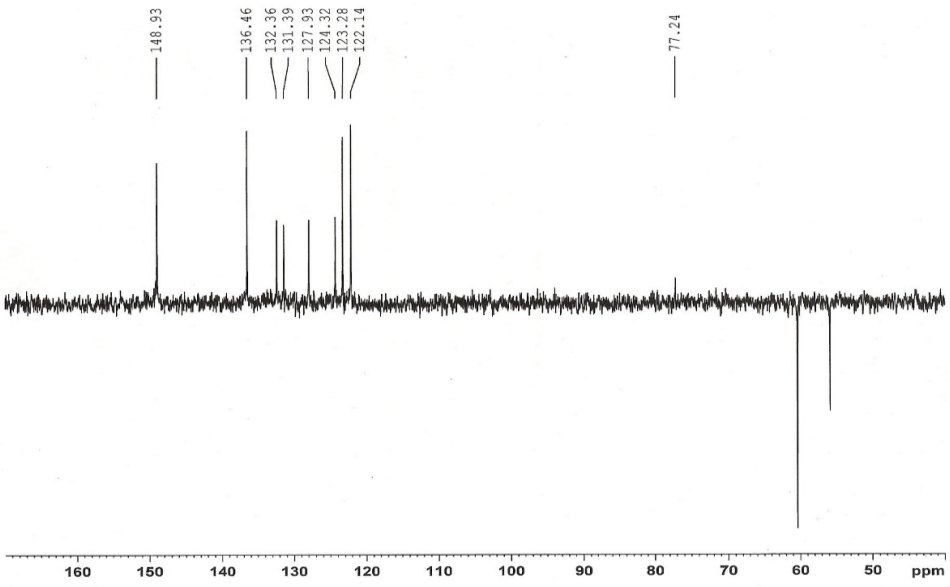


**Figure S11**. DEPT 135 NMR spectrum of 2-[bis(2-pyridylmethyl)aminomethyl]nitro benzene **(c)** in $CDCl_3$

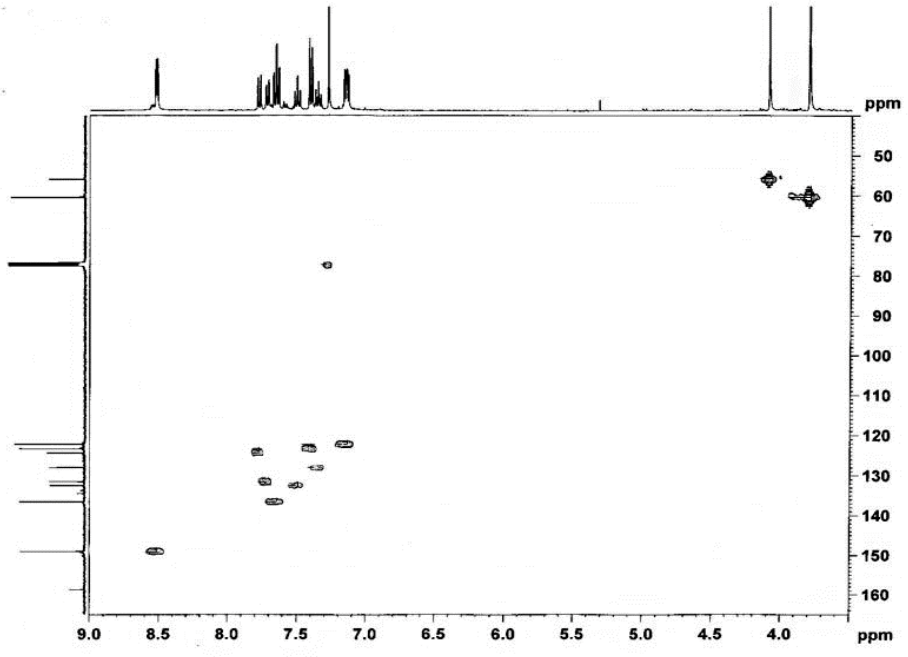


**Figure S12**. HMQC NMR spectrum of 2-[bis(2-pyridylmethyl)aminomethyl] nitrobenzene (**c**) in $CDCl_3$

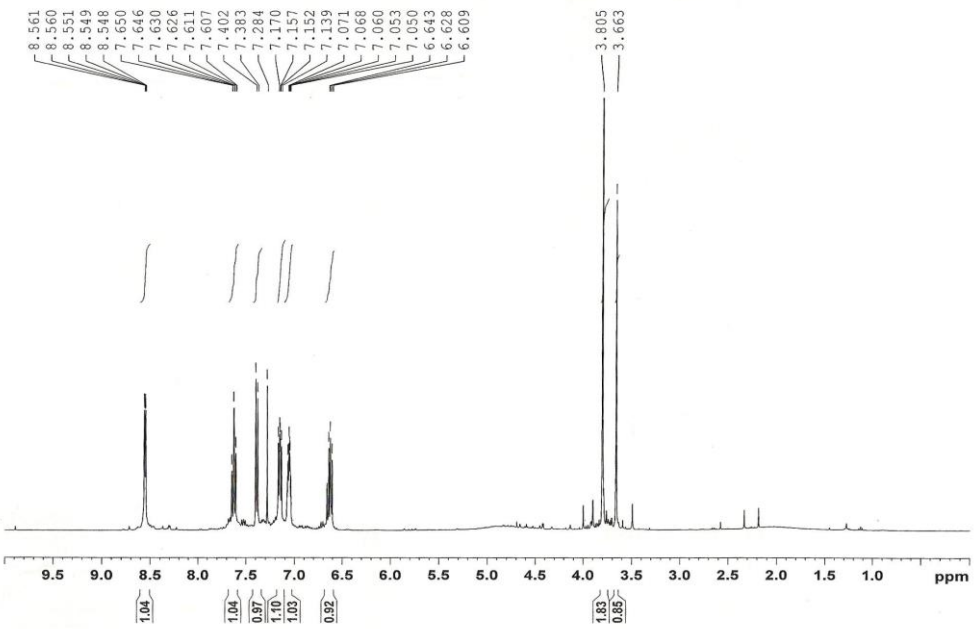


**Figure S13**. $^{1}$H NMR spectrum of 2-[bis(2-pyridylmethyl)aminomethyl]aniline (**d**) in $CDCl_3$

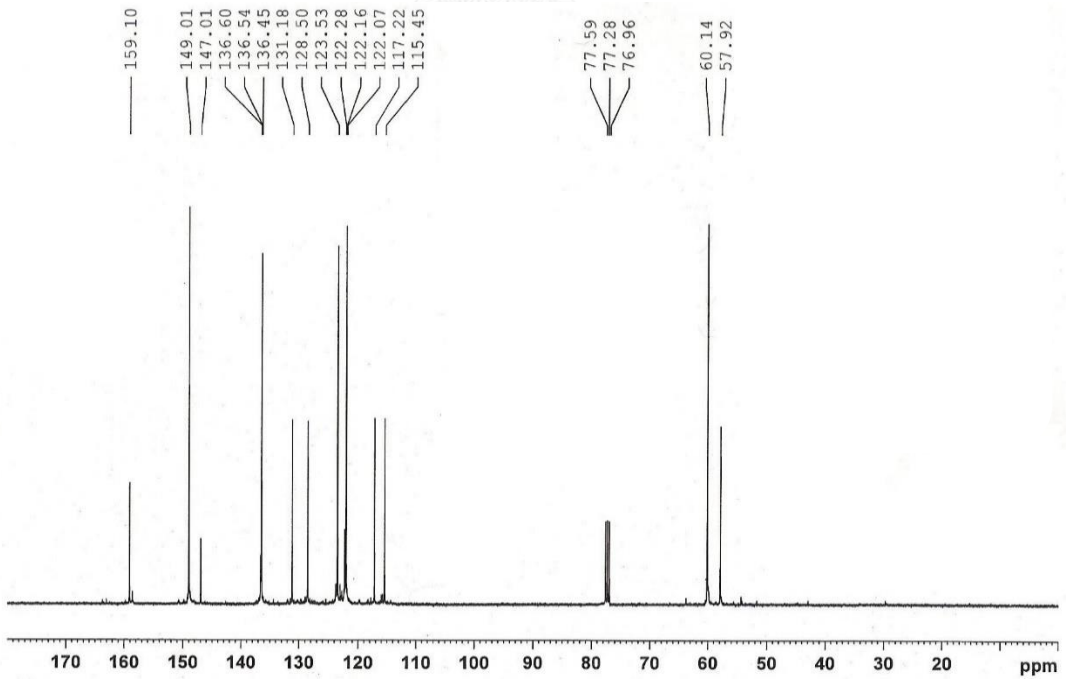


**Figure S14**. $^{13}$C NMR spectrum of 2-[bis(2-pyridylmethyl)aminomethyl]aniline (**d**) in $CDCl_3$

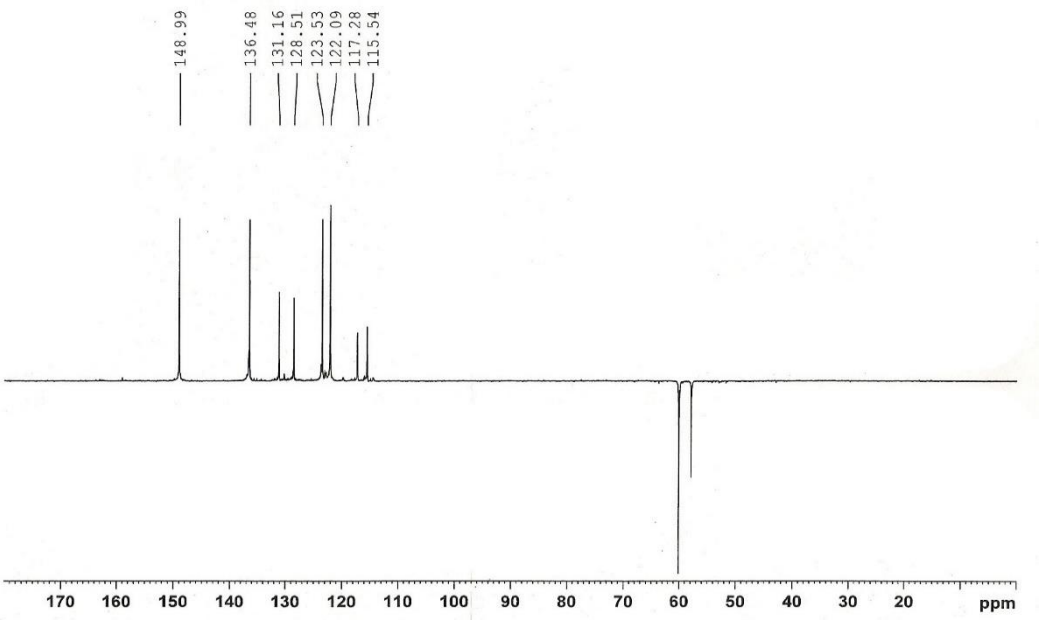


**Figure S15**. DEPT 135 NMR spectrum of 2-[bis(2-pyridylmethyl)aminomethyl]aniline (**d**) in $CDCl_3$

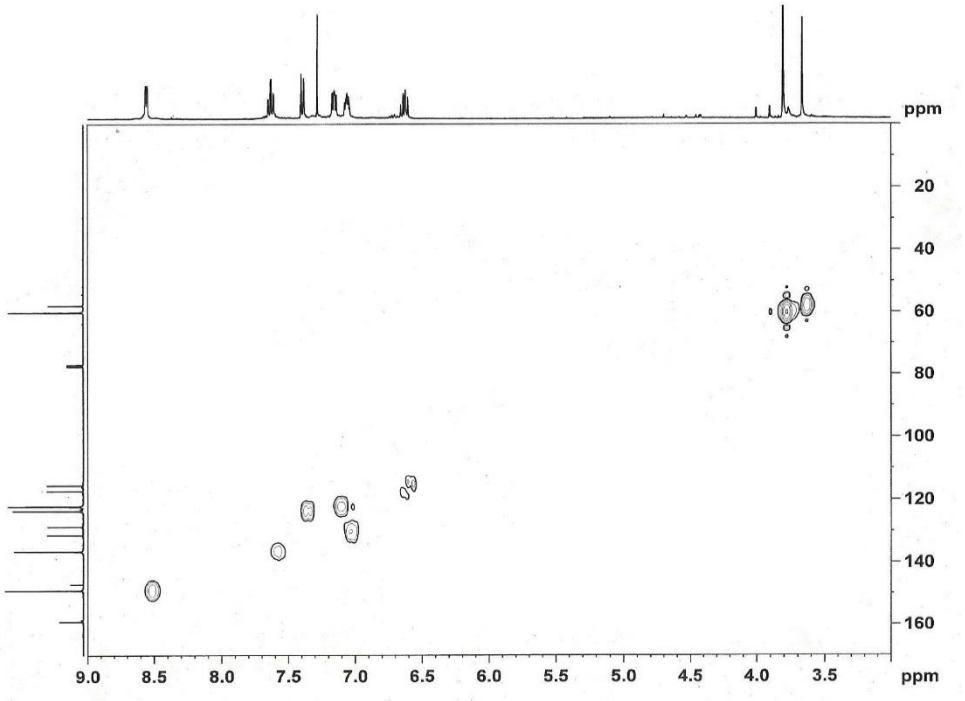


**Figure S16**. HMQC 135 NMR spectrum of 2-[bis(2-pyridylmethyl)aminomethyl]aniline in $CDCl_3$

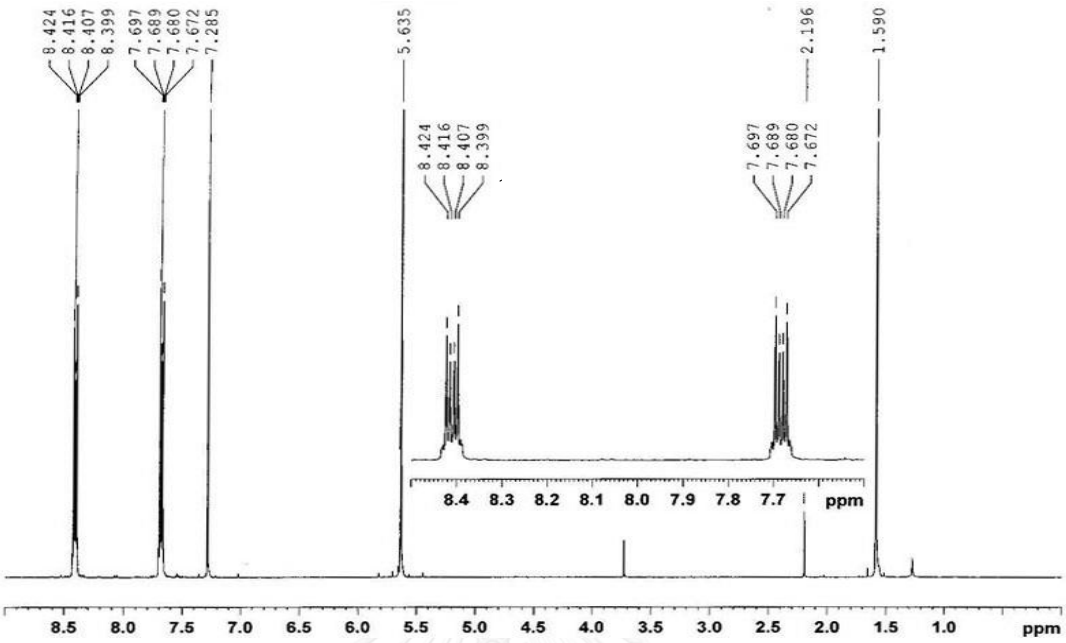


**Figure S17**. $^{1}H$ NMR spectrum of 9,10-bis(chloromethyl)anthracene (**e**) in $CDCl_3$

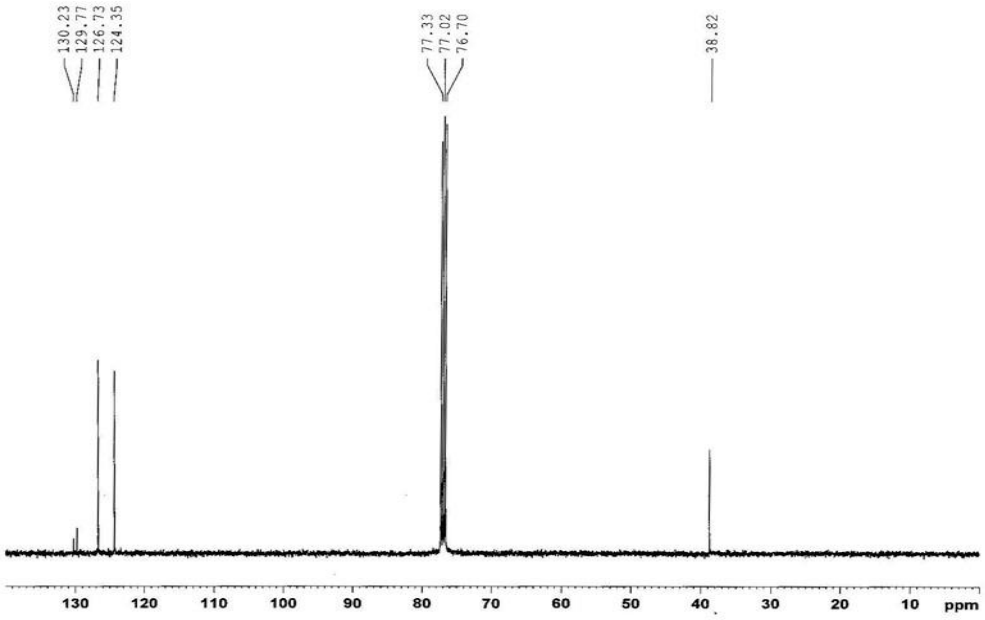


**Figure S18**. $^{13}C$ NMR spectrum of 9,10-bis(chloromethyl)anthracene (B) in $CDCl_3$

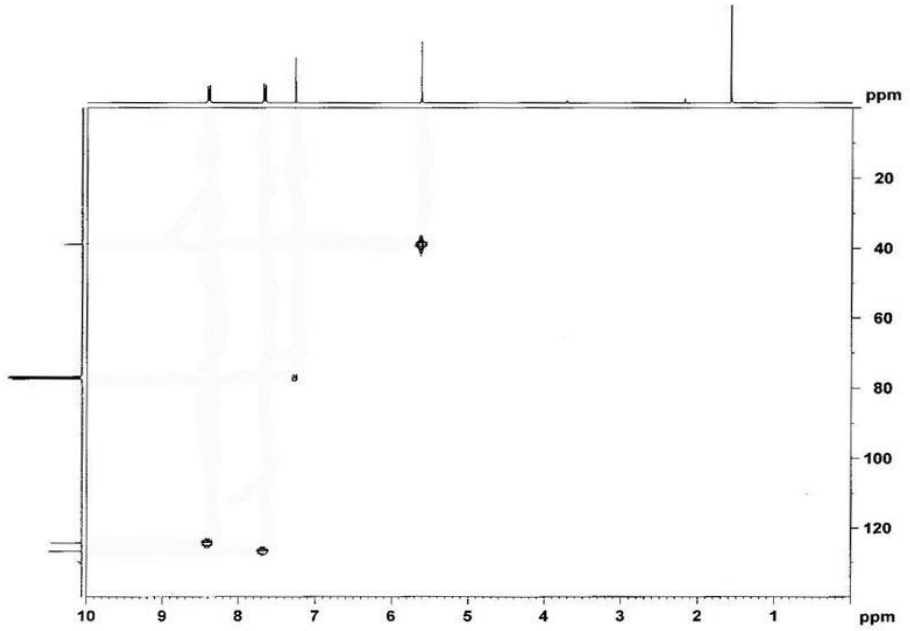


**Figure S19**. HMQC NMR spectrum of 9,10-bis(chloromethyl)anthracene (**e**) in $CDCl_3$

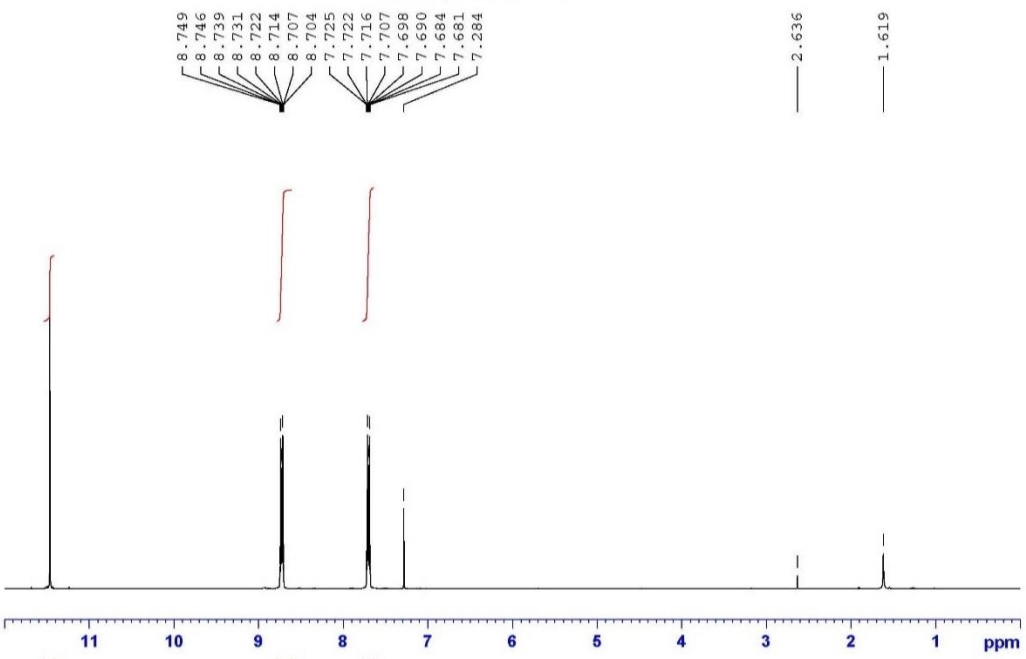


**Figure S20**. $^1H$ NMR spectrum of anthracene-9,10-dicarboxaldehyde (**f**) in $CDCl_3$

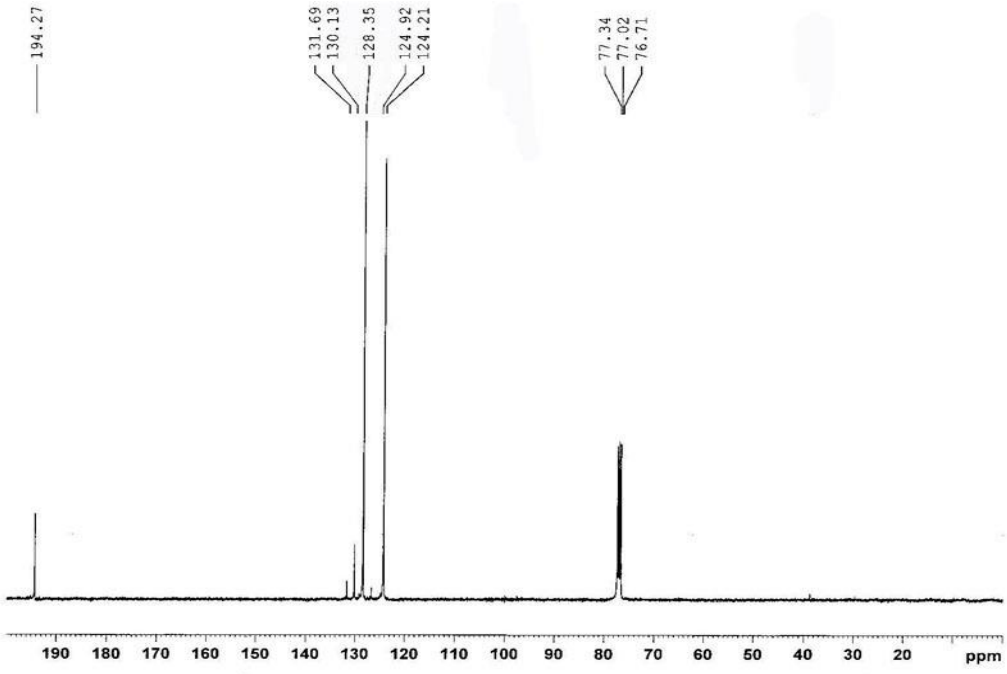


**Figure S21**. $^{13}C$ NMR spectrum of anthracene-9,10-dicarboxaldehyde (**f**) in $CDCl_3$

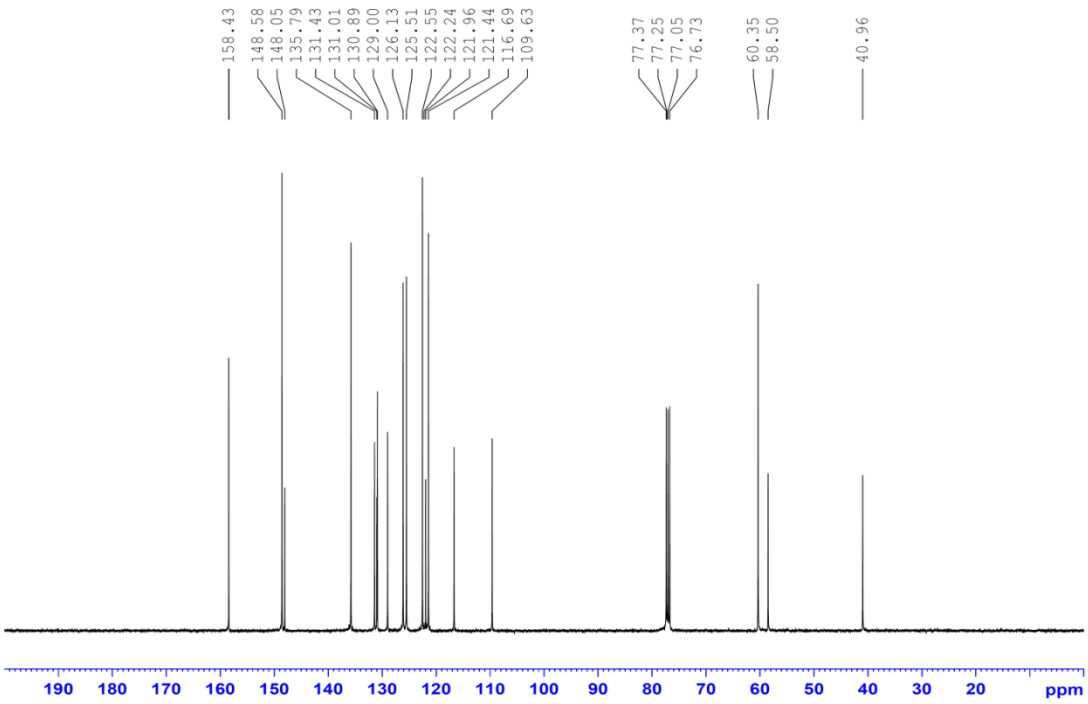


**Figure S22**. $^{13}C$ NMR spectrum of **L2** in $CDCl_3$

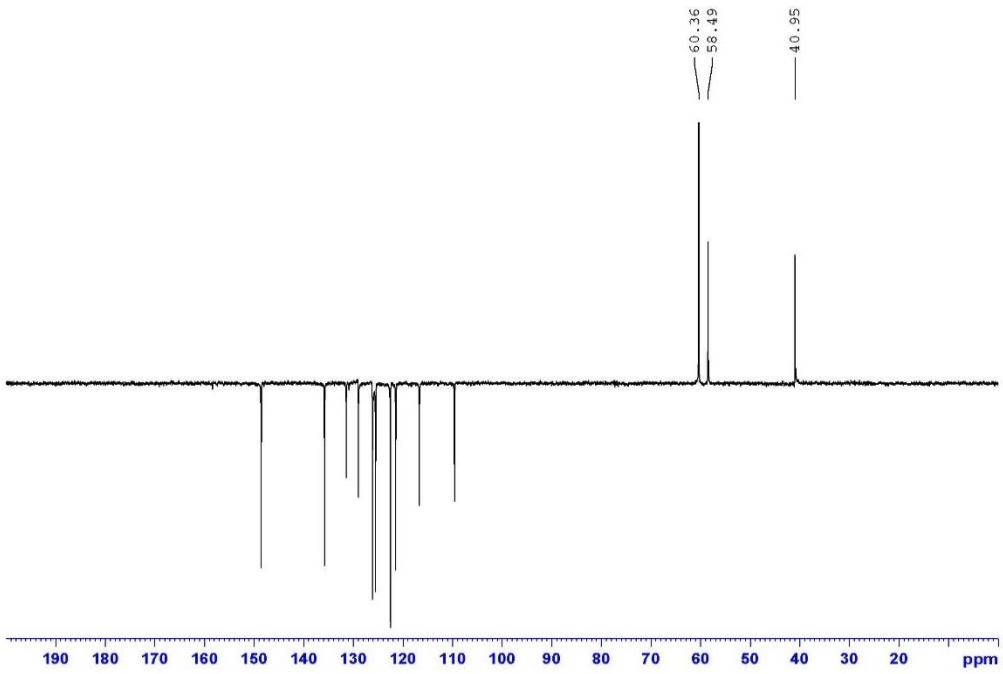


**Figure S23**. DEPT 135 NMR spectrum of **L2** in $CDCl_3$

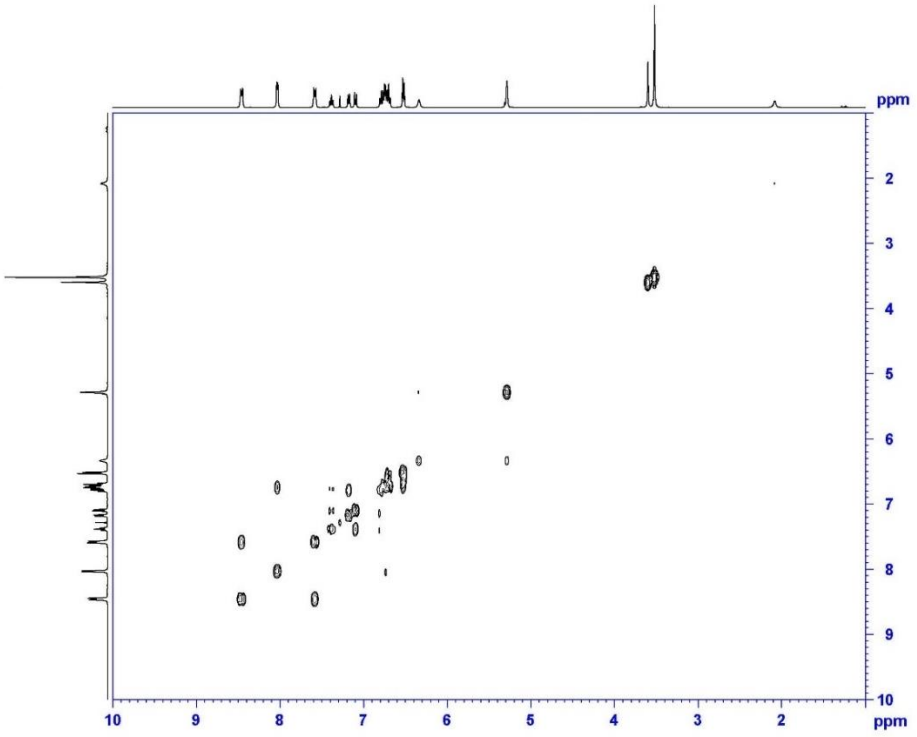


**Figure S24**. COSY NMR spectrum of **L2** in $CDCl_3$

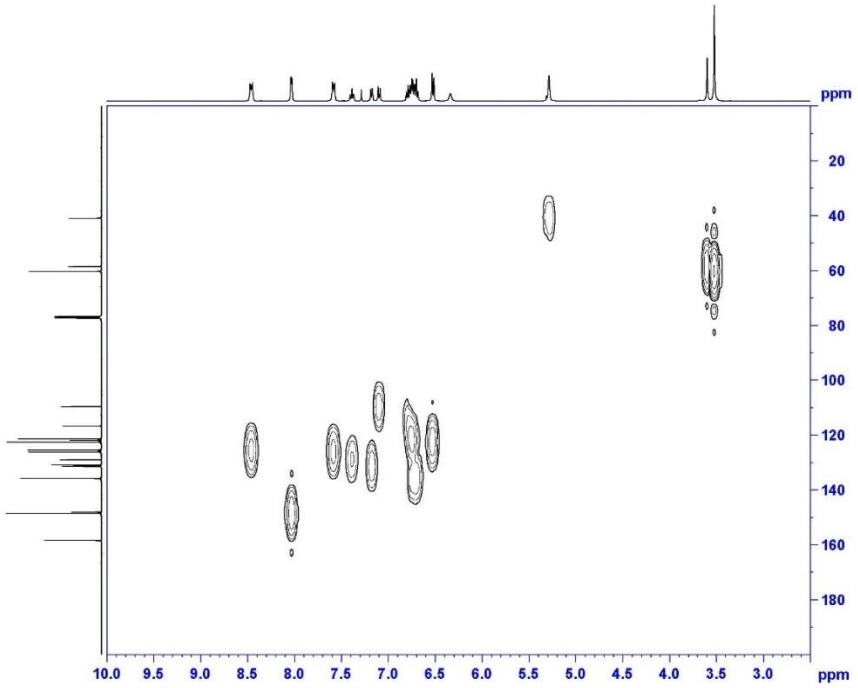


**Figure S25**. HMQC NMR spectrum of **L2** in $CDCl_3$

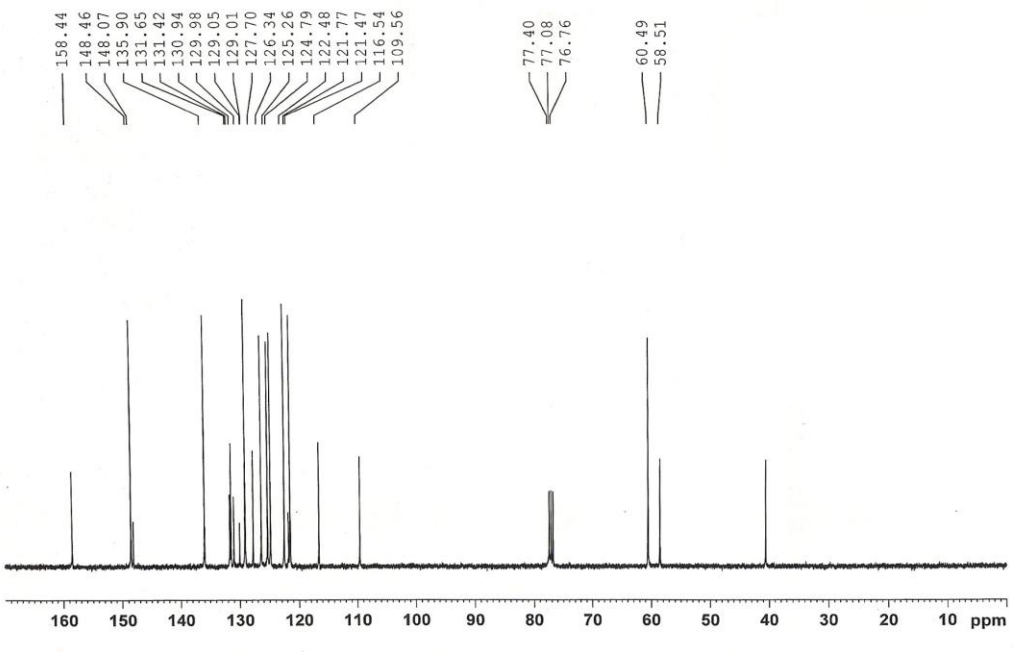


**Figure S26**. $^{13}C$ NMR spectrum **L3** in $CDCl_3$

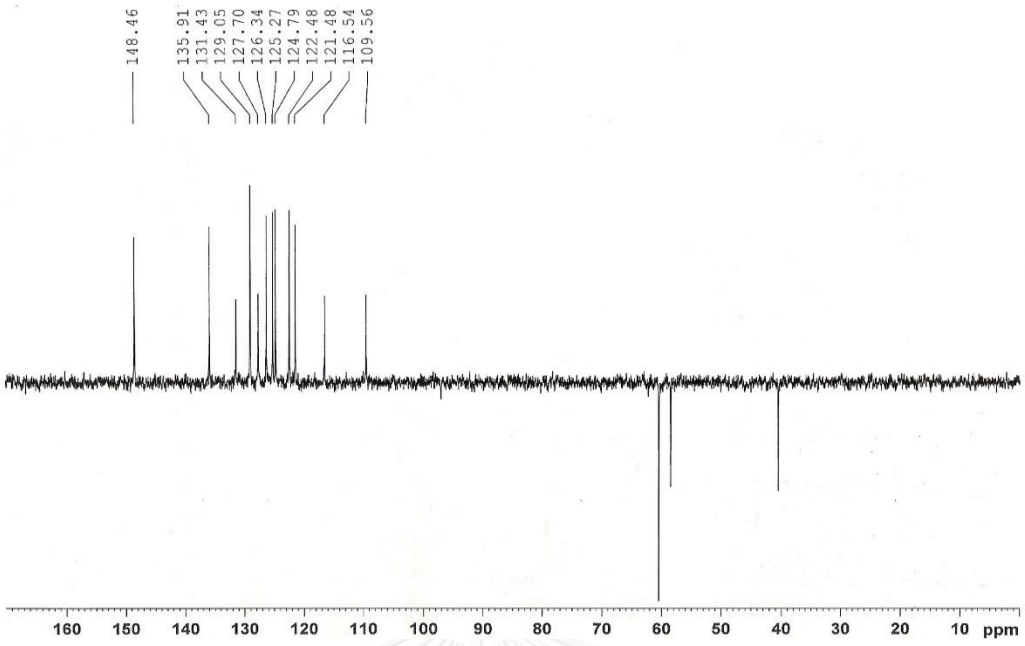


**Figure S27**. DEPT-135 NMR spectrum of **L3** in $CDCl_3$

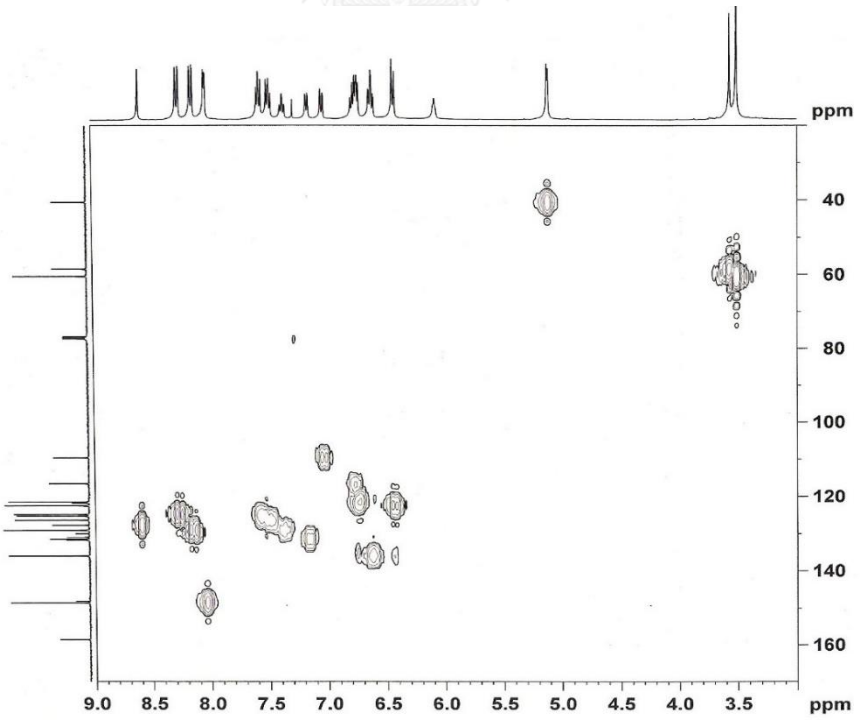


**Figure S28**. HMQC NMR spectrum of **L3** in $CDCl_3$

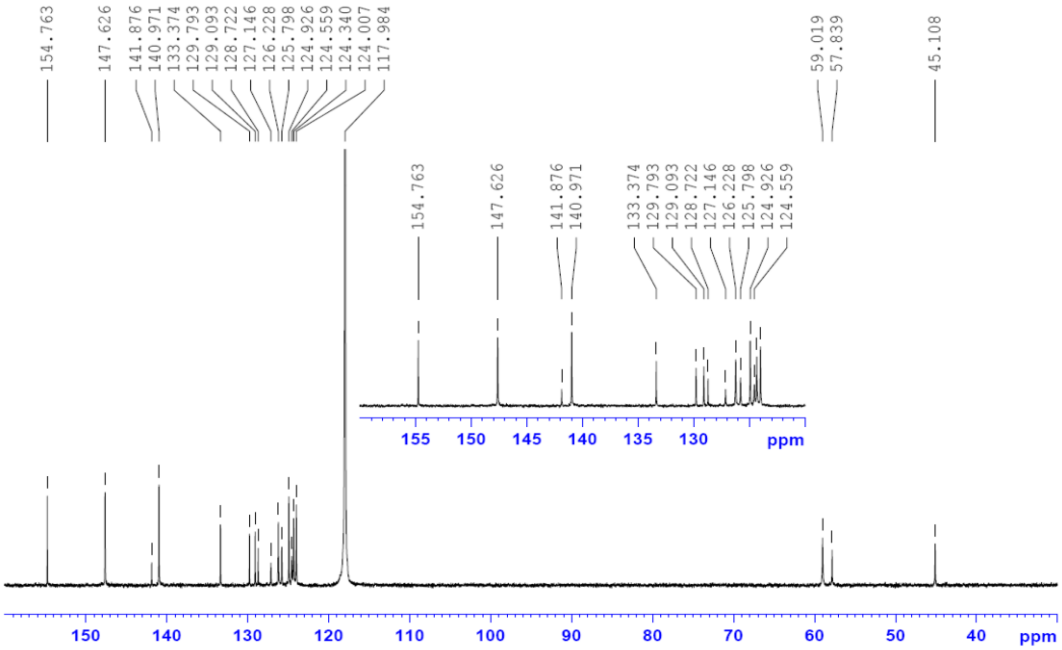


**Figure S29**. $^{13}$C-NMR spectrum of **$Zn_2$L2** in 20% $D_2O/CD_3CN$

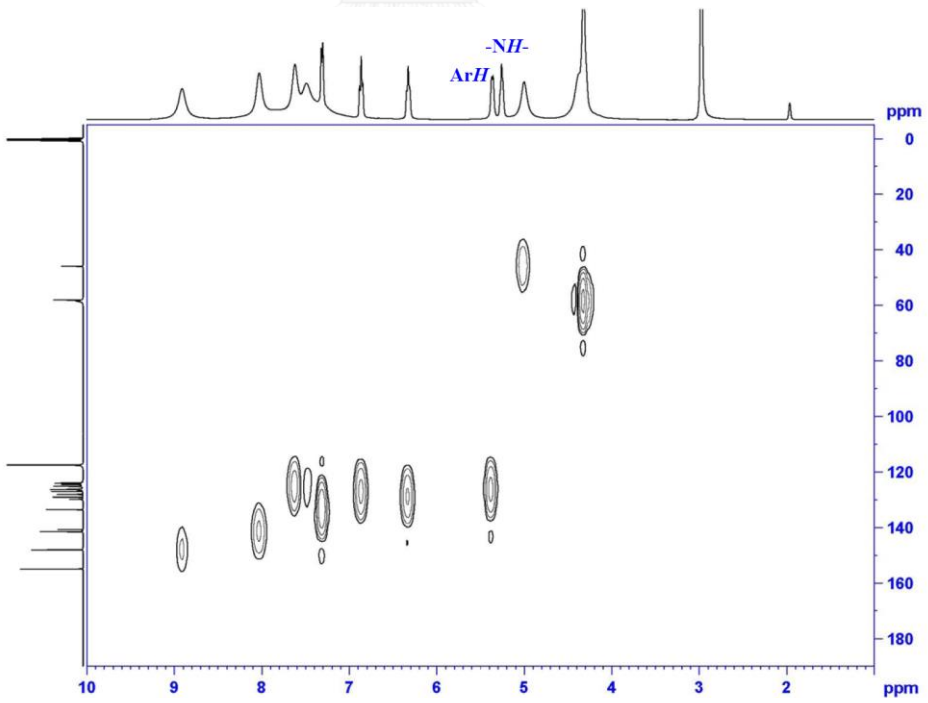


**Figure S30**. HMQC-NMR spectrum of **$Zn_2$L2** in 20% $D_2O/CD_3CN$

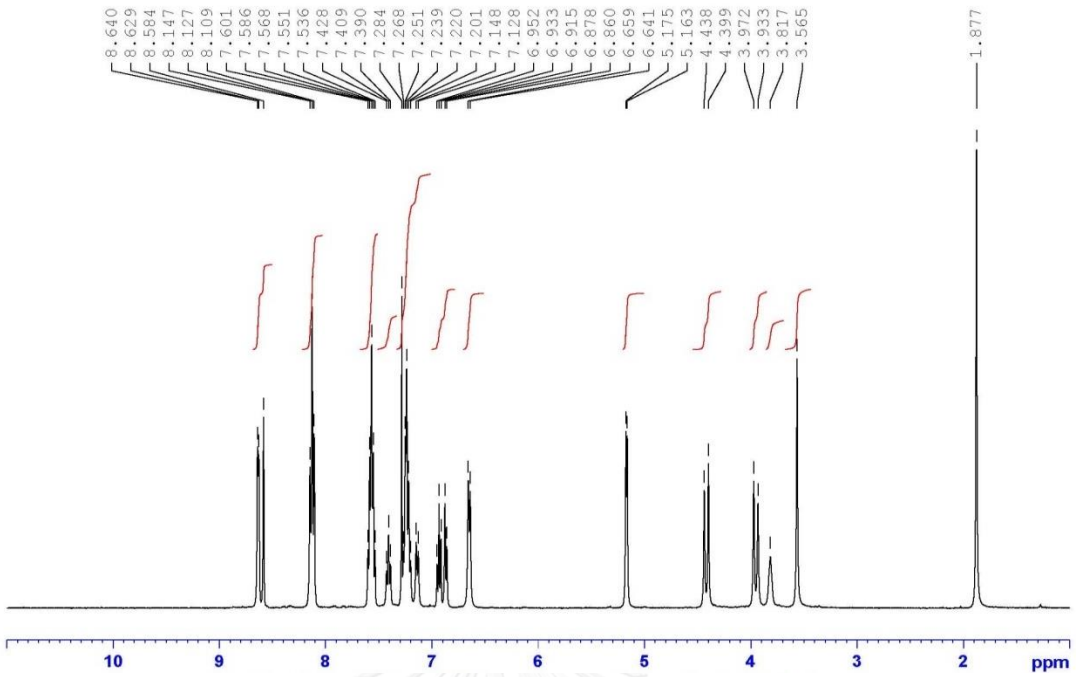


**Figure S31**. $^{1}H$ NMR spectrum of **ZnL3** in $CDCl_3$

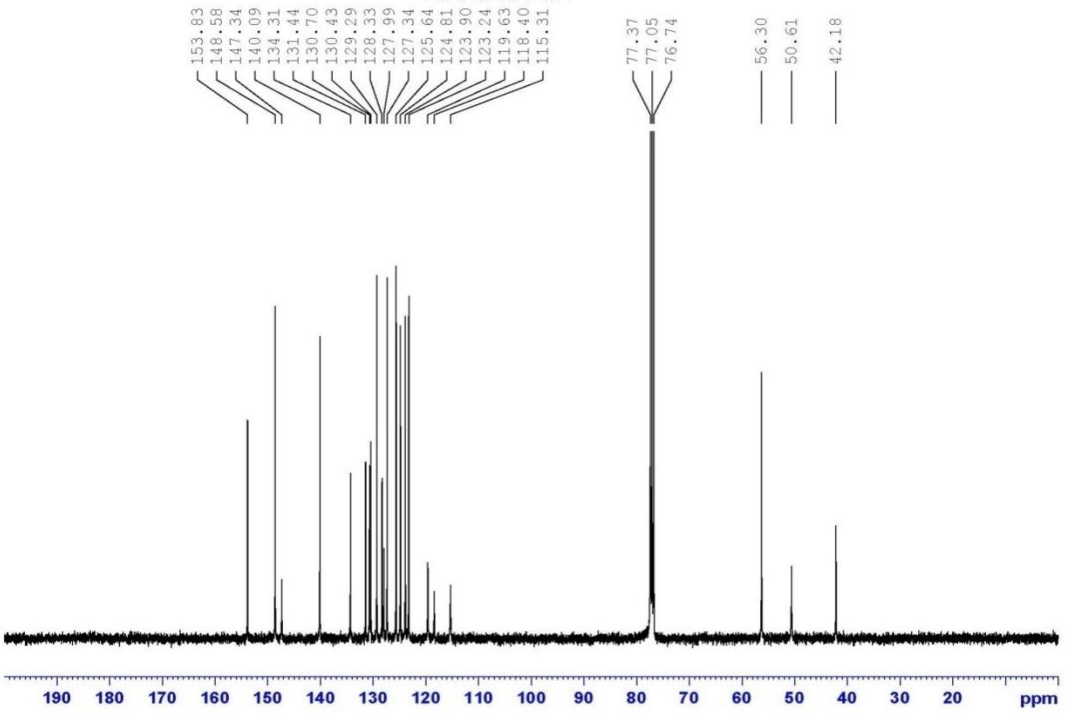


**Figure S32**. $^{13}C$ NMR spectrum of **ZnL3** in $CDCl_3$

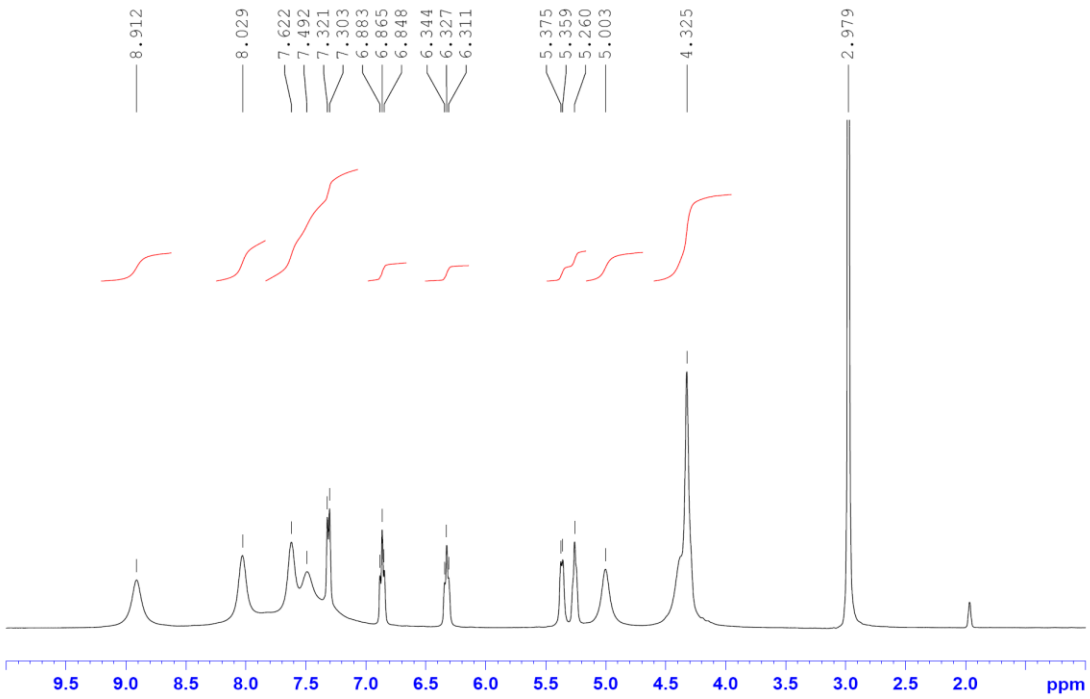


**Figure S33**. $^{1}$H NMR spectrum of **$Zn_2$L2** in $CD_3CN$

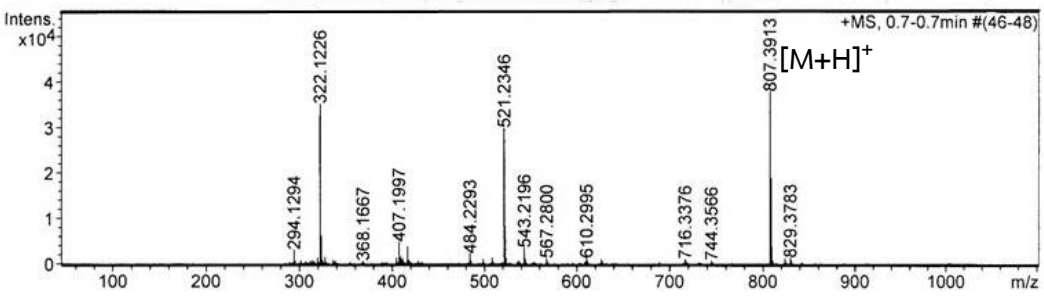


**Figure S34**. Mass spectrum of (N,N'E,N,N'E)-N,N'-(anthracene-9,10-diylbis(methan-1-yl-1-ylidene))bis(2-((bis(pyridin-2-ylmethyl)amino)methyl)aniline) **(h)**

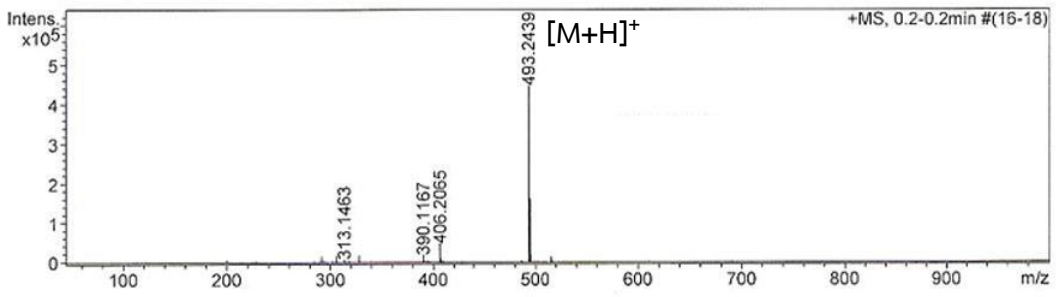


**Figure S35**. Mass spectrum of (E)-N-(anthracen-9-ylmethylene)-2-((bis(pyridin-2-ylmethyl)amino)methyl)aniline (**g**)

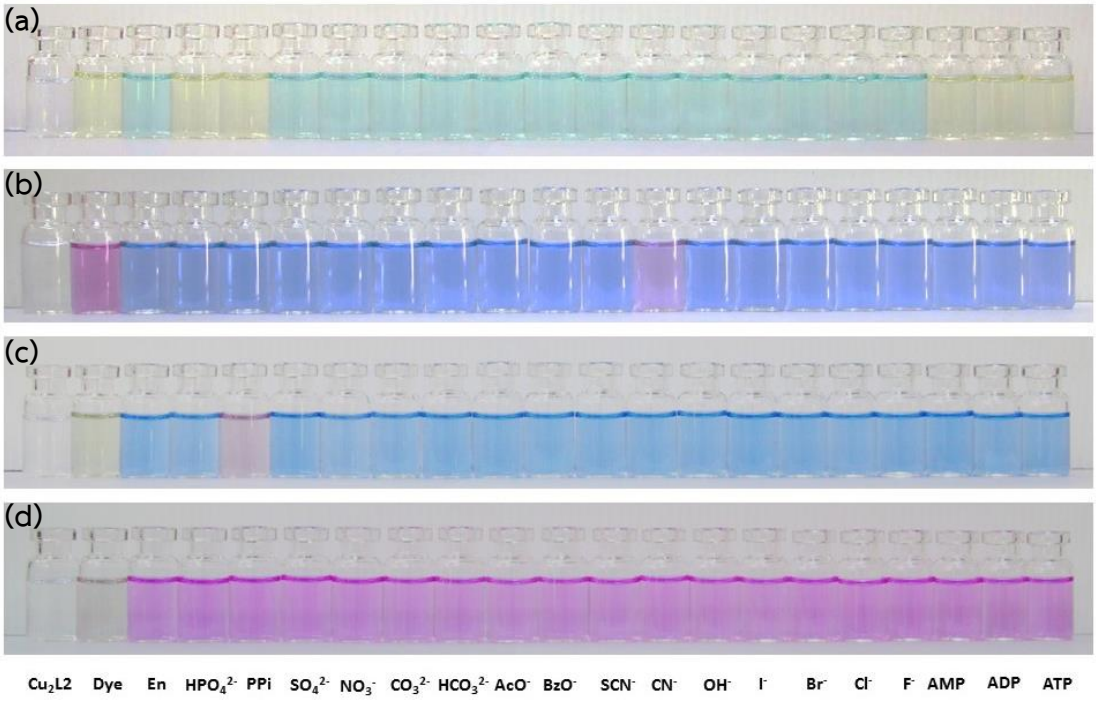


**Figure S36**. Color changes of the **$Cu_2$L2**-based (20 μM, 2 mL) ensembles with various indicators (400 μM, 0.2 mL) at a 1:2 receptor to indicator ratio (a) **PV**, (b) **BPG**, (c) **MTB** and (d) **XO** in the presence of various anions (1 mM, 0.3 mL in 20% (v/v) $H_2O/CH_3CN$ buffered at pH 7.4 with HEPES.

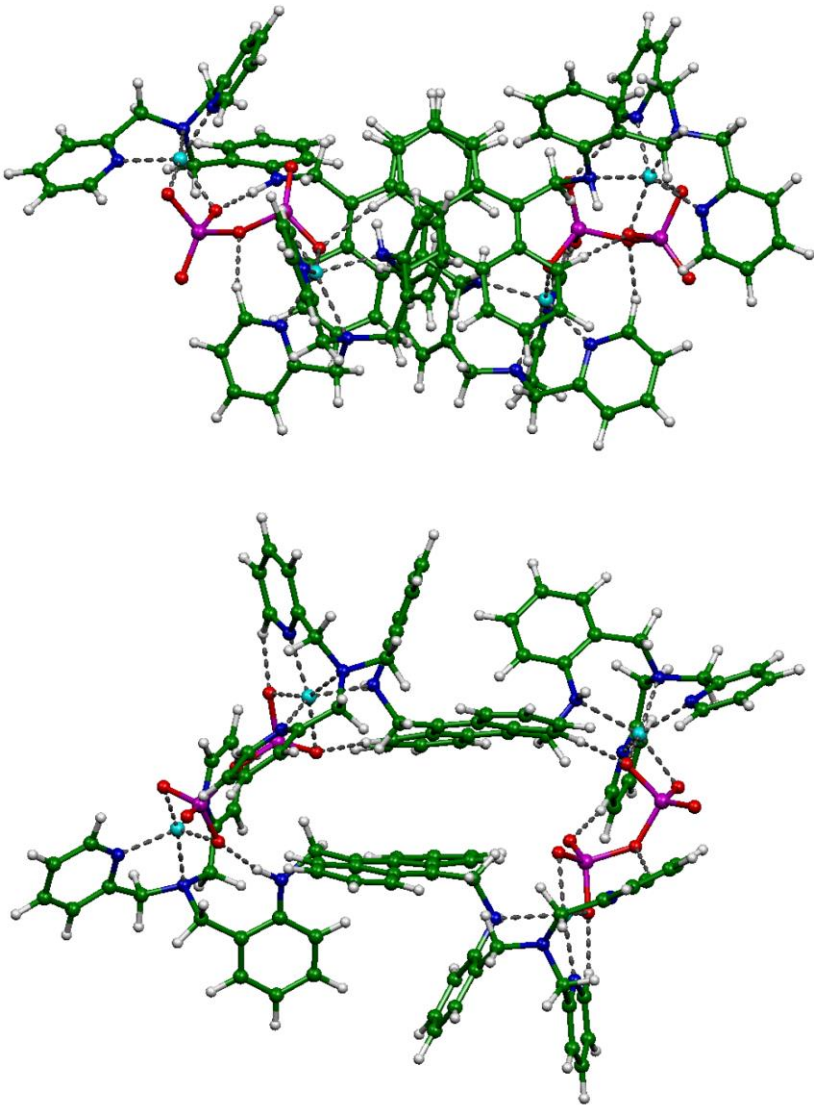

**Figure S37**. DFT/B3LYP/LANL2DZ-optimized structure of the dimeric 2:2 species of C1 conformer. Top and bottom images are top and front views, respectively.

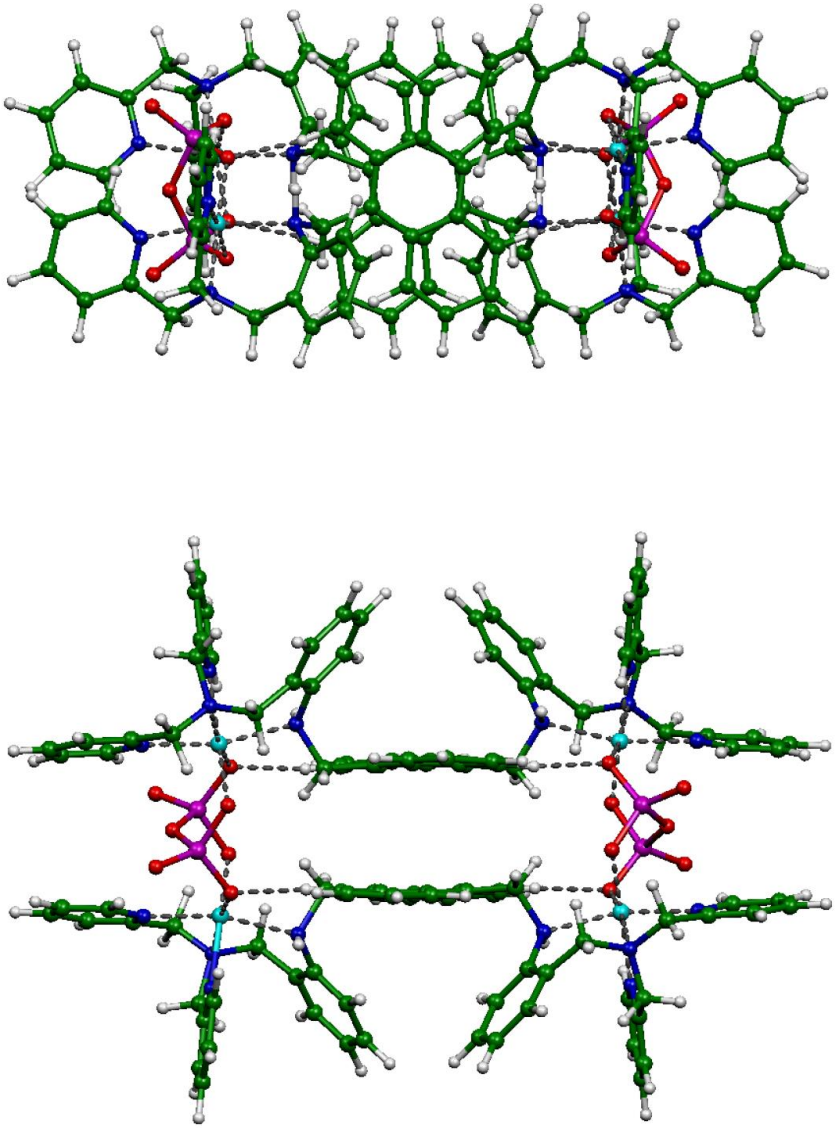

**Figure S38**. DFT/B3LYP/LANL2DZ-optimized structure of the dimeric 2:2 species of C2 conformer as the most stable one. Top and bottom images are top and front views, respectively.

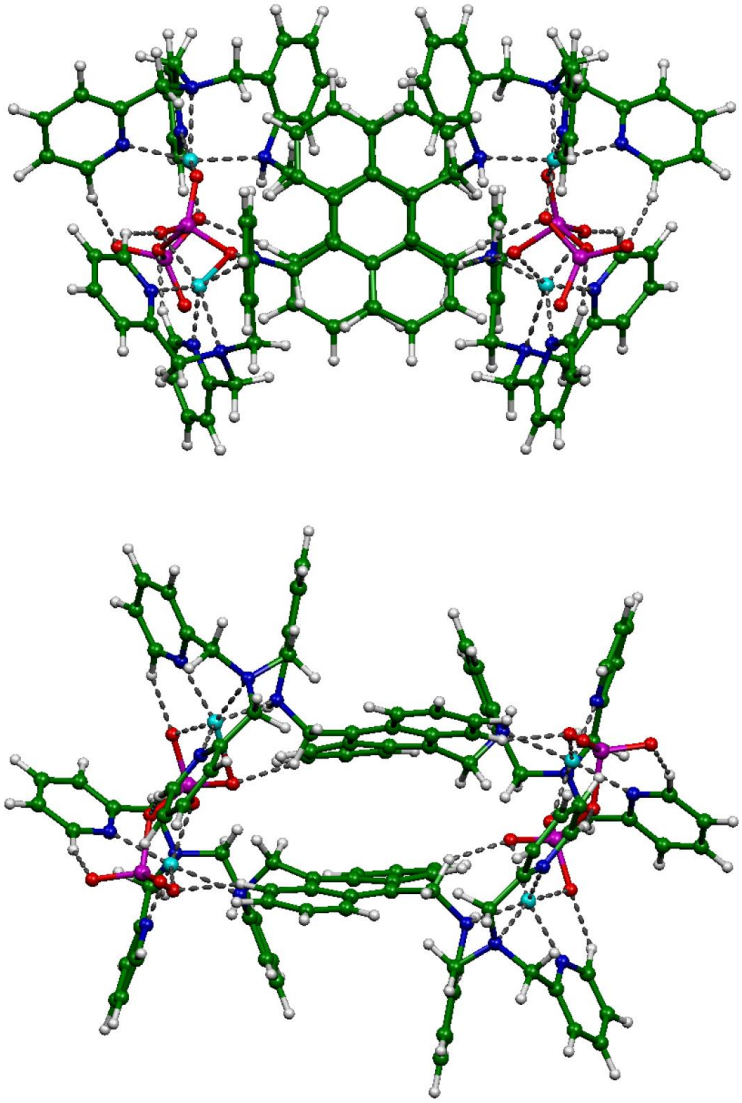

**Figure S39**. DFT/B3LYP/LANL2DZ-optimized structure of the dimeric 2:2 species of C3 conformer. Top and bottom images are top and front views, respectively.

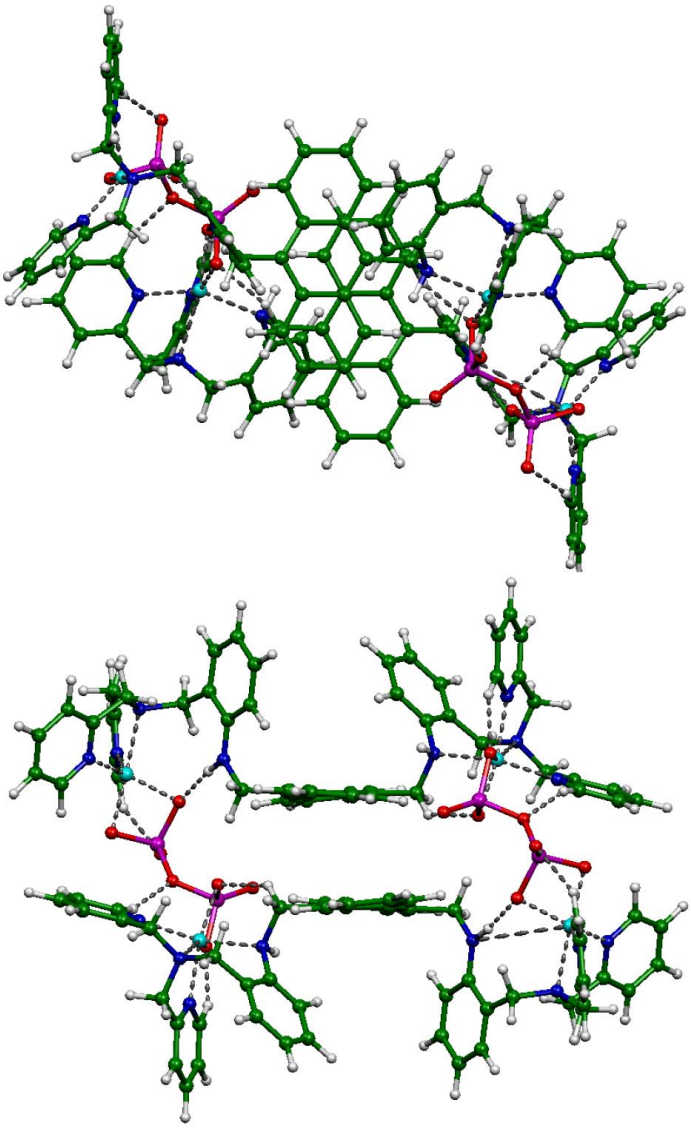

**Figure S40**. DFT/B3LYP/LANL2DZ-optimized structure of the dimeric 2:2 species of P1 conformer. Top and bottom images are top and front views, respectively.

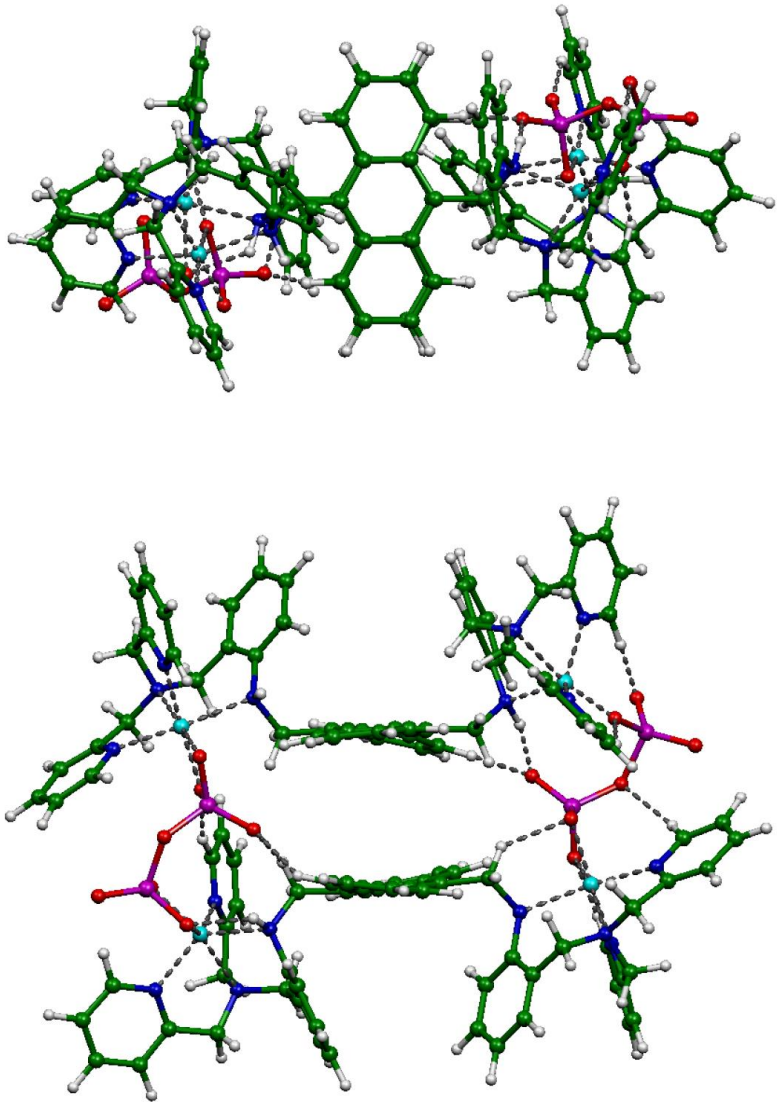

**Figure S41**. DFT/B3LYP/LANL2DZ-optimized structure of the dimeric 2:2 species of P2 conformer. Top and bottom images are top and front views, respectively.

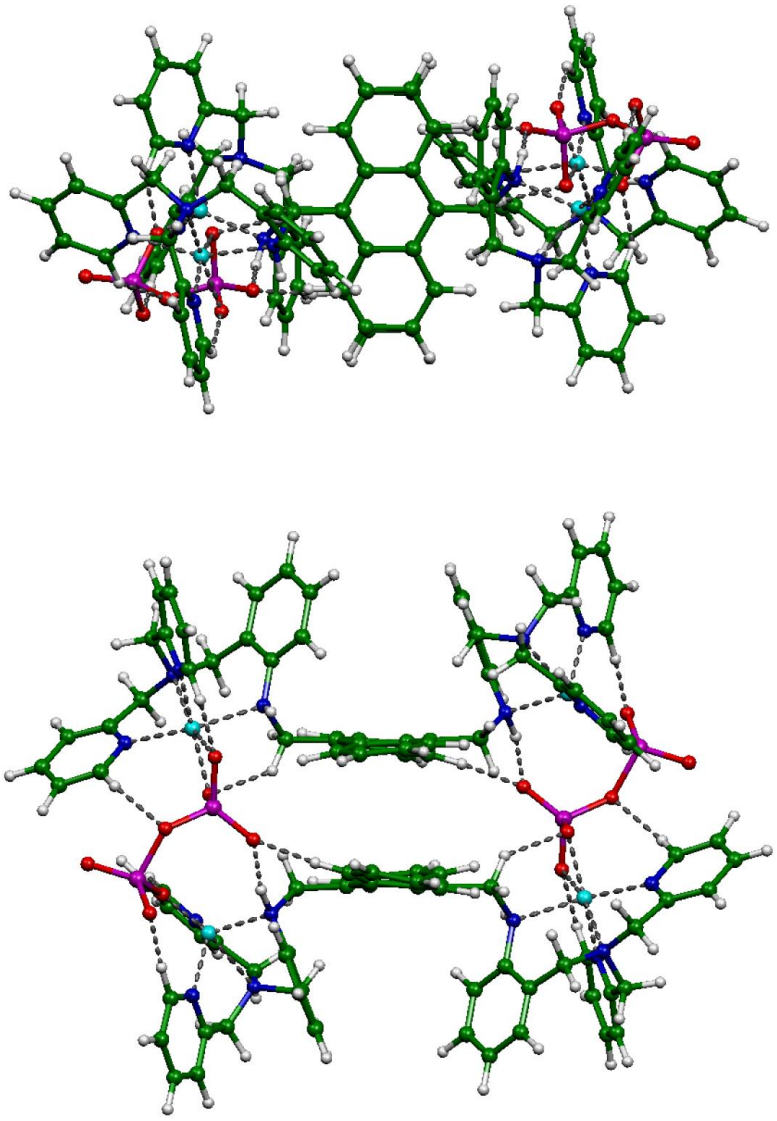

**Figure S42**. DFT/B3LYP/LANL2DZ-optimized structure of the dimeric 2:2 species of P3 conformer. Top and bottom images are top and front views, respectively.

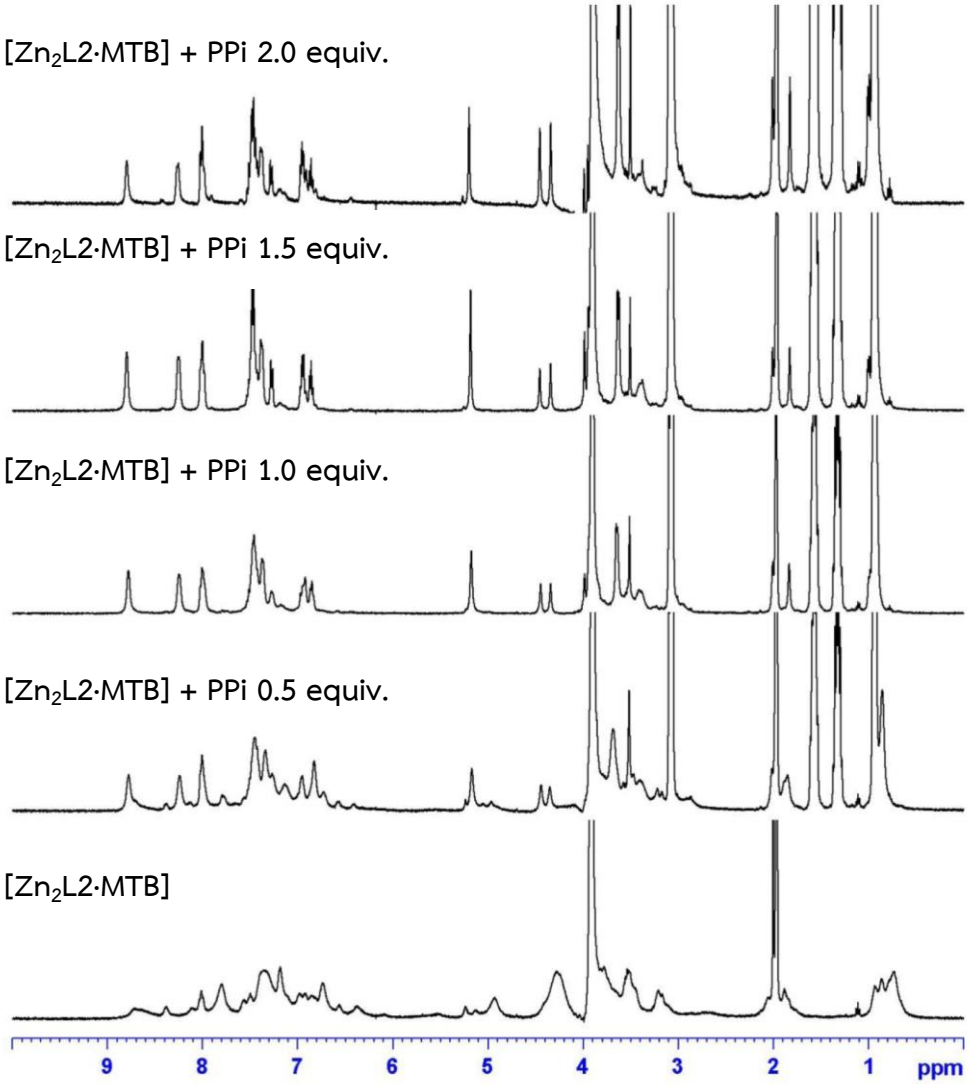


**Figure S43**. $^{1}$H NMR spectra of 1:1 ratio of ensemble formation between **$Zn_2$L2:MTB** (5 mM) upon addition of various concentrations of **PPi** (0.05 M) in 80/20 (%v/v) $CD_3CN/D_2O$.

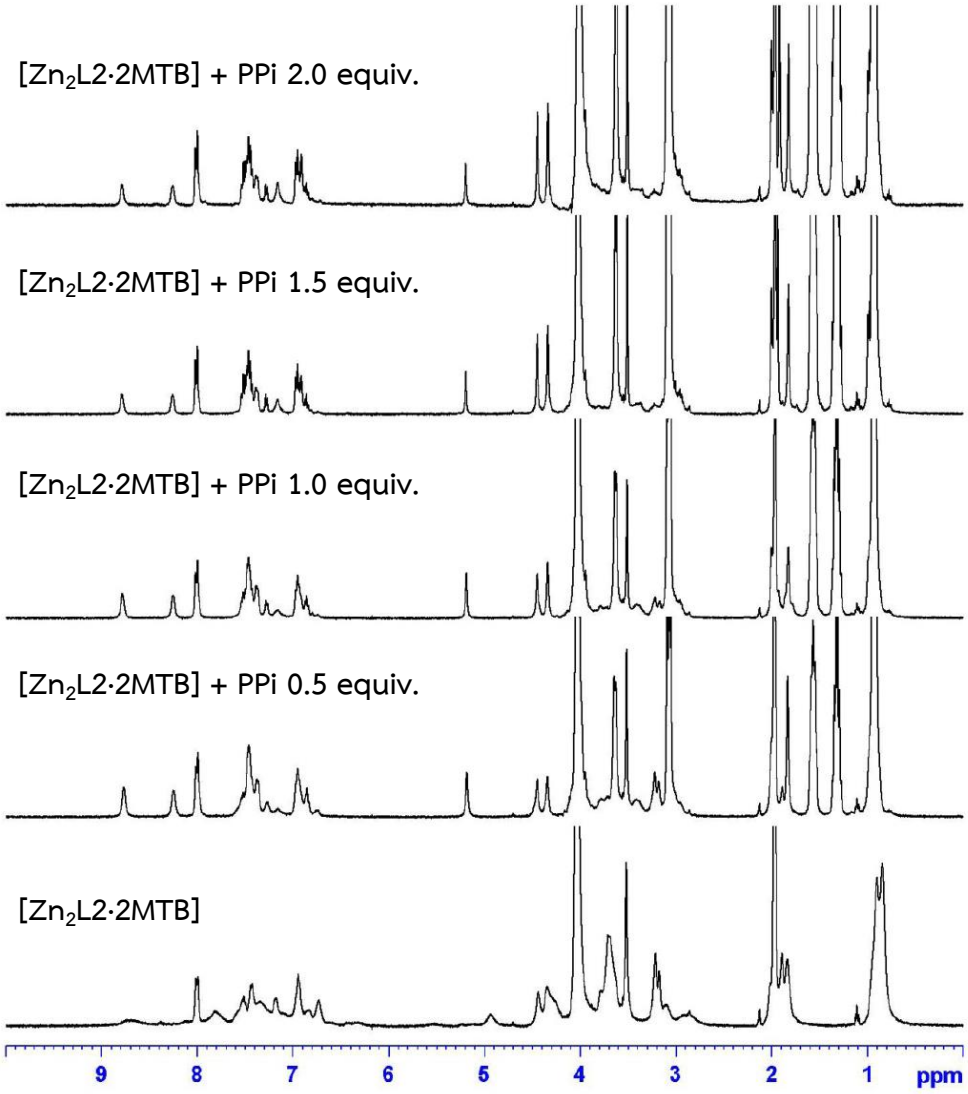


**Figure S44**. $^{1}$H NMR spectra of 1:2 ratio of ensemble formation between **$Zn_2$L2**:**MTB** (5 mM) upon addition of various concentration of **PPi** (0.05 M) in 80/20 (%v/v) $CD_3CN/D_2O$.

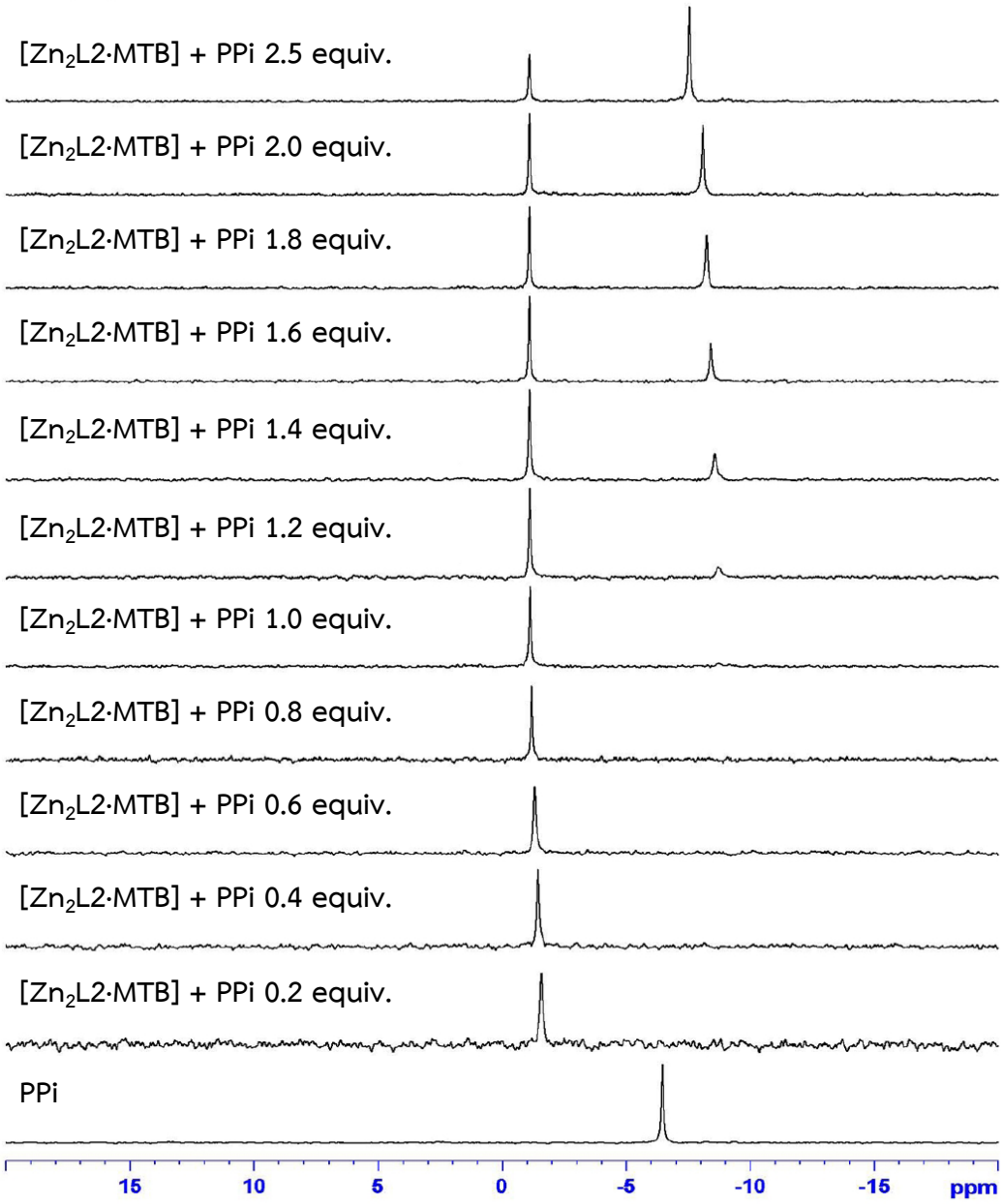


**Figure S45**. $^{31}$P NMR spectra of [**$Zn_2$L2·MTB**] (5 mM) upon addition of various concentrations of **PPi** (0.05 M) in 80/20 (%v/v) $CD_3CN/D_2O$.

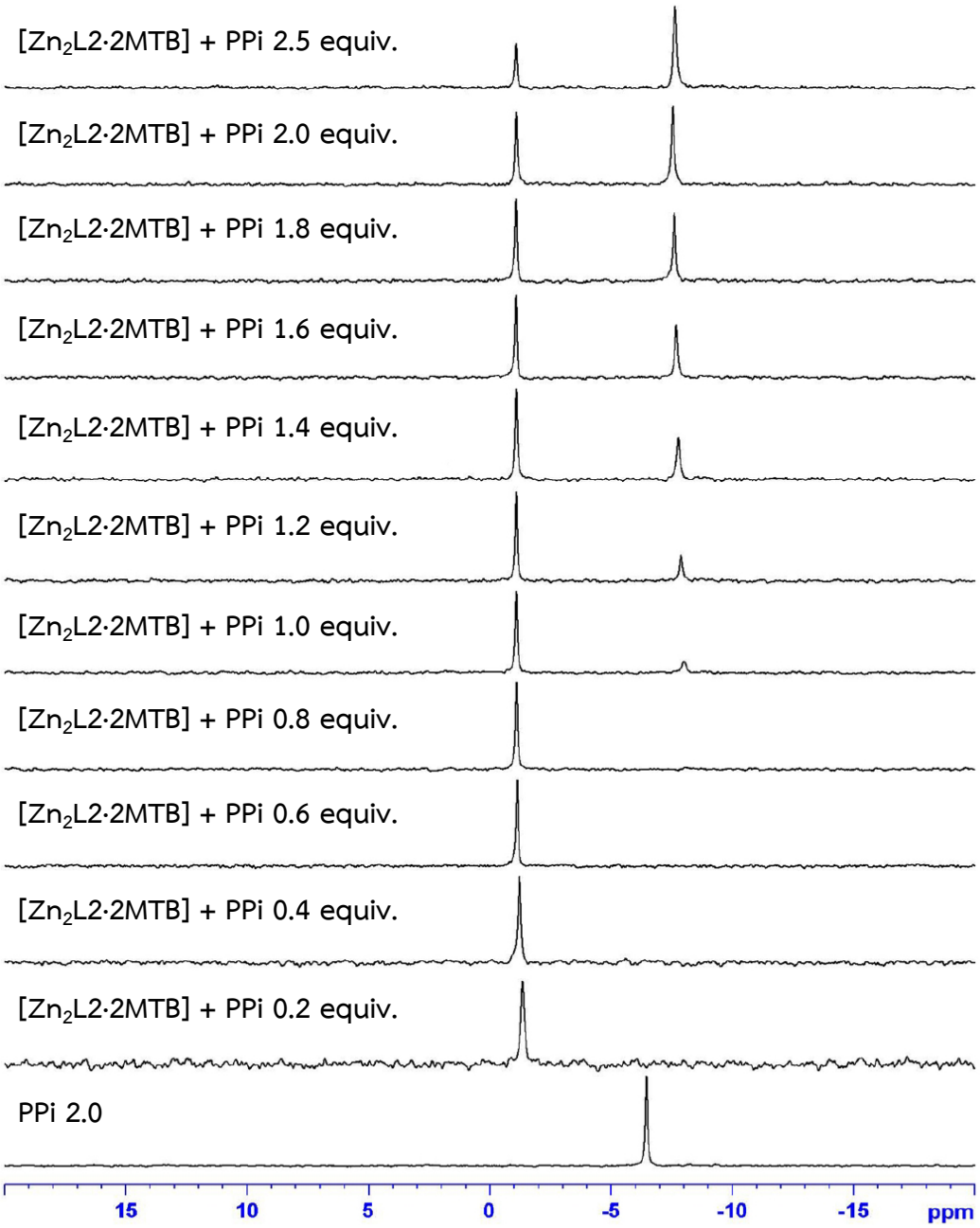


**Figure S46**. $^{31}$P NMR spectra of [**$Zn_2$L2·2MTB**] (5 mM) upon addition of various concentrations of **PPi** (0.05 M) in 80/20 (%v/v) $CD_3CN/D_2O$.

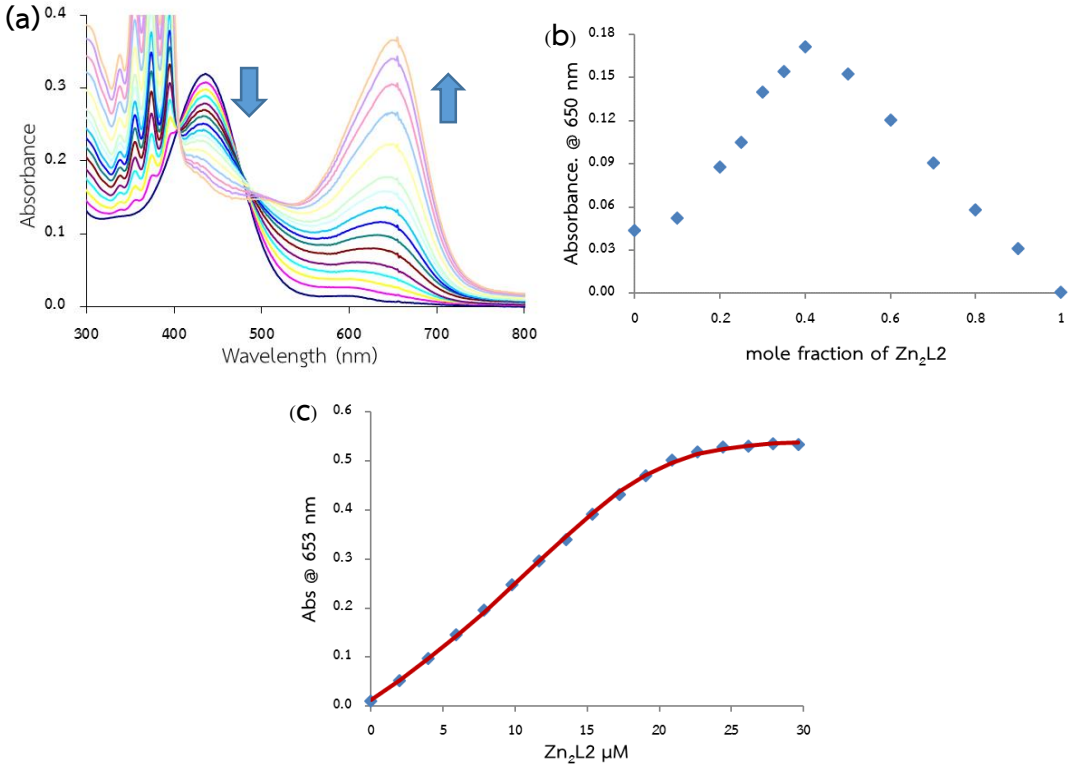


**Figure S47**. (a) UV-vis spectra obtained by addition of **$Zn_2$L2** (400 μM) to a solution of indicator **PV** (20 μM) in HEPES buffered pH 7.4 in 80/20 (%v/v) acetonitrile/aqueous solution, (b) Job's plot analysis of [**PV·$Zn_2$L2**] ensemble, (c) A plot of absorption against concentration of **$Zn_2$L2** titrated in **PV**. The red solid line is nonlinear least-squares fittings of the titration profiles using SPECFIT32 program.

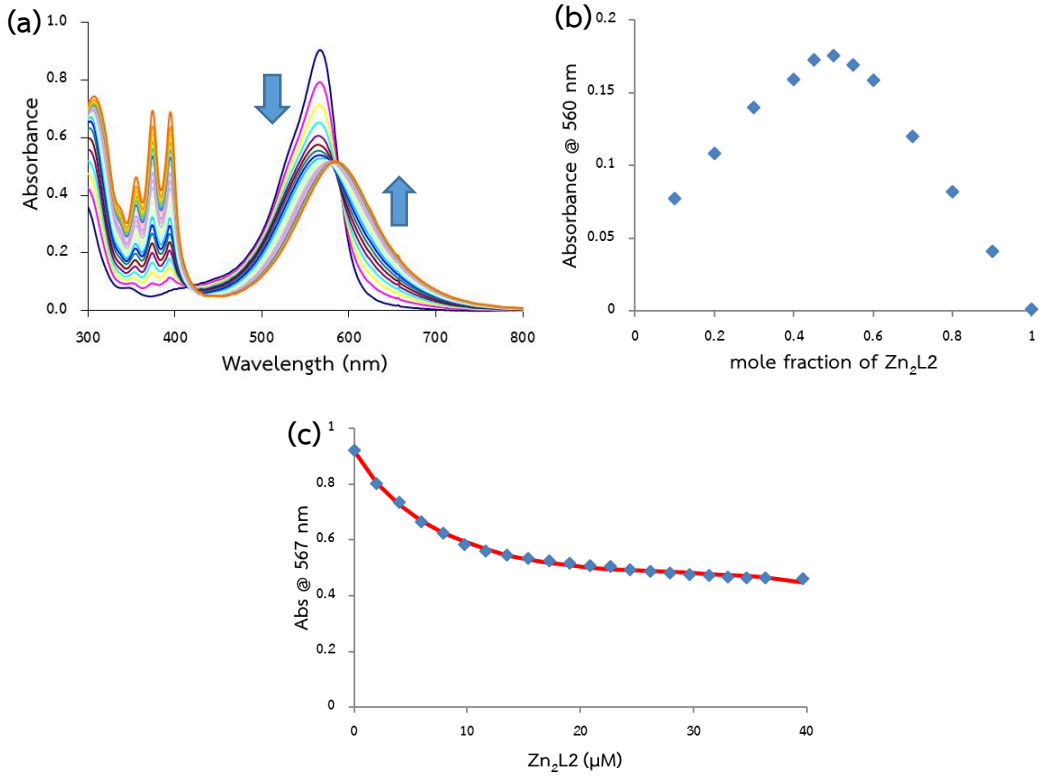


**Figure S48**. (a) UV-vis spectra obtained by addition of **$Zn_2$L2** (400 μM) to a solution of indicator **BPG** (20 μM) in HEPES buffered pH 7.4 in 80/20 (%v/v) acetonitrile/aqueous solution, (b) Job's plot analysis of [**BPG·$Zn_2$L2**] ensemble, (c) A plot of absorption against concentration of **$Zn_2$L2** titrated in **BPG**. The red solid line is nonlinear least-squares fittings of the titration profiles using SPECFIT32 program.

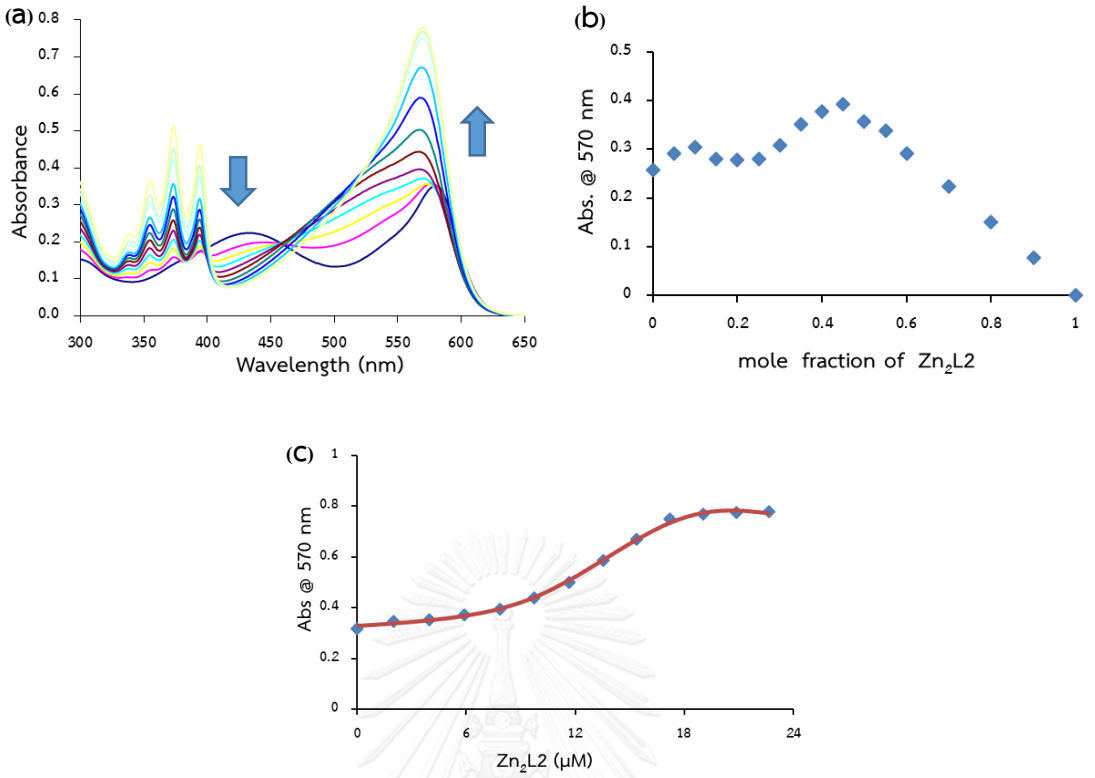


**Figure S49**. (a) UV-vis spectra obtained by addition of **$Zn_2$L2** (400 μM) to a solution of indicator **XO** (20 μM) in HEPES buffered pH 7.4 in 80/20 (%v/v) acetonitrile/aqueous solution, (b) Job's plot analysis of **[XO·$Zn_2$L2]** ensemble, (c) A plot of absorption against concentration of **$Zn_2$L2** titrated in **XO**. The red solid line is nonlinear least-squares fittings of the titration profiles using SPECFIT32 program.

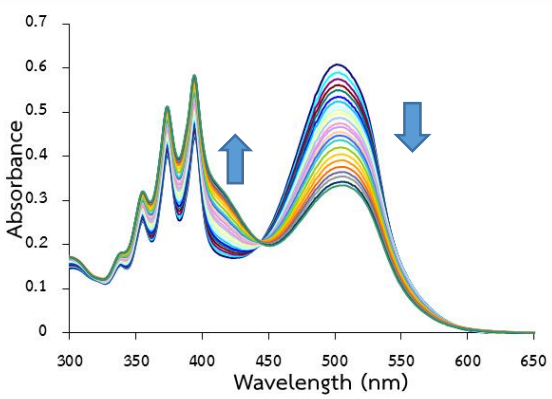


**Figure S50**. UV/vis spectra obtained by addition of **His** (1 mM) to a solution of [**$Zn_2$L2•2PAR**] ensemble (20 μM) in HEPES buffered pH 7.4 in 80/20 (% v/v) acetonitrile/aqueous solution.

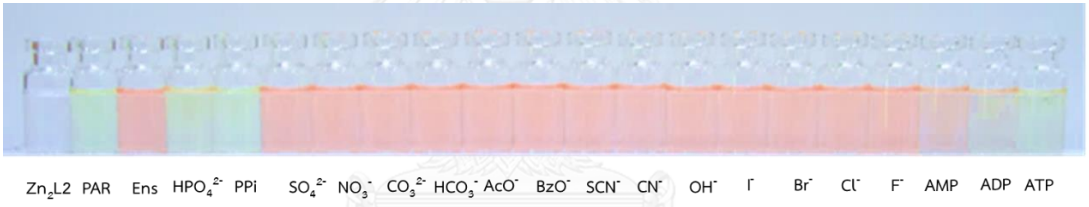


**Figure S51**. Color changes of [**$Zn_2$L2•PAR**] ensemble (20 μM) in the present of various anions in 10 mM HEPES buffered pH 7.4 in 80/20 (% v/v) acetonitrile/aqueous solution.

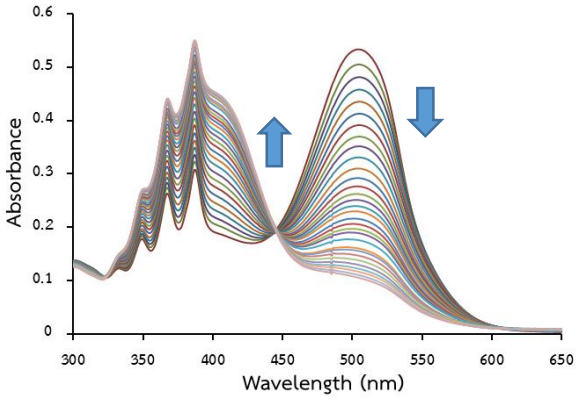


**Figure S52**. UV/vis spectra obtained by addition of His (1 mM) to a solution of [**ZnL3•PAR**] ensemble (20 μM) in HEPES buffered pH 7.4 in 80/20 (% v/v) acetonitrile/aqueous solution.

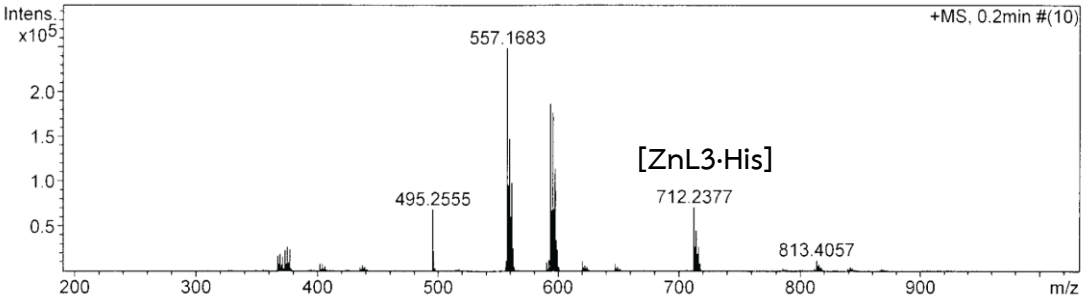


Chulalongkorn University

**Figure S53**. HR-MS spectrum of the solution mixture between **ZnL3** and **His**.

**(a)**

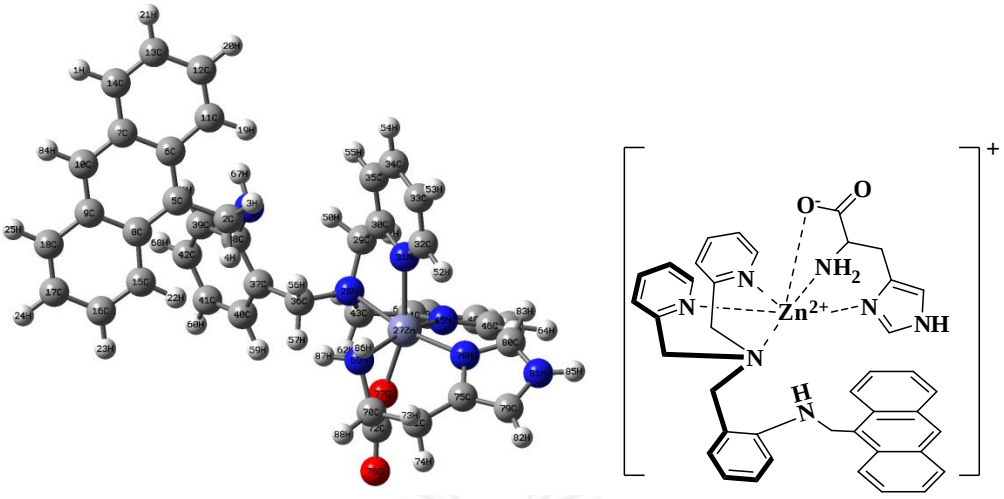


**(b)**

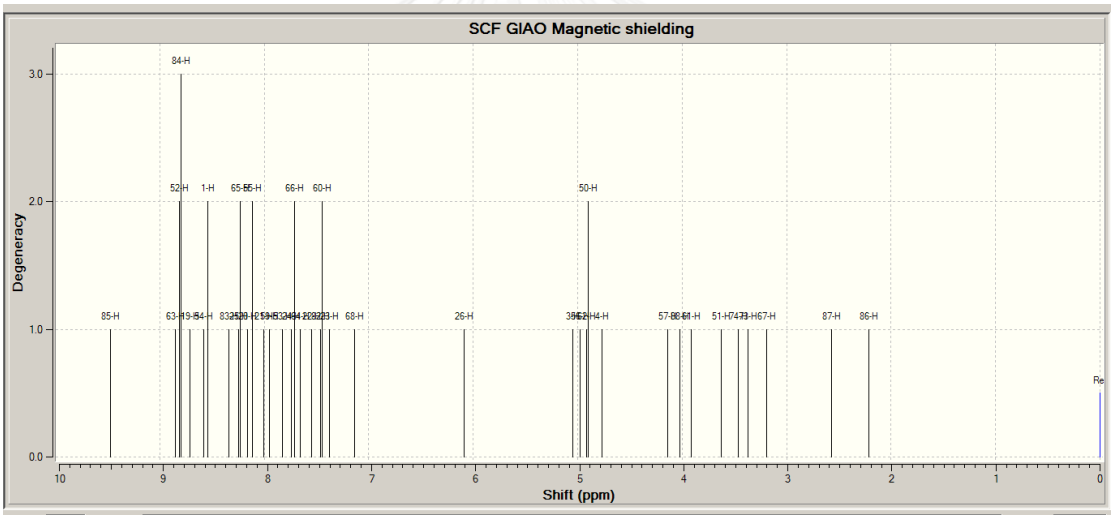


**Figure S54.** (a) The B3LYP/6-31+G(d,p) optimized structure of *N,N,O* conformer (**1**), where O in in the equatorial position and (b) $^{1}$H-NMR spectrum of the conformer (**1**), simulated using the GIAO/B3LYP/6-31+G(d,p) method with CPCM/UFF solvent effect for water.

(a)

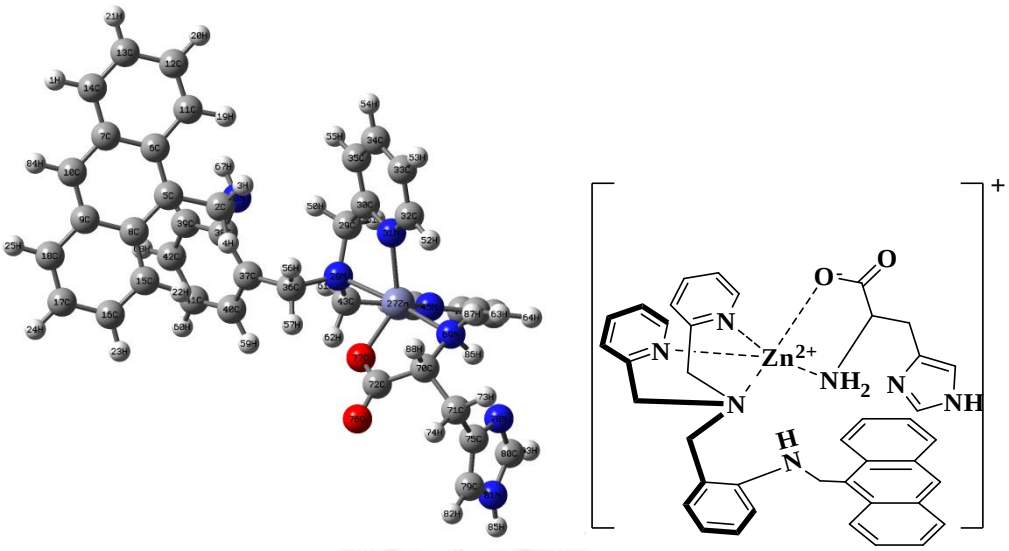


**(b)**

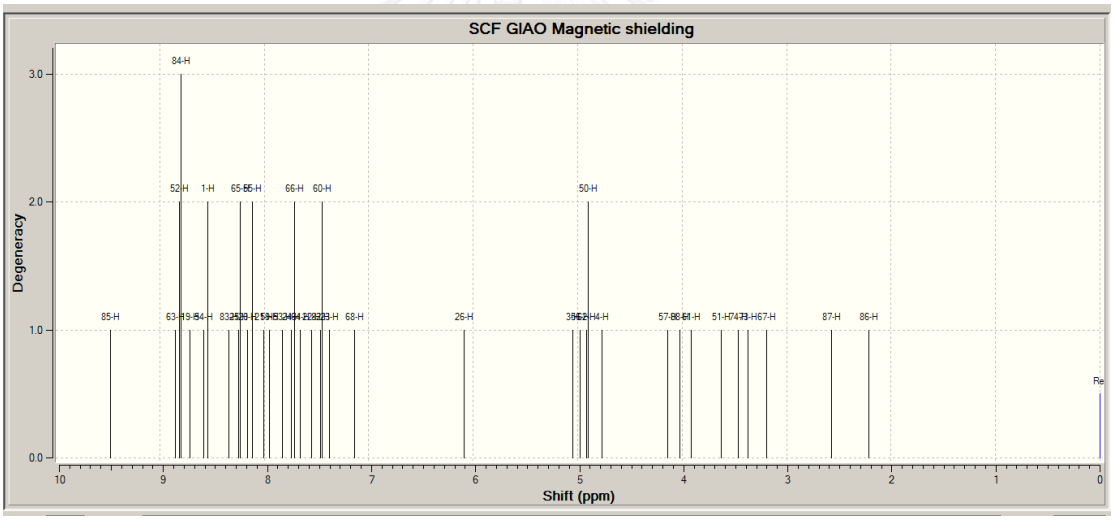


**Figure S55.** (a) The B3LYP/6-31+G(d,p) optimized structure of *N,O*-conformer (**2**) and (b) $^{1}$H-NMR spectrum of the conformer (**2**), simulated using the GIAO/B3LYP/6-31+G(d,p) method with CPCM/UFF solvent effect for water.

(a)

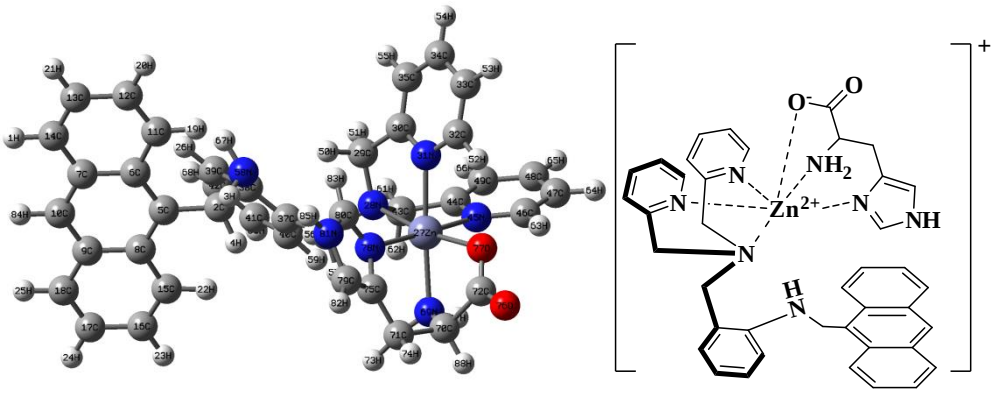


(b)

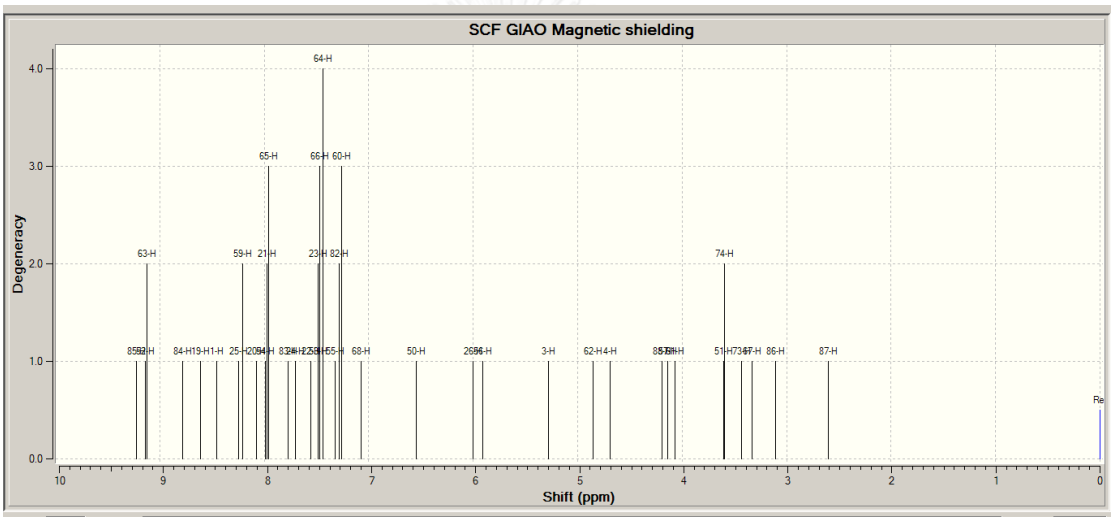


Chulalongkorn University

**Figure S56.** (a) The B3LYP/6-31+G(d,p) optimized structure of *N*,*N*,*O*-conformer (**3**), where O in in the equatorial position and (b) $^{1}$H-NMR spectrum of the conformer (**3**), simulated using the GIAO/B3LYP/6-31+G(d,p) method with CPCM/UFF solvent effect for water.

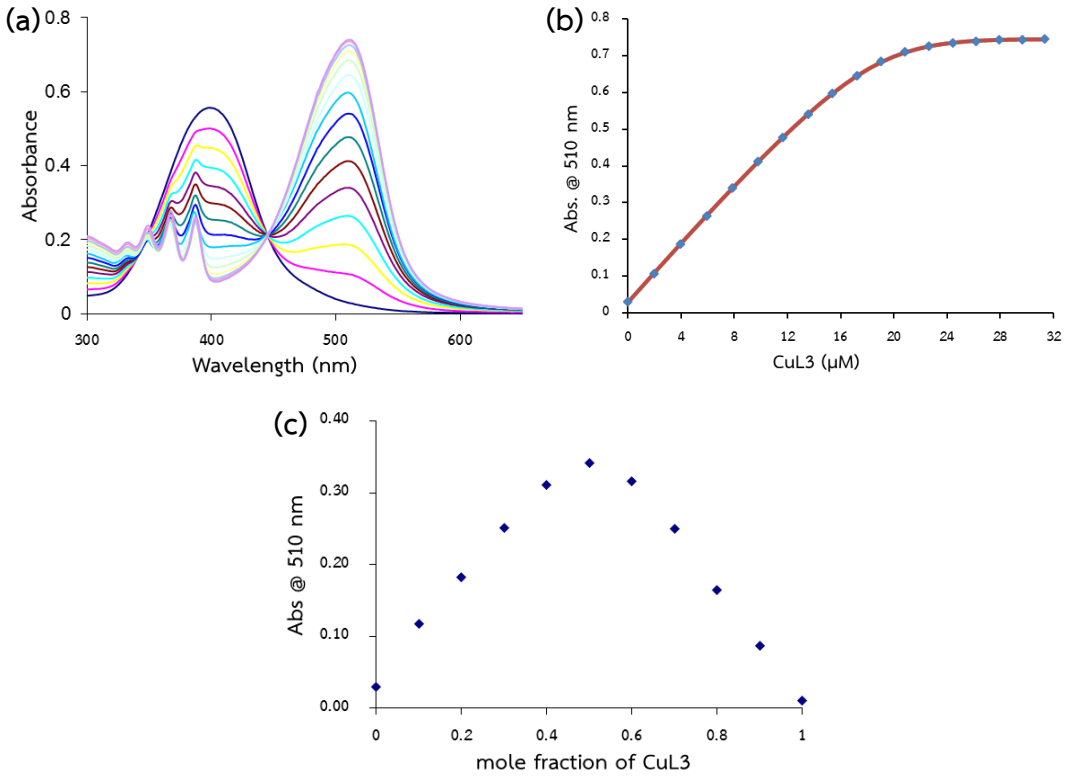


**Figure S57**. (a) UV/vis spectra obtained by addition of **CuL3** (400 μM) to a solution of **PAR** (20 μM), (b) a plot of absorption against concentration of **CuL3** titrated in **PAR** and (c) Job's plot analysis in HEPES buffered pH 7.4 in 80/20 (% v/v) $CH_3CN/H_2O$ solution. The blue solid line is nonlinear least-squares fittings of the titration profiles using SPECFIT 32 program.

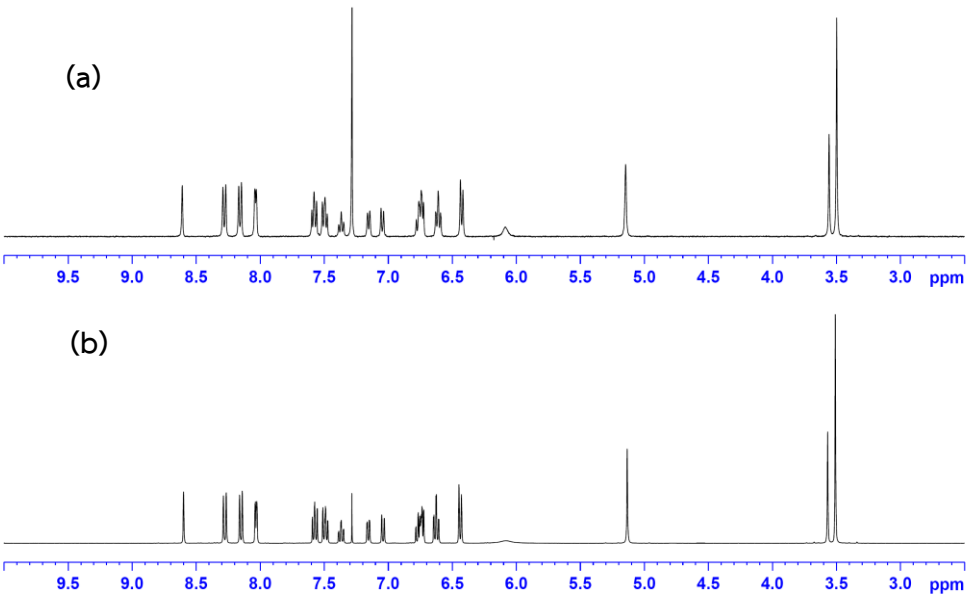


**Figure S58.** $^{1}$H-NMR spectra of (a) free **L3** and (b) solid evidence from electrochemical studies in $CDCl_3$.

จุฬาลงกรณ์มหาวิทยาลัย
Chulalongkorn University

**Table S1**. Crystallographic data and final refinement parameters for ligand **L3** and **CuL3** complex.

| | **L3** | **CuL3** |
|---|---|---|
| Chemical formula | $C_{34}H_{32}N_4O$ | $C_{35}H_{34}Cl_2CuN_4O$ |
| Formula weight | 512.64 | 661.10 |
| Crystal size | 0.25 × 0.3 × 0.2 | 0.26 × 0.3 × 0.32 |
| Colour | yellow | yellow |
| Temperature (K) | 293(2) | 293(2) |
| Crystal system | Triclinic | Orthorhombic |
| Space group | *P-1* | *Pbca* |
| *a* (Å) | 11.459(3) | 15.9666(4) |
| *b* (Å) | 11.615(3) | 13.5534(4) |
| *c* (Å) | 12.520(3) | 28.1590(8) |
| $\alpha$ (°) | 108.116(6) | 90 |
| $\beta$ (°) | 101.413(6) | 90 |
| $\gamma$ (°) | 110.757(6) | 90 |
| *V* (Å$^3$) | 1389.1(6) | 6093.7(3) |
| *Z* | 2 | 8 |
| $\rho_{calc}$ (g cm$^{-3}$) | 1.226 | 1.441 |
| $\mu$ (mm$^{-1}$) | 0.075 | 0.928 |
| *F(000)* | 544 | 2744 |
| θ range for data collection | 1.82 to 28.00° | 1.45 to 28.02° |
| Index ranges | -15<=h<=15 | -21<=h<=21 |
| | -15<=k<=15 | -17<=k<=17 |

จุฬาลงกรณ์มหาวิทยาลัย
Chulalongkorn University

| | -16<=l<=16 | -37<=l<=37 |
|---|---|---|
| Reflections collected / observed | 16762 / 6694 | 69843 / 7366 |
| $R_{int}$ | 0.0710 | 0.0975 |
| Data / restraints / parameters | 6694 / 0 / 364 | 7366 / 0 / 408 |
| GOF | 1.020 | 1.166 |
| $R_1$ [$I > 2\sigma(I)$] | 0.0846 | 0.0721 |
| $wR_2$ [$I > 2\sigma(I)$] | 0.1405 | 0.1226 |
| $R_1$ [all data] | 0.2049, | 0.1025 |
| $wR_2$ [all data] | 0.1796 | 0.1325 |

**Table S2.** Total and relative energies of all the B3LYP/6-31+G(d,p) optimized structures of three conformers of the relevant complexes.

| Conformers | $E_{total}$ [a] | $\Delta E_{rel}$ [b] |
|---|---|---|
| **C1** [c] | -3860.0862499 | 2.96 |
| **C2** [d] | -3860.0909651 | 0.00 |
| **C3** [c] | -3860.0900861 | 0.55 |

[a] Total energies are in au. [b] Relative energies compared with the most stable conformer (C2), in kcal/mol. [c] Distort octahedral structure. [d] Distort pyramidal structure.

# VITA

| | |
|---|---|
| Name | Sarayut Watchasit |
| Date of birth | June 3, 1985 |
| Place of birth | Trat Province, Thailand |
| Present address | Burapha University, Chonburi, Thailand |

Education

| | |
|---|---|
| 2004 - 2008 | Bachelor of Science (B.Sc.), Faculty of Science, Burapha University, Chonburi, Thailand |
| 2008 - 2010 | Master of Science (M.Sc.), Faculty of Science, Burapha University, Chonburi, Thailand |
| 2010 - 2015 | Doctor of Philosophy (Ph.D.), Faculty of Science, Chulalongkorn University, Bangkok, Thailand |

Awards or Grants

| | |
|---|---|
| 2008 - 2010 | PERCH-CIC |
| 2010 - 2015 | The Royal Golden Jubilee Ph.D. Program |

จุฬาลงกรณ์มหาวิทยาลัย
Chulalongkorn University